Winter 2004

Analysis of Human Thermal Comfort Using a Coupled Model for Predicting Human Body-Environment Heat and Mass Exchange

Ahmed M. Al-Mogbel
Old Dominion University

ANALYSIS OF HUMAN THERMAL COMFORT USING A COUPLED MODEL FOR PREDICTING HUMAN BODY-ENVIRONMENT HEAT AND MASS EXCHANGE

by

Ahmed M. Al-Mogbel

M.S. August 2000, Old Dominion University, Virginia
B.S. December 1991, King Saud University, Saudi Arabia

A Dissertation Submitted to the Faculty of Old Dominion University in Partial Fulfillment of the Requirement for the Degree of

DOCTOR OF PHILOSOPHY

MECHANICAL ENGINEERING

OLD DOMINION UNIVERSITY
December 2004

Approved by:

Dr. Sushil K. Chaturvedi (Director)

Dr. Surendra N. Tiwari

Dr. Devendra S. Parmar

Dr. Tarek Abdel-Salam

ABSTRACT

Analysis of Human Thermal Comfort Using a Coupled Model for Predicting Human Body- Environment Heat and Mass Exchange

Ahmed M. AL-Mogbel
Old Dominion University, 2004
Director: Dr. Sushil K. Chaturvedi

Recent advances in computational fluid dynamics (CFD) make it possible to accurately predict many features of airflow within ventilated spaces. The present study investigates thermal comfort aspects of an occupant in a conditioned space, using a CFD code.

The heat and mass transfer between the human body and the surrounding environment is analyzed by a coupled model that accounts for dispersal of metabolically generated heat in the body to the surroundings by the combined mechanisms of radiation, convection, respiration and evaporation. A two-node model in which two coupled non-linear algebraic equations govern the skin temperature and the body core temperature analyzes heat transfer inside the body. The energy interaction between the body and the surroundings is modeled by coupled equations for mass, momentum and energy transport. Since energy and mass (water vapor) interactions between the body and surroundings modify the air temperature and humidity, the numerical algorithm adopted incorporates the coupling between the body and the surroundings, using interfacial boundary conditions for temperature and humidity at the skin surface.

A segmented body model has also been developed to take into account the spatial variation of body skin temperature. The proposed segmented model shows more details and incorporates wider variations of body properties. Thermal comfort indices namely, Effective Draft Temperature (EDT), Predicted Mean Vote (PMV) and Percentage of People Dissatisfied (PPD) are used to map the regions of thermal comfort and discomfort. Results presented for several supply air conditions and metabolic activity rate show that of all the variables considered in this study the supply air temperature most strongly influences thermal comfort conditions, followed by the metabolic activity rate. The supply air relative humidity has the least effect. The body skin and core temperatures are most influenced by the metabolic activity rate, followed by the supply air temperature. Simulations with varying supply air turbulence intensity show that it has minimal effect on thermal comfort conditions in the room. Regions of thermal comfort and discomfort mapped on PMV-EDT diagrams show that out of 20 supply air and metabolic activity conditions considered in this study, the room averaged PMV index predicted 15 of them to be in the thermal comfort zone and remaining five were shown to lie in the thermal discomfort zone. The EDT index predicted 18 of the 20 conditions as belonging to the comfort zone. Although in the majority of cases both indices are in agreement regarding their prediction, the PMV index provides a conservative estimate of thermal comfort conditions. The segmented body model points to the fact that results predicted by it provide a more conservative estimate of thermal comfort as compared to the regular (unsegmented) model.

ACKNOWLEDGMENTS

First, Praise be to God (Allah), the Cherisher and Sustainer of the worlds. This study would not have been possible without grace God (Allah) has bestowed upon me. Many people have helped me during my graduate studies, and I would like to thank all of them for their patience and support. I am massively indebted to Dr. Sushil K. Chaturvedi, who has given me so much guidance, insight and encouragement throughout this work. Everyone in the Mechanical Engineering Department has helped me at some point along the way. I am especially grateful to Dr. Surendra Tiwari, Dr. Devendra Parmar and Dr. Tarek Abdel-Salam for many kindnesses over the years.

I wish to thank Adel Alharbi who gave me encouragement, enlightenment and help through several discussions. No study of this size can be completed without disruption of one's normal family routine. This project could not have been completed without the support, encouragement, love and caring of my father, mother, wife and the entire family.

The positive attributes of this report derive from those mentioned above and many other sources. The conclusions and any errors, omissions or mistakes within this report are attributable only to the author.

TABLE OF CONTENT

Page

ACKNOWLEDGEMENTS vi

LIST OF TABLES vii

LIST OF FIGURES viii

LIST OF SYMBOLS xi

CHAPTER

Introduction 1
1.1 Background 1
1.2 Review of Literature 4
1.2.1 Room Airflow Models 4
1.2.2 Human Thermal Mathematical Models 8
1.3 Objectives 11
1.4 Outline of the Dissertation 12

I. Thermal Comfort 14
2.1 Introduction 14
2.1.1 The Dry Bulb Temperature 16
2.1.2 The Air Velocity 16
2.1.3 The Relative Humidity 17
2.1.4 The Activity Level 17
2.1.5 The Mean Radiant Temperature 18
2.1.6 The Turbulence Intensity Level 19
2.2 Heat Balance Equation 19
2.3 Thermal Comfort Indices 23
2.3.1 EDT 23
2.3.2 PMV 24
2.3.3 PPD 25

III. The Mathematical Model 27
3.1 Computational Fluid Dynamics (CFD) 27
1.2 Governing Equations 28
3.2.1 Continuity Equation 28
3.2.2 Momentum Equation 29
3.2.3 Energy Equation 31
3.2.4 Mass Diffusion Equation 31

3.2.5 General form of Equations 32
1.3 Turbulence Model 33
1.4 Coupled Nature of the Problem 36

IV. Solution Procedure 40
4.1 Introduction 40
4.2 The Two Node Model for Human Thermo-Regulation Process 41
4.3 The Algorithm of the Coupled Solution Procedure 44
4.4 Model Geometry 46
4.5 Boundary Conditions 50
4.6 Model Validation 51

V. Results and Discussions 58
5.1 Introduction 58
5.2 Effect of Occupation in Conditioned Room 58
5.2.1 Room Temperature and Relative Humidity 59
5.2.2 Thermal Comfort Indices 60
5.3 Effect of Physical Variables on Thermal Comfort 65
5.3.1 Effect of Supply Air Temperature 65
5.3.2 Effect of Supply Air Velocity 74
5.3.3 Effect of Relative Humidity 81
5.3.4 Effect of Metabolic Activity 87
5.4 Effect of the Turbulence Intensity Level 93
5.5 Segmented Body Model 97
5.5.1 Variation of Skin Temperature and Convective Heat Transfer Coefficient 97
5.5.2 Thermal Comfort Using Segmented Model 99
5.6 Effect of Environmental and Physical Parameters on the Skin and the Core Temperatures 106
5.7 The EDT-PMV Comfort Map 111
5.8 Correlation of Skin Temperature with PMV 111

VI. Conclusions 120

References 123

VITA 128

LIST OF TABLES

Table Page

2.1 PMV Thermal Sensation Scale 25

4.1 Comparison of Hear Release from Human Body with Murakami Model 56

LIST OF FIGURES

Figure Page

2.1 The human body interactions with surrounding 15

2.2 The total heat production from the human body 20

2.3 PPD as function of PMV 26

3.1 The types of grid mesh 38

4.1 Two-Node body heat transfer model 42

4.2 Flow chart of numerical methodology 45

4.3 Human body model 48

4.4 the occupied ventilated room 49

4.5 Grid independency by vertical temperature distribution 53

4.6 Grid independency by vertical velocity distribution 54

4.7 Comparison of predictions of vertical temperature with different Models 55

5.1 Temperature contours for the empty room 62

5.2 Temperature contours for the occupied room 62

5.3 Relative humidity contours for the empty room 63

5.4 Relative humidity contours for the occupied room 63

5.5 EDT index for the empty room 64

5.6 EDT index for the occupied room 64

5.7 Temperature contours for different inlet temperatures 69

5.8 Velocity contours for different inlet temperatures 70

5.9 PMV index for different inlet temperatures 71

5.10 EDT index for different inlet temperatures 72

5.11 Inlet temperatures vs. PMV & PPD 73

5.12 Temperature contours for different Inlet velocities 76

5.13 Velocity contours for different inlet velocities 77

5.14 PMV index for different inlet velocities 78

5.15 EDT index for different inlet velocities 79

5.16 Inlet velocity vs. PMV & PPD 80

5.17 Temperature contours for different relative humidity 82

5.18 Velocities contours for different relative humidity 83

5.19 PMV index for different relative humidity 84

5.20 EDT index for different relative humidity 85

5.21 Relative humidity vs. PMV & PPD 86

5.22 Temperature contours for different metabolic activity 88

5.23 Velocity contours for different metabolic activity 89

5.24 PMV index for different metabolic activity 90

5.25 EDT index for different metabolic activity 91

5.26 Metabolic activity rate vs. PMV & PPD 92

5.27 Temperature contours for different intensity levels 94

5.28 Velocity contours for different intensity levels 95

5.29 EDT index for different intensity levels 96

5.30 Body skin temperatures 98

3.31 Convective heat transfer & coefficient 98

5.32 Temperature contours for different metabolic activity 101

5.33 Velocity contours for different metabolic activity 102

5.34 PMV index for different metabolic activity 103

5.35 EDT index for different metabolic activity 104

5.36 Metabolic activities vs. PMV & PPD 105

5.37 Core and skin temperatures as function of room inlet air temperature 107

5.38 Core and skin temperatures as function of air velocity 108

5.39 Core and skin temperatures as function of relative humidity 109

5.40 Core and skin temperatures as function of metabolic rate 110

5.41 Thermal comfort zone for different inlet air temperature 113

5.42 Thermal comfort zone for different inlet air velocity 114

5.43 Thermal comfort zone for relative humidity 115

5.44 Thermal comfort zone for different metabolic rate 116

5.45 Thermal comfort zone for different metabolic rate (segmented body) 117

5.46 PMV index vs. body skin temperature for all different parameters 119

LIST OF SYMBOLS

c_p specific heat or heat capacity, J/g.°C

E_{sk} total evaporative heat transfer from skin, W/m^2

H height of human body, m

K effective conductance between the core node and the skin layer, 5.28 $W/(m^2 K)$

M metabolic heat production, W/m^2

m_{bl} blood flow rate, $kg/(m^2s)$

m_{sk} sweat rate generated from skin, $kg/(m^2s)$

P_a water vapor pressure in ambient air, Pa

Q_{cv} convective heat transfer rate, W/m^2

Q_r radiant heat transfer rate, W/m^2

Q_{res} total heat transfer rate through respiration, W/m^2

Q_{sk} total (sensible+latent) heat transfer rate from skin, W/m^2

S_{cr} rate of heat storage in core node, W/m^2

S_{sk} rate of heat storage in skin layer, W/m^2

S source term

T_a ambient air temperature,°C

T_{cr} temperature of core node of human body,°C

T_{sk} temperature of skin layer,°C

T_w wall surface temperature,°C

u X-direction velocity, m/s

V mean velocity, m/s

W work rate transfer, W

w skin wettedness (including diffusion and regulatory sweat)

x,y,z coordinates

Greek Symbols

Γ Diffusion coefficient

ϕ Dummy variable

μ The viscosity, kg/m s

μ_l The laminar viscosity, kg/m s

ρ Density, kg/m^3

CHAPTER I[1]

INTRODUCTION

1.1 Background

Thermal comfort is a major concern in the daily life of human beings. Analysis of thermal comfort deals with factors that affect human thermal comfort, and indices that characterize it. The growing modernization of society is causing a majority of people in technologically advanced countries to spend most of their lives in an environment in which thermal conditions are maintained in a narrow band by heating and cooling systems.

Definition of thermal comfort and its characterization is a challenging problem because different individuals in the same environment may have differing perception of thermal comfort or lack of it. One of the widely quoted definitions of thermal comfort can be stated as: the condition of mind that expresses satisfaction with the thermal environment [1]. Many thermal comfort indices are based on statistical analysis of occupant's perception of thermal comfort. For instance if 95 percent of occupants find the environment to be comfortable, then it may be deemed that maintained thermal conditions are in the comfort zone.

Thermal comfort is a condition that results from complex interactions between the human body, surrounding air, the building envelope and thermal comfort equipment. Since maintaining thermal comfort requires energy consuming equipment, it is imperative that a balance be reached between the need to maintain an optimum level of

[1] The journal mode for this is the *AIAA Journal*

comfort and the associated energy cost. It has been reported that deviation of indoor conditions from thermal comfort zone can lead to discomfort as well as decline in productivity of workers [1]. For many years since the seventies, researchers in this field have investigated strategies for providing thermal comfort at reasonable energy cost. After the oil crisis in the 70's, and due to threat of diminishing of high quality fossil energy resources, new design strategy for building has led to tightening of building envelopes with increased building insulation, and reduced air infiltration. Although this has kept energy cost required to achieve thermal comfort in check, it has also raised the spectre of poor indoor air quality, and has led to many sick building episodes.

There has been a resurgence of studies in recent years dealing with the topic of thermal comfort in the indoor environment [2-5]. Many of these studies have investigated factors that govern thermal comfort as experienced by building occupants. These factors can be lumped into two categories. The first category involves ambient or environmental variables including air temperature, humidity, velocity, turbulence intensity and mean radiant temperature. The second category includes life style factors such as physical activity level and clothing. Physical activity level of occupants also affects thermal comfort due to metabolic heat generation. Clothing has a direct impact on thermal comfort. The insulation and porosity properties of clothing material affect the heat and vapor exchange between the human body and its surroundings, thereby altering the comfort level experienced by persons in a conditioned space. It is important to emphasize that the collective effect of these factors eventually governs the human thermal comfort in an indoor environment.

Instead of analyzing all factors governing thermal comfort simultaneously, the approach of previous researchers has been to consider some of the parameters, and combine them into comfort indices. Working on those lines, several past studies have developed empirical comfort indices by combining two or more of the variables into a single index [6]. For example, the effective draft temperature (EDT) index combines dry bulb temperature and room air velocity to characterize the effect of air draft on human thermal comfort. The effective temperature (ET) index combines the effects of temperature and humidity. Another thermal comfort index namely percent person dissatisfied (PPD) combines the effects of air temperature, velocity and turbulence intensity on human thermal comfort. However, it should be stated that there is no single index that is capable of taking into account all seven factors listed earlier.

It is well known that variables such as air velocity, humidity, temperature and turbulence intensity can vary with location inside a conditioned space. As a result the perception of comfort also changes as an occupant moves from one location to another. For instance, a person sitting or standing under an air-conditioning supply vent is likely to have a sensation of cold as compared to a person, situated away from the supply vent, who may be quite comfortable with maintained conditions. This spatial variation of variables governing thermal comfort exists in most indoor environment and it must be taken into account to ensure that a vast majority of occupants experience thermal comfort. In the past, the HVAC engineers have assumed uniformity of variables affecting thermal comfort to arrive at design values for operating conditions that must be maintained in the room. Recent advances in prediction of indoor airflow patterns using computational fluid dynamics (CFD) codes has made it possible to determine the spatial

variation of temperature, humidity, velocity and turbulence intensity in an indoor environment. The present study employs a computational fluid dynamics code to map regions of thermal comfort, using two different thermal comfort indices, namely EDT and percent mean vote (PMV). These indices are described in Chap. 2.

1.2 Review of Literature

Numerous mathematical models for airflow in conditioned spaces as well as heat and moisture flow from human body have been developed. Most of these studies have dealt either with the indoor flow modeling itself, or with heat and mass transfer from the human body. As a result of this dichotomy, in this literature review, these two kinds of mathematical models will be discussed separately.

1.2.1 Room Airflow Models

Airflow modeling in conditioned spaces has progressed significantly within the past thirty years. Many researchers have made contributions to the controlled room airflow modeling, by applying a variety of turbulence models in conjunction with computational fluid dynamics modeling. The following review will summarize the room airflow research using computational fluid dynamics (CFD) modeling.

Nielsen [7] made pioneering contributions by implementing CFD and 2-D turbulence modeling to predict air movement and heat transfer in buildings. He used the standard k-ε turbulence model to simulate air movement in a room, and he demonstrated through comparison with experimental values the fact that room airflow model predictions were sufficient for design purposes (Nielsen et al. [8]). However, the

computational modeling could not handle the flow through rooms with small inlets or relatively long rooms where flow instabilities may be expected. Gosman and Nielsen [9] also used a three-dimensional k-ε turbulence model to predict velocity, pressure, turbulent kinetic energy, and the dissipation rate distribution in a room. They used algebraic substitutions for differential equations to reduce computational time. Three-dimensional information about the flow patterns in rooms with small inlet regions incorporated wall jet assumptions at the inlet. This eliminated the need for a denser grid in that region. His prediction of the maximum velocity was accurate to within five percent of the experimental results.

Awbi has performed significant numerical research in the area of room ventilation system. He used the k-ε turbulence model to solve two-dimensional ventilation problems in wall jets and room ventilation systems [10]. To evaluate ceiling diffusers, velocity profiles and temperature distributions from the 2-D program were compared to measured values from an experimental room which was designed especially for evaluating the performance of ceiling diffusers. Good agreement between experimental and numerical results was found everywhere except near the floor. With the 3-D program, results were obtained for experiments with obstacles interrupting a wall jet. Awbi concluded that the obstacles enhance jet diffusion. In some instances it was shown that the jet reattached to boundaries. However as the height of the obstacle was increased the attachment was less frequent.

The CFD techniques were shown to be a useful tool for practical applications by Awolesi, Awbi, Seymour and Hiley [11]. They studied ventilation and contamination problems in an industrial workshop by conducting measurements and performing

computational analysis of air movement. In addition to industrial workshops, numerical simulations were performed of air movement in offices, classrooms and clean rooms. Awbi [12] noted that more work was needed before CFD programs could be used as design tools. He also stated that considerable progress was still needed to improve computational modeling in terms of grid coverage, stability of algorithms and boundary conditions.

In 1990, Chen and Kooi [13] applied the k-ε model to study cavity flow. Most of their work dealt with the prediction of velocity and temperature distributions in an enclosure with natural convection flow. They concluded that in order to simulate indoor air movement near a wall, a low Reynolds number k-ε model needs to be used to produce more accurate velocity profiles. They also found that more realistic convective heat transfer results are obtained in the wall regions of the room when one uses the low Reynolds number turbulence model. Chen and Kooi validated the low Reynolds number turbulence model through comparison with experimental cavity flow data and showed that the high Reynolds number turbulence model with wall functions were inaccurate in predicting the near-wall velocity profile. Because the distance from the wall to the first grid point in most room simulations is greater than the thickness of the boundary layer, Chen and Kooi claimed that the high Reynolds number k-ε model is not suitable for heat transfer analysis in room airflow applications. This is because the convective heat transfer coefficients from the high Reynolds number model are inaccurate. The high Reynolds number turbulence model uses experimental approximations and does not determine the wall heat transfer in the inner layer of the boundary layer which makes it impossible to compute heat loss or gain through the boundaries.

Chen and Jiang [14] have found that with simple thermal and flow boundary conditions, the standard k-ε model may correctly predict room airflow. They also pointed out that standard k-ε models use semi-empirical wall function formulas when predicting the heat transfer on a solid surface. But for room airflow, the wall function method is not suitable. The low-Reynolds number k-ε models alterative is also difficult to use because large number of grid points are required in the near-wall region [15]. Thermal comfort and indoor air quality were analyzed with a low Reynolds number k-ε model while varying the location and type of diffuser [16]. This study showed that both the diffuser type and location have an impact on thermal comfort and indoor air quality. From these studies it is evident that air quality and thermal comfort can be better analyzed and improved if computational airflow simulations become more accurate and dependable.

Murakami et al. investigated computationally many aspects of room airflow. Three-dimensional simulations of ventilated rooms were performed [17] showing "fairly good agreement" between computational and empirical results. According to Murakami, one of the most appropriate uses of the k-ε model is modeling of airflow in clean rooms where turbulence is high. Murakami et al. used the wall function method in their analysis. Dimensionless physical quantities were obtained which agreed well with experimental values. Murakami et al. concluded that the k-ε model could appropriately be used to model airflow in clean rooms. They also pointed out that the computational results compared well with empirical mean velocity data.

In 1989, Murakami and Kato analyzed different turbulence models and showed how they are affected by variations in the inlet and outlet geometries [18]. The geometry of the inlet openings and the location, size and number of outlets were varied. Techniques

for modeling the boundary conditions at the wall from the log-law and the power law were, outlined, and implemented. Three types of log-law techniques and a power law type boundary condition were studied and produced similar results. According to their study the power law type of boundary condition is preferred because of simplicity.

Murakami and Kato [19] used the k-ε model to predict three-dimensional turbulent recirculating flows in ventilated rooms. Addressing problems associated with the k-ε model, Murakami and Kato suggested using advanced turbulence modeling to handle the effect of buoyancy and boundary fitted coordinates to simulate complicated room geometries. They used generalized curvilinear coordinates for complex geometries since a normal, rectangular Cartesian grid did not sufficiently match the boundaries. Their grid system fits a curve to the boundary and alters the distance between nodes. The grid can then be transformed from generalized curvilinear coordinates to a rectangular grid.

1.2.2 Human Thermal Mathematical Models

Many past studies have dealt with human body models from the thermo-regulation perspective. In these studies, mathematical models for the human body based on thermodynamic and transport processes have been developed for the prediction of thermal behavior of either the entire human body or a part of it.

In 1911, Lefevre [20] made a first known human model for entire body. This model presented the body as sphere with a core to predict the heat transfer from the body to the environment. Givoni and Goldman [21] presented an empirical model to predict the thermal responses for the entire human body. Their model was based on experimental

data that was obtained from a real human subjected to the experiment, and the data from experiments were converted to best fit curves to determine the thermal response of the human body. Although this model was a well known thermal model for human body at the time it was proposed, it has very limited application due to its one-node thermal model and due to the fact that model was developed for hot environments only.

Machle and Hatch [22] developed an unsteady state model using heat balance for the entire human body. Their model was the first attempt to use a two-node thermal model for the entire human body which deals with the human body as two concentric shells. This model could not give a detailed approach to calculate the skin temperature distribution for different surrounding environments. In 1971, Gagge et al. [23] developed the well-known two-node human thermal model. This model represents a more realistic approach to the entire human body. Since its introduction, the model has been widely used for many applications because of its simplicity. This model is a modification of the Machle and Hatch model, but instead of using a one heat balance equation as Machle and Hatch did, Gagge used two energy balance equations, one for the skin node and another for the core node. Later in 1986 [24], Gagge et al. modified his model, to predict, besides the energy transfer to and from the human body, the thermal control functions such as the blood flow rate, the sweat rate, the metabolic rate and the skin mass fraction, all of which are treated as functions of skin and core temperatures.

Jones and Ogawa [25] presented in 1992 a segmented two-node model. This model was based on Gagge model, but with more than two-nodes for the entire human body (multi-node thermal model). In this model the core was considered as in previous models as single node, but the skin node is divided into an arbitrary number of segments.

Each segment constitutes a specified fraction of the total surface area. Because of limitations of the two-node models, restricting the applications for different environments to which the human body is subjected, Jones and Ogawa developed this model by applying the energy balance equation to each body segment to have more detailed results that provided spatial variation of temperature of the body.

Smith [26] developed a three-dimensional, transient, thermal model for the human body. This model divided the human body into four parts: the body tissue, the circulatory system, the respiratory system, and the thermal control system. Each body part is connected to other by the central and superficial vessels, and all of the body parts are assumed to have a similar vascular network. The main work that Smith did in this model is the human circulatory system in which the system was modeled as a right-angle-intersecting network of circular blood vessels that circulate blood through the body. Smith used this model to predict the nude human thermal response under uniform and nonuniform environmental conditions for sedentary human. Smith ignored in this model the effect of the moisture accumulation on the skin surface, which meant that all sweat was assumed to immediately evaporate away from the skin surface.

Murakamai et al. [27] presented a three-dimensional thermal model to predict the heat release from the human body. A human thermo-physiological model was developed to calculate the sensible and latent heat transfer from the human body. Flow, temperature and moisture fields were investigated with three-dimensional CFD. In this model Murakamai et al. used generalized curvilinear coordinate system to represent the complicated shape of the human body. This model adopted Gagge's two-node model to

simulate the metabolic heat production and the thermoregulatory control processes of the human body.

Alfahaid has developed [28] a three-dimensional multi-element human model, to predict the flow and temperature patterns, and investigate the thermal comfort conditions, for indoor environments using displacement ventilation. This model was used for two cases namely the unoccupied and occupied rooms. In the occupied rooms, a standing person and a person sitting on a chair, has been analyzed.

1.3 Objectives

The principal goal of this study is to develop a mathematical model for predicting human thermo-regulatory responses, and the associated thermal comfort sensation, for different environmental and metabolic heat generation conditions. A two-node model for predicting heat and mass exchanges between a human body and its environment is developed and coupled to a CFD code for predicting the temperature, humidity and velocity distributions around the body. The zones of thermal comfort are predicted by employing two different types of thermal comfort indices. In order to predict air movement in the room and around the body, a RNG k-ε model has been adopted as the main turbulence model for the simulation.

Several previous studies have dealt with the indoor airflow to investigate thermal comfort (sensation) of the human. The present study, using computational techniques, predicts the physiological thermal comfort of the human body positioned in an indoor environment. The first step in achieving the objectives of this study is to develop a 3-D

model of human body which realistically takes into accounts the shape and size of different organs. The problem addressed here is a coupled problem because the metabolic heat production in the body can have an influence on the microclimate around the body. Also, the local properties of the microclimate around the body can affect the local heat and mass transfer characteristics of the body. The two combined numerical codes, one for predicting the body temperature and another for heat transfer from the body have been implemented to characterize the thermal environment around a human body. Both are coupled at the body surface through surface temperature as well as heat and mass balance equations.

The first code, developed during this study, calculates the internal heat transfer inside the human body, based on the human thermo-physiological model. The second code, a commercial CFD code, predicts heat and mass transfer from the body surface to the surrounding environment by means of a coupled simulation of airflow, convection, radiation and moisture transport.

Also, a segmented body model has been proposed to characterize the spatial variations of the body skin temperature. This model takes into consideration more details and accurate variation of the body properties.

1.4 Outline of the Dissertation

In Chap. 2, an introduction to human thermal comfort is presented. This chapter gives a detailed account of heat balance equation formulation, which forms the basis for the present work. Various types of thermal comfort indices are introduced and discussed. In Chap. 3, a detailed mathematical model is provided that gives a full description of

mathematical equations and numerical techniques used in this work. First, an introduction of the CFD simulations in the area of the human thermal models is presented. Following it, a set of governing equations of the current model is given. Finally, the turbulence model used for simulating the indoor airflow is discussed, and a comparison of different available grid technique is presented. The solution procedure of the current model is discussed in Chap. 4. First, an algorithm describing solution procedure is provided. A detailed discussion of the human body shape modeling is presented, and the required boundary conditions for the present work are covered. Finally, the results obtained from the CFD code are validated by comparing them with results in the literature. In Chap 5, the simulation results for different cases are discussed. Effects of supply air temperature, velocity, relative humidity, turbulence intensity, and metabolic heat generation rate are analyzed. Different thermal comfort indices are employed to predict zones of comfort and discomfort. Chapter 6 presents conclusions and recommendations for future work.

CHAPTER II

THERMAL COMFORT

2.1 Introduction

Thermal comfort is attained when there is a balance between the generation of metabolic heat within the body and the loss of heat from the body via the mechanisms of conduction, convection, radiation and evaporation. In this thermally balanced state, a person will feel neither too hot nor too cold. Since different people have a different sense of warmth or cold, there will always be some people who feel uncomfortable in an environment where others are comfortable. However, it should be pointed out that generally people respond in similar way to different environmental conditions, and as a result, as temperature moves away from a neutral balance point, a greater number of people will feel increasingly uncomfortable.

The heat generated in the body by metabolism depends primarily on the activity being undertaken. The greater the physical exertion, the greater will be the metabolic heat generated within the body. The amount of heat actually transferred by the different mechanisms of heat transfer will be influenced by a number of factors. These may be behavioral factors such as: activity level, and clothing insulation or environmental factors such as: air velocity, humidity, air temperature, and mean radiant temperature (see Fig.

2.1). The multiciplicity of factors governing human thermal comfort makes analysis of this phenomenon quit complex.

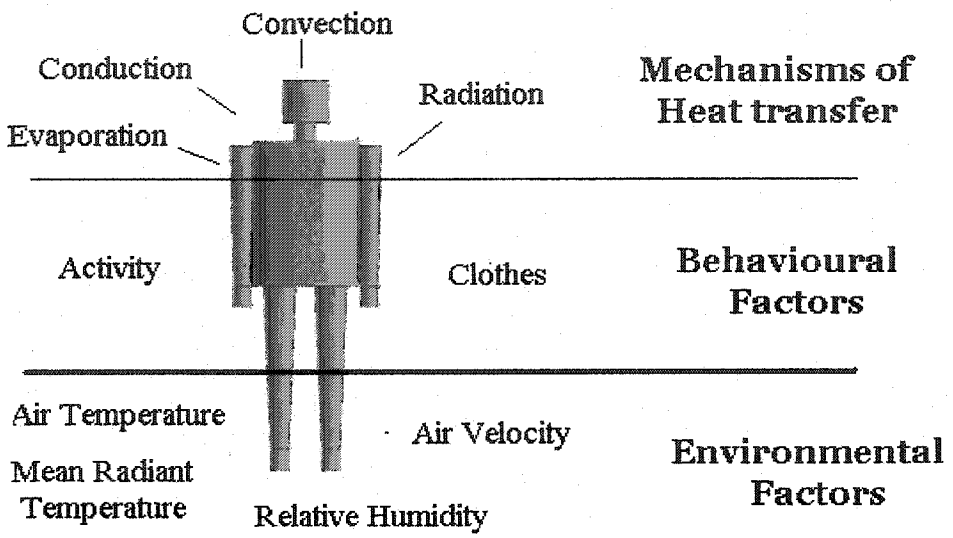

Figure 2.1 The human body interactions with surrounding

It is also not possible to include all factors simultaneously since it would make the analysis intractable. This fact is reflected in the literature in which researchers have tended to include only few of these factors to assess their impact on thermal comfort. Of all these factors, perhaps clothing is the most difficult one to incorporate in the statistical analysis of thermal comfort since people can choose to wear different types of clothing to adjust their garments depending on ambient conditions. Also, clothing adds several layers of analysis that must account for insulation (heat transfer), and porosity (mass transfer) nature of the clothing.

In different climates the body uses different mechanisms of heat transfer and the building needs to facilitate the mechanism most appropriate to the ambient conditions. In hot tropical climates human body principally uses evaporation to keep cool. When the air is also humid, then evaporation is reduced and therefore it is important that there is air movement in order to promote evaporation and provide cooling. Minimizing exposure to gain energy directly from the sun will also lessen the need for cooling. In cold dry climates the direct gain from the sun may be able to offset the high convective and radiative losses to cold surroundings.

The factors determining thermal comfort of human body in most climates are described in the following paragraphs.

2.1.1 The Dry Bulb Temperature

Dry bulb temperature has significant influence on thermal comfort. Basically, the dry bulb temperature is the ambient air temperature. It is difficult to specify a single temperature as the best temperature for thermal comfort. If the occupants of a room are sedentary or mostly seated then they will not generate as much body heat compared to those who are working very strenuously. Therefore the design room temperature will most likely vary with activity. Also clothing has to be considered. In winter time room occupants may wear heavier clothes than in the summer and some accommodation of the seasons may be necessary in deciding room conditions. ASHRAE standard [1] suggests that the optimal dry bulb temperature be in 20 ^{o}C and 26 ^{o}C temperature range.

2.1.2 The Air Velocity

Air velocity has significant influence on thermal comfort. In order to keep the same thermal sensation if the temperature is increased, the air velocity also has to be increased. Large air movements in rooms can cause discomfort especially if the air is cold in winter time. Cooler air tends to travel at floor level and can cause discomfort at the lower extremity of the body. Very low levels of air movement can also cause a feeling of discomfort and stuffiness in a room especially if the ceiling height is low and the dry bulb temperature is too high. Air velocities between 0.10 m/s and 0.45 m/s are generally acceptable [1], but this depends on conditions such as dry bulb temperature, humidity and clothing.

2.1.3 The Relative Humidity

Optimum value of relative humidity is important for both comfort and health issues. It has been found by Arundel and Sterling [29], that an increase in relative humidity enhances mildew growth, and low relative humidity results in respiratory problems due to dryness The bacterial population typically increases below 30% and above 60% of relative humidity. Relative humidity below 40% may cause respiratory infections [30]. Conversely, low relative humidity produces ozone which irritates the mucous membrane and eyes. Wright [31] discovered that bacteria e.g. mycoplasma laidlawii prefer relative humidity above 75% or below 25%. The optimal relative humidity range should be from 40% to 60%. This range of relative humidity is included in the recommendations of ASHRAE Standard [1].

2.1.4 The Activity Level

Activity level has a significant effect on thermal comfort. Metabolic rate measurements can be performed to measure heat generated by a body for different activity levels. Metabolic rate increases in proportion to exercise intensity. By ASHRAE definition [1], the metabolic rate is the rate at which energy is produced by the body and is expressed in met units. One met is defined as 58.2 W/m^2 (the energy produced per unit surface area of a seated person). During the elevated activity, a higher heat loss to the surrounding is required for thermal balance. If humidity is high, the heat dissipation ability of the body is reduced and the sweat rate increases. This results in wet skin, which may persist after the activity rate has subsided and the skin cooled off. Discomfort can result from increased skin temperature during the intermittent exercise or residual wet skin after the exercise.

2.1.5 Mean Radiant Temperature

Radiant temperature is the mean temperature of individual exposed surfaces in the environment. If radiant heating is used in a room then there will be an exchange of radiant energy from the heater to the room surfaces and occupants. It is possible to feel uncomfortable in a room with radiant heating, particularly if overhead heating panels emit radiant heat downwards onto the head. Similarly it is possible to feel uncomfortable if a room surface is cold and the body radiates heat to that surface. This can happen when people occupy an unheated building and the walls and other surfaces are cold. Even when the central heating system has been on for a while the air temperature may be satisfactory but the surfaces are still at a temperature much less than the air temperature, thus causing an excessive radiant heat exchange from body to surfaces.

According to ASHRAE standard [1] the dry bulb temperature should not exceed the mean radiant temperature of the surroundings in summer. In winter the dry bulb temperature should be less than the mean radiant temperature. This means that in winter the mean radiant temperature should be higher than the dry-bulb. In practice this is difficult to achieve since external walls and windows are at a lower temperature than the air inside a room unless radiant panels are attached to walls.

2.1.6 Turbulence Intensity Level

The turbulence intensity, I, is defined as the ratio of the root-mean-square of the velocity fluctuations, u', to the mean flow velocity, u_{avg} [6]. Turbulence intensity of 1% or less is generally considered low and turbulence intensities greater than 10% are considered high. For the indoor airflow, most studies chose the turbulence intensity level around 5% [32].

2.2 Heat Balance Equation

The heat transfer between the human and its surrounding environment can be formulated based on the activity level. The heat generation by a human can either stay in the human body causing the body's temperature to increase, or it can be transferred to the surroundings through either the skin or the respiration process. Several modes of heat transfer are involved in transport of heat released from the body to the environment and from the environment to the body, to keep the body temperature in a narrow range: the sensible heat loss from the skin, and the latent heat loss from the evaporation of sweat, and the evaporation of moisture during the respiration (Figure 2.1).

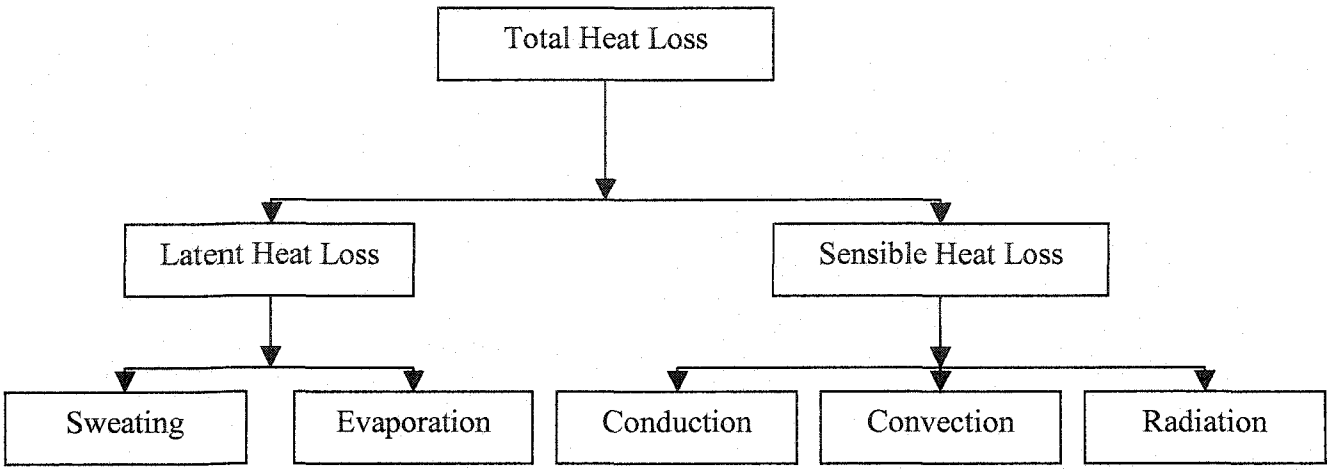

Figure 2.2 The total heat production from the human body

The body energy balance of these different modes including the external work can be expressed as [6]:

$$M - W = Q_{sk} + Q_{res} + S \tag{2.1}$$

This equation states that heat generation of the body is equal to the heat loss when the body is in thermal equilibrium with the surrounding environment. The heat generation is the internal heat production, which is the difference between the metabolic rate (M) and

the mechanical work (W). The symbol S represents energy storage while symbols Q_{sk} and Q_{res} represent heat transfer from skin and heat transfer through respiration.

The heat loss through the respiratory system can be expressed as:

$$Q_{res} = C_{res} + E_{res} + E_{sw} \tag{2.2}$$

This equation states that the heat released due the body's respiration is equal to both convective and evaporative heat loss from the respiration of the body (C_{res} & E_{res}), and the heat loss by evaporation of sweat secretion (E_{sw}). Fanger [2] developed a mathematical model to approximate these heat loss terms due the respiratory system as:

$$C_{res} = 0.0014M(34 - T_a) \tag{2.2a}$$

$$E_{res} = 0.0173M(5.87 - P_a) \tag{2.2b}$$

$$E_{sw} = 0.42[(M - W) - 58.15] \tag{2.2c}$$

The heat loss through the skin can be expressed as :

$$Q_{sk} = C + R + E_{sk} \tag{2.3}$$

Equation (2.3) states that the heat released from the body's skin is equal to the sensible heat loss from the skin that combines both convective (C) and radiative (R) heat loss, and evaporative heat loss from the skin (E_{sk}). The heat loss by convection from the human body can be expressed by the following equation:

$$C = f_c\, h_c\, (T_{cl} - T_a) \tag{2.3a}$$

where f_c is the clothing area factor which depends on garment insulation values, t_{cl} is the mean temperature of the clothed body (for this study it is assumed to be equal to the skin temperature of the nude body), and h_c is the convective heat transfer coefficient in (Kcal/m^2 hr $^\circ$C). The magnitude of h_c depending on the type of convection process. A formula developed by Seppenan [33] to estimate the h_c for the standing person in moving air is:

$$h_c = 14.8\ V^{0.69} \qquad 0.15 < V < 1.5$$

$$h_c = 4.0 \qquad 0 < V < 0.15$$

The heat loss by radiation from the human body can be expressed by the Setefan-Boltzmann's law [1]:

$$R = \varepsilon \sigma [(T_{cl} + 273)^4 - (T_r + 273)^4] \qquad (2.3b)$$

where ε is the emittance of the skin body, σ is the Setefan-Boltzmann constant: 3.96 x 10^{-8} in (Kcal/m^2 hr$^\circ$ K^4), and t_r is the mean radiant temperature in $^\circ$C.

The heat loss by evaporation from the skin can be expressed as [6]:

$$E_{sk} = w\ \alpha_e\ (P_{sk,s} - P_a) \qquad (2.3c)$$

where w is the wet skin fraction which is the ratio of the actual evaporation heat loss to the maximum possible evaporation heat loss, α_e is the evaporative heat transfer

coefficient in (W/m2 k Pa), $P_{sk,s}$ is the saturated water vapor pressure at t_{sk} at skin surface Pa, and P_a is the water vapor pressure in ambient air in Pa.

The heat stored in the body can be expressed as :

$$S = S_{sk} + S_{cr} \tag{2.4}$$

where S_{sk} is the heat storage in skin compartment of the body in (W/m^2), and S_{cr} is the heat storage in core compartment of the body in (W/m^2). In steady state the storage term is zero.

2.3 Thermal comfort Indices

There are several thermal comfort indices that can be used to predict comfort levels. These indices describe specific zones that can be the best for human body comfort, and have been proposed to simplify the description of the thermal environment and the stress imposed by it. The thermal comfort indices comprise two or more of the environmental factors. The thermal comfort indices which will be used in this study, include among others effective draft temperature (EDT), predicted mean vote (PMV), and percentage of dissatisfaction (PD).

2.3.1 Effective Draft Temperature (EDT)

EDT index combines dry bulb air temperature and air velocity. It is the simplest

of a variety of thermal indices available and it captures the first order effect of air temperature and air velocity. It takes into accounts effects on human thermal comfort arising from air temperature and air velocity variation in the room.

The EDT index, first proposed by Rydberg and Norback [34], and later modified by Koestel and Tuve [35], combines temperature and air velocity. The effective draft temperature values between –1.7 and 1.1 characterize thermal comfort. Values less than –1.7 represent cool sensation while values above 1.1 represent warm sensation. This expression for EDT is given by :

$$EDT = (T_x - T_{ave.}) - 8\,(V_X - 0.15) \qquad (2.7)$$

where T_x is the local air temperature in °C, $T_{ave.}$ is the mean room temperature in °C, and V_x is the local air speed in m/s.

2.3.2 Predicted Mean Vote

The predicted mean vote PMV is a seven-point scale that describes occupant thermal comfort as a function of occupant activity level and occupant thermal load, and was set by Fanger[2]. The PMV varies from a low of –3 and a high of +3. Negative values suggest that the occupant feels cold; positive values suggest that the occupant feels warm, and a value of 0 suggests that the occupant feels comfortable. Table 2.1 shows the relationship between the thermal sensation scale and the PMV values. The PMV is expressed as [6]:

$$PMV = [0.303^{-0.036\,M} + 0.028]\,L \qquad (2.5)$$

where the parameter M is the occupant metabolic rate and L is the thermal load on the body.

Table 2.1 PMV Thermal Sensation Scale

Thermal sensation	Numerical range (PMV)
Hot	+2 to +3
Warm	+1 to +2
Slightly Warm	+0.5 to + 1
Comfort	-0.5 to +0.5
Slightly Cool	-1 to -0.5
Cool	-2 to -1
Cold	-3 to -2

2.3.3 Percentage of People Dissatisfied (PPD)

The PPD is the percentage of people dissatisfied with thermal comfort at a specific PMV [1]. Fanger has also derived this index [2] that reduces to a sole function of the PMV. This index can be expressed as a function of PMV as given below:

$$PPD = 100 - 95^{[-(0.03353\,PMV^{\wedge}4 + 0.2179\,PMV^{\wedge}2)]} \qquad (2.6)$$

Figure 2.3 illustrates the functional relationship between the PMV and PPD [1]. This relation shows that even when the PMV is neutral (a value of 0), 5% of the occupants are still dissatisfied.

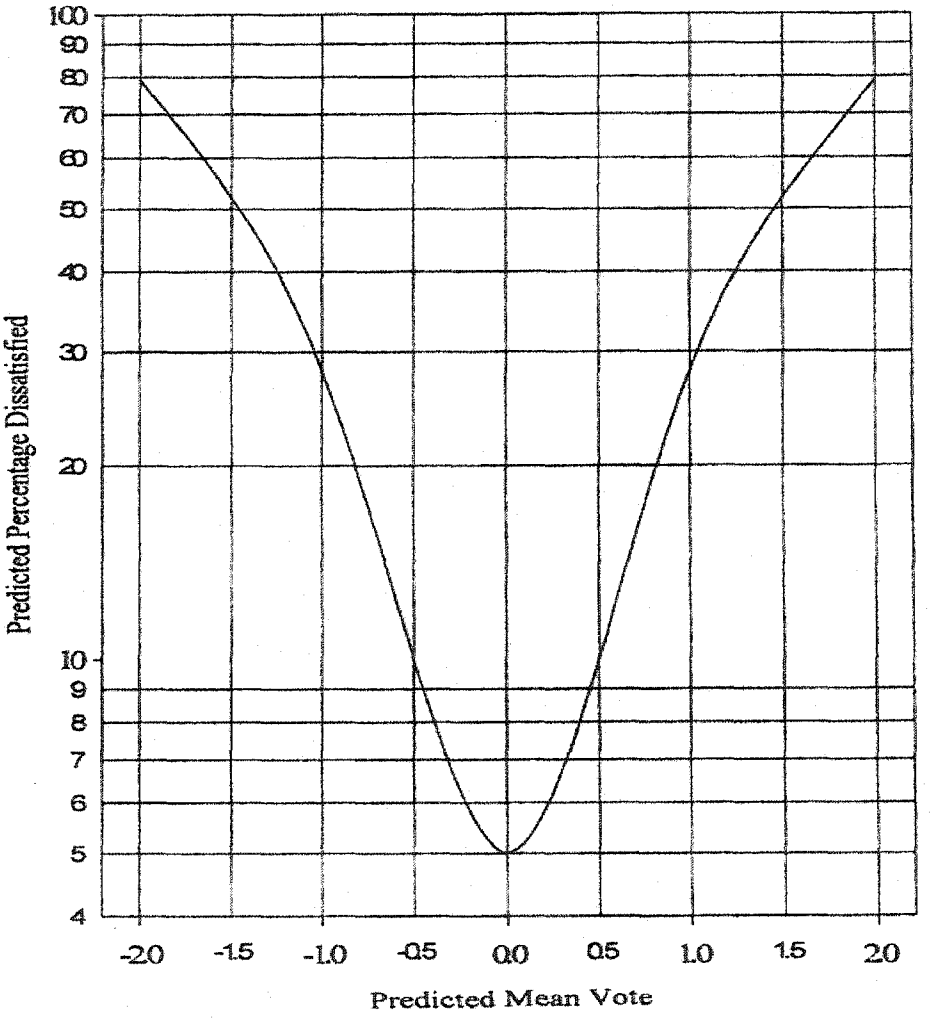

Figure 2.3 PPD as function of PMV

CHAPTER III

THE MATHEMATICAL MODEL

3.1 Computational Fluid Dynamics (CFD)

Computational fluid dynamics methodology aims to provide a numerical solution of the mathematical equations governing fluid motion and related physical processes. The description of fluid motion in rooms often requires treatment of heat and mass transfer phenomena due to sensible and evaporative heat transfer from human body to the surrounding room air. Due to the turbulent nature of air flow near vents as well as near the human body [36], it is also necessary to incorporate turbulence modeling in the mathematical analysis of room air flow. Computational fluid dynamics has become a very important tool for simulation of indoor airflow problems in recent years. The main advantage of using CFD over other tools for airflow simulation is its ability to simulate a wide range of configurations [5].

Computational fluid dynamics in its infancy was first deployed for simulation of indoor airflow patterns for simple geometries primarily due to the computer processing power limitation at that time. Subsequently more practical indoor airflow problems have been solved using CFD tools due to rapid advancement in computer software and hardware technologies. Currently CFD has matured to the extent that it has become possible to numerically investigate complex indoor climates with sufficient accuracy and acceptable CPU time. In order to establish CFD as a tool for indoor air flow simulations,

many efforts have been directed to improve the reliability of the CFD-techniques through precise comparison with accurate full-scale measurement results which take into account effects of multiple heat sources and obstacles in the indoor environment [16].

Though CFD has been successfully applied for airflow analysis for relatively complicated geometries, it is important to develop simple models and methods to simulate indoor airflow so that heating, ventilating and air-conditioning (HVAC) designers can finish computer predictions in short time to meet the engineering demand on a personal computer for design calculations. The main factors affecting the simulation speed are the method of describing inlet boundary conditions, turbulence model used, and the numerical method for solving the discretized equations [19]. In the following section, governing equations for room airflow will be introduced.

3.2 Governing Equations

The set of equations governing the fluid flow and heat and mass transfer in a human thermal comfort model are quite involved, and the appearance of specific terms in the equations depend on the case of interest due to different assumptions and possible simplifications.

In this study the flow is assumed to be three-dimensional, non-isothermal and turbulent. This leads to the following set of governing equations.

3.2.1 Continuity Equation

The mass conservation equation, also known as the continuity equation, is derived by balancing mass flow rate for a control volume in the fluid where the incoming mass

flow equals the outgoing mass flow plus any accumulation of mass inside the control volume. In the cartesian tensor notation the time averaged continuity equation is expressed as,

$$\frac{\partial \rho}{\partial t} + \frac{\partial}{\partial x_i}(\rho u_i) = 0 \tag{3.1}$$

where ρ is the density of the fluid, t is the time, and u_i is the mean velocity component in the i direction.

3.2.2 Momentum Equation

The time averaged momentum equations for turbulent flow are derived from Newton's second law of motion and can be expressed as [4]:

$$\frac{\partial}{\partial t}(\rho u_i) + \frac{\partial(\rho u_i u_j)}{\partial x_j} = \frac{\partial}{\partial x_j}\left(\mu_l\left(\frac{\partial u_i}{\partial x_j} + \frac{\partial u_j}{\partial x_i}\right) - \overline{\rho u_i' u_j'}\right) - \frac{\partial p}{\partial x_i} + B_i + S_u \tag{3.2}$$

where p is the pressure in Pa, μ_l is the laminar dynamic viscosity (kg/m s), B_i is the volume force in the i direction (N/m^3), and S_u is the source term (N/m^3). The term on the left side of the Eq. (3.2) is the net supply of momentum from the surroundings, also referred to as the convection term. The shear force or the diffusion term is the first term on the right side; the second term is pressure gradient term which represents the normal forces, and the last two terms represent both the buoyancy forces that act on the fluid and the source term respectively.

In the diffusion term, the quantity [$-\overline{\rho u_i' u_j'}$] is the Reynolds stresses. It represents the turbulent transport of fluid across the main flow direction and it influences the flow in the same way as the increased shear stress. The turbulent stresses are assumed to be proportional to the gradient of the mean velocity and turbulence is assumed to be isotropic [5].

$$-\overline{\rho u_i' u_j'} = \mu_t \left(\frac{\partial u_i}{\partial x_j} + \frac{\partial u_j}{\partial x_i} \right) - \frac{2}{3} \rho k \delta_{ij} \tag{3.3}$$

where μ_t is the turbulent viscosity (kg/m s), k is the turbulent kinetic energy ($m^2/s^{2)}$, and δ_{ij} is the Kronecker delat (equals 1 for $i = j$ & equals 0 for $i \neq j$). In the real fluid flow an effective viscosity, μ_{eff} can be formed as sum of the laminar and the turbulent viscosity:

$$\mu_{eff} = \mu_l + \mu_t \tag{3.4}$$

The buoyancy term in the momentum equation, B_i ,can be obtained by using the Boussinesq approximation [5] as,

$$B_i = -\rho \beta g_i (T - T_o) \tag{3.5}$$

where β is the thermal expansion coefficient, g_i is the gravitational acceleration in the i direction (m/s^2), T is the mean temperature of the fluid (^oC), and T_o is Boussinesq operating temperature (^oC).

Inserting the above expressions for the Reynolds stresses and for the buoyancy

term in the momentum equation leads to:

$$\frac{\partial}{\partial t}(\rho u_i)+\frac{\partial(\rho u_i u_j)}{\partial x_j}=\frac{\partial}{\partial x_j}\left(\mu_{eff}\left(\frac{\partial u_i}{\partial x_j}+\frac{\partial u_j}{\partial x_i}\right)\right)-\frac{\partial p}{\partial x_i}-\frac{2}{3}\rho k\delta_{ij}-\rho\beta g_i(T-T_o)+S_u \qquad (3.6)$$

3.2.3 Energy Equation

The energy equation describes the temperature distribution throughout the non-isothermal flow domain. This equation is derived from the first law of thermodynamics to the an elemental central volume, and can be expressed as [4]:

$$\frac{\partial}{\partial t}(\rho c_p T)+\frac{\partial(\rho c_p u_j T)}{\partial x_j}=\frac{\partial}{\partial x_j}\left(\lambda_{eff}\frac{\partial T}{\partial x_j}\right)+S_t \qquad (3.7)$$

where c_p is the specific heat at constant pressure (J/kg°C), λ_{eff} is the effective conductivity (W/m°C), and S_t is the source term (W/m3). The effective conductivity can be expressed as,

$$\lambda_{eff} = \lambda_l + \lambda_t \qquad (3.8)$$

where λ_l is the laminar thermal conductivity, a thermodynamic property, and λ_t is the turbulent conductivity, which depends on the local flow field.

3.2.4 Mass Diffusion Equation

The convection–diffusion equation has been included in the governing equations in this study for indoor airflow model to take into account the distribution of water vapor mass fraction within environment surroundings the human body. The basic assumption

for this equation is that the moisture transport modeling considers the air as a mixture of dry air–vapor (two species models). Moreover, no chemical interaction exists between these two species and their mixture is assumed as an ideal gas [37]. As a result, the vapor represents a scalar transported by the airflow, but at the same time, the water vapor properties have an effect on the airflow-governing equations. The conservation of the vapor mass fraction m_i (defined as the ratio of the vapor mass contained in a given volume to the total mass of the mixture contained in the same volume) is expressed as [4]:

$$\frac{\partial}{\partial t}(\rho m_i)+\frac{\partial}{\partial x_i}(\rho u_i m_i)+\frac{\partial}{\partial x_i}J_i = S_c \tag{3.9}$$

where J_i is the mass flux of species or the diffusion flux in (kg/s m^2), and S_c is the source term in (kg of species / kg of air . s). In the previous equation, the second term on the left-hand side represents the convective term while the next one represents the diffusion flux. Taking into account the Fick's law of diffusion (diffusion due to concentration gradients by means of a diffusion coefficient D_i) and the additional mass diffusion caused by the turbulent flow (which introduces the turbulent Schmidt number Sc_t), the diffusion flux can be written as,

$$J_i = -\left(\rho D_i + \frac{\mu_t}{Sc_t}\right)\frac{\partial m_i}{\partial x_i} \tag{3.10}$$

3.2.5 General form of Equations

It is possible to write above equations in a more general form for facilitating the discretization and the solution of these equations. If the dependent variable ϕ, a diffusion coefficient Γ, and a source term S_ϕ are used as general variables the following form of the differential equations can be written as,

$$\frac{\partial}{\partial t}(\rho u_i)+\frac{\partial(\rho u_i \phi)}{\partial x_i}=\frac{\partial}{\partial x_i}\left(\Gamma_\phi \frac{\partial \phi}{\partial x_i}\right)+S_\phi \tag{3.11}$$

with different meaning of ϕ, Γ and S_ϕ for respective equations. The second term on the left side is the convection term, the first term on the right side is the diffusion term and the last term is the source term.

3.3 Turbulence Model

Several considerations influence the choice of turbulence model. The most important ones, which guide the selection for a good turbulence model, include the accuracy and the simplicity of the turbulence model. Another important criterion in this choice is related to the computational resources required in the application of the turbulence model. Finally, the amount of time available for the simulation is an important factor in these considerations.

In a relatively recent study, Chen [38] compared the performance of five different models for simulating simple indoor air flows and found that the standard and RNG k-ε predicted actual flows patterns best. The Re Normalization Group (RNG) model was

found to perform slightly better than the standard k-ε model. In the standard k-ε model, which is the simplest of all models of turbulence, there are two separate transport equations for the turbulent kinetic energy and length scales to be independently determined. The standard k-ε model has become a very useful tool of practical engineering flow calculations in the time since it was first proposed by Launder and Spalding [39]. The advantages of this model are: low computational cost, and reasonable accuracy for a wide range of turbulent flows, which explain its popularity in industrial flow and heat transfer simulations. In the RNG model, which is derived from the Navier-Stokes equations, using a mathematical technique called ``renormalization group" (RNG) methods, the constants are determined from theory. Standards values for these constants are suggested by Yakhot and Orzag [40].

Although the standard and RNG k-ε models are almost similar, there are some important differences or some improvements in the RNG model that the standard model does not have. These differences can cause the two models to produce markedly different results. The first difference or the improvement for the RNG model is that the standard k-e model is based on the assumption of high Reynolds number flow, while the RNG model is not. The RNG is equally valid for low and high Reynolds number flows [38]. This is an important capability for a model that will be used to simulate indoor airflows because they are generally wall-bounded, and thus have regions of low Reynolds number flow [35]. An additional benefit of this low Reynolds number extension is that the governing equations can be integrated through the turbulent boundary layer and into the viscous sub-layer adjacent to wall. This means that the wall–functions that are used in the

standard model are not necessary, so its applications for the complex indoor airflows may not be justified.

A second improvement for the RNG model is the addition of the rate of strain term in the RNG dissipation rate equation. This term varies in size, as well as in sign, and can have a significant influence on the turbulent viscosity, especially in regions of large-strain rate. It is this feature that allows the RNG model to partially account for the strong anisotropy in regions of large shear, thus enabling it to provide improved predictions of separated flows and anisotopic large-scale eddies [38]. The third improvement in the RNG model is the inclusion of the effect of swirl on turbulence, enhancing accuracy for swirling flows. Finally, the RNG theory provides an analytical formula for turbulent Prandtl numbers, while the standard k-ε model uses arbitrary specified constant values. These improvements and the benefits the RNG model have, make it as the attractive model for indoor airflow simulations. Therefore, the RNG k-ε model has been selected in this study as the main turbulence model for the simulation.

The turbulent viscosity μ_t for the RNG k-ε model is determined from the same equation as in the standard k-ε model:

$$\mu_t = \rho C_\mu \frac{k^2}{\varepsilon} \tag{3.12}$$

where ρ represents the density; k and ε correspond to the turbulence fields: turbulent kinetic energy and its rate of dissipation, respectively. The model coefficient C_μ is no

longer constant (usually 0.09) as in the standard model, but with use in the RNG theory, C_μ is equal 0.0845. The values for both k and ε are determined by using RNG k-ε model transport equations as [40] which can be expressed as,

$$\frac{\partial}{\partial t}(\rho k)+\frac{\partial}{\partial x_i}(\rho k u_i)=\frac{\partial}{\partial x_i}\left(\delta_k \mu_{eff}\frac{\partial k}{\partial x_i}\right)+G_k-\rho\varepsilon+S_k \tag{3.13}$$

and,

$$\frac{\partial}{\partial t}(\rho \varepsilon)+\frac{\partial}{\partial x_i}(\rho \varepsilon u_i)=\frac{\partial}{\partial x_i}\left(\delta_\varepsilon \mu_{eff}\frac{\partial \varepsilon}{\partial x_i}\right)+C_{1\varepsilon}\frac{\varepsilon}{k}(G_k)-C_{2\varepsilon}\rho\frac{\varepsilon^2}{k}-R_\varepsilon+S_\varepsilon \tag{3.14}$$

where G_k is the generation of turbulence kinetic energy due to the mean velocity gradients, the quantities α_k and α_ε are the inverse effective Prandtl numbers for k and ε, respectively, S_k and S_ε are source terms, and $C_{1\varepsilon}$ & $C_{2\varepsilon}$ the model constants. Using the RNG methodology [41], these four unknown coefficients are determined as,

$$C_{1\varepsilon}=1.42-\frac{\eta(1-\eta/\eta_\infty)}{1+\beta\eta^3} \quad ; \quad C_{2\varepsilon}=1.68 \tag{3.15a}$$

$$\delta_k=0.7179 \quad ; \quad \delta_\varepsilon=0.7179 \tag{3.15b}$$

where,

$$\eta=S_t\cdot k/\varepsilon \quad ; \quad \eta_\infty=4.38 \tag{3.15c}$$

$$\beta = 0.015 \qquad ; \qquad S_t = \left(2S_{ij}S_{ij}\right)^{1/2} \tag{3.15d}$$

where S_{ij} is the mean rate of strain.

3.4 Coupled Nature Of The Problem

The human thermal model used in the simulation is based on a set of partial differential and algebraic governing equations described earlier. These equations are solved numerically with appropriate initial and boundary conditions. The first part of the model enables calculation of heat transfer inside the human body based on the human thermo-physiological model which uses a set of algebraic thermal equations (2.1)-(2.3) that are solved numerically by a two-node model for human body (to be described in detailed in Chap. 4). In the second part of the simulation, which predicts the heat and mass transfer between the body surface and the surrounding environment, a finite volume method is used to solve the partial differential equations (3-1)-(3-14). Using this method, the calculation domain is divided into a finite number of control volumes and grid points, so that there is one volume surrounding each grid point.

The commercial CFD code "FLUENT" is implemented [42] for the indoor airflow problems. "FLUENT" can convert the partial differential governing equations into algebraic equations which can be solved numerically. An appropriate numerical scheme is used (segregation solver) to discretize the governing equations in the domain. Using this numerical scheme, "FLUENT" is employed to solve the governing equations for the conservation of mass, momentum, energy and other scalars of turbulence and

chemical species. A control-volume-based technique is used to perform the solution in three steps. The first step divides the domain into discrete control volumes by using a computational grid. The second step integrates the governing equations on the individual control volumes to construct algebraic equations for the discrete dependent variables of the velocities, pressure, temperature, and conserved scalars. The final step linearizes the discretized equations, so the solution of the resultant linear equation system can be yielded to update the values of the dependent variables.

The two widely used types of grid mesh or control volume for the numerical technique are the structured and the unstructured grids or hexahedral and tetrahedral control volumes.

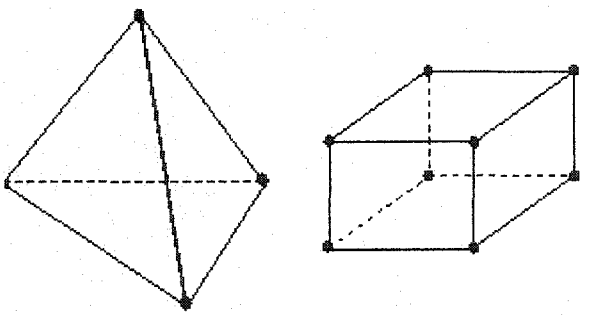

Figure 3.1 The types of grid mesh: a) Tetrahedral grid; b) Hexahedral grid

Both types have almost similar solution procedure. The discretization of computational domain in this study is achieved by means of an unstructured mesh. The grid contains tetrahedral elements obtained due to a mesh generation algorithm based on

the Delaunay criterion. This meshing technique is by far the most popular of the grid generation methods for doing the indoor air flow simulations for more than one reason [42]. First, the unstructured grid is ideally suited for the discretization of complicated geometrical domains that gives more details and descriptions for the grid. Secondly, the flow field in the domain is a complex one, therefore there is no advantage in using a hexahedral (structured) mesh since the flow is not aligned with the mesh. Finally, another advantage of the unstructured mesh is the simplicity of refining the grid based on geometric or numerical solution data. This property is very useful for the regions of the domain where strong flow gradients occur (boundary layers). The grid in these zones can be refined without adding unnecessary cells in the other parts of the domain as classically happens in the structured grid approach.

Solving the equations on an unstructured grid uses combined solution process consisting of both the Gauss-Seidel method with the multi grid method [42]. The purpose of using this combined of numerical scheme is to accelerate the convergence for the large number control volumes as in the current model. For this numerical scheme the second-order discretization is applied in order to obtain more accurate results and reduce the numerical discretization error.

The convergence criteria for the acceptable level of error are the normalized residual and the global conservation imbalance, which provides a way of establishing how well conservation has been maintained. In this study, if the normalized residual for all variables are below 1.0E-04 and the global conservations imbalances are less than 1%, the solution is assumed to have converged.

CHAPTER IV

SOLUTION PROCEDURE

4.1 Introduction

The mathematical model described in the preceding chapter forms a set of differential and algebraic governing equations for the human body system in an indoor environment. The purpose of this model is to create a tool for predicting human body comfort sensation by means of a CFD code and a two-node human body thermo-regulation model. The model permits simulation of flow phenomena observed close to a human body so that thermal comfort predictions can be made, taking into account factors that can influence human body thermoregulatory response. The main focus of this dissertation is the development of a coupled model that takes into account thermoregulatory heat generation and its dispersal by ambient air to predict zones of thermal comfort and discomfort.

In this chapter, first the two-node model for human thermo-regulation will be discussed, followed by description of the algorithm for the coupled human body room air model for prediction of thermal comfort indices. After this, the human body geometry modeling and boundary conditions for the CFD model will be discussed. The last section in this chapter will provide details of model validation that would also include check for grid independency.

4.2 The Two-Node Model for Human Thermo-Regulation

Prediction of zones of thermal comfort in an indoor environment requires an analysis of thermo-regulatory processes in human body and transport of metabolically generated heat and water vapor from the body to the surrounding air for their subsequent dispersal by air movement in the room. The processes are coupled, and require simultaneous solution of energy equation for the human body, as well as solution of heat, mass and momentum equations for the surrounding air. Solution of coupled equations yields body core and skin temperatures, convective and radiative heat fluxes from or to the body, air temperature, humidity, velocity and turbulence intensity. These variables are then used to calculate spatial variation of thermal comfort indices, and maps of region thermal comfort.

In the present study, the Gagge's two-node model has been used because of its ability to model sweating [3]. This two-node model, shown in Fig. 4.1, deals with whole-body heat balance rather than localized heat balance. All physical mechanisms for thermo-regulatory heat dispersal are shown in Fig. 4.1. The human skin and the body core (everything except skin) are designated as nodes 2 and 1. T_{sk} and T_{cr} designate body skin and core temperatures respectively. The core temperature is governed by metabolic heat generation, heat conduction, respiration and blood flow response to metabolic heat generation. The skin temperature is governed by radiation and convection of heat, evaporation of sweat and sensible heat arriving at skin through conduction in the core.

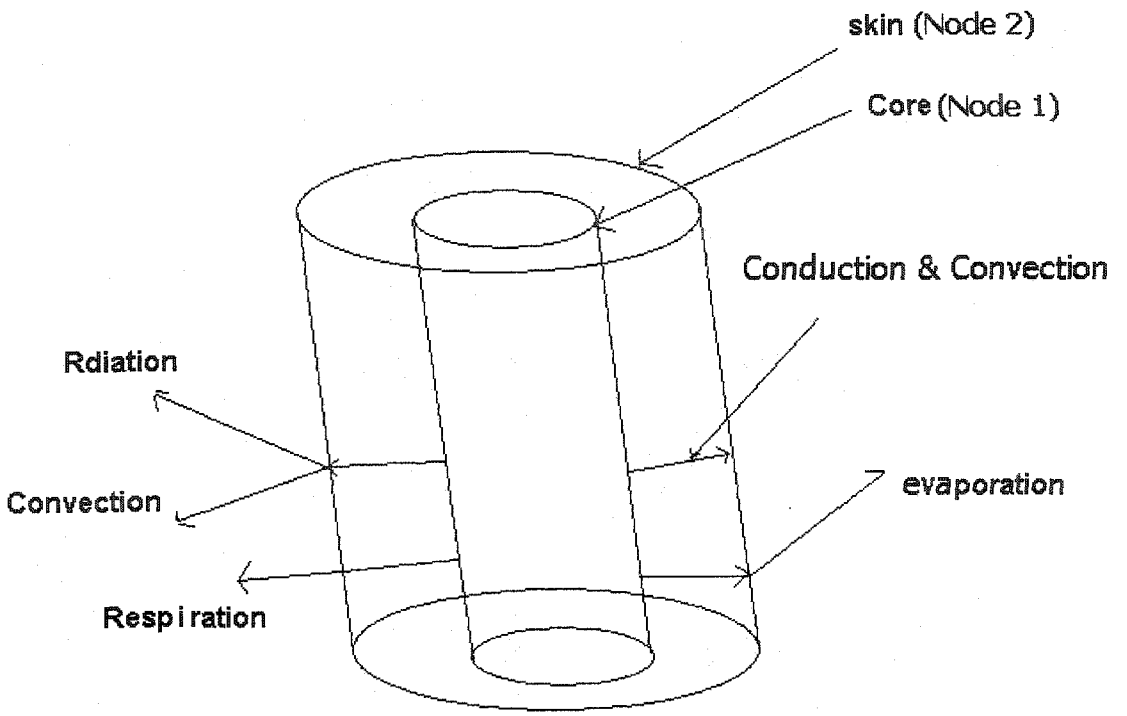

Figure 4.1 Two-Node body heat transfer model.

As stated earlier, in this model the body core (symbol cr) and the body skin (sk) are treated as two nodes for which governing equations for energy transport are formulated. These equations can be expressed as [6]:

$$S_{cr} = (M - Q_{res}) - K(T_{cr} - T_{sk}) - c_{p,,bl}\, m_{bl}(T_{cr} - T_{sk}) \qquad (4.1)$$

$$S_{sk} = K\,(T_{cr}-T_{sk}) + c_{p,,bl}\,m_{bl}\,(T_c-T_{sk}) \quad - E_{sk} - (Q_{cv}-Q_r) \tag{4.2}$$

where S_{cr} and S_{sk} are the sensible heat storage terms. In the current steady state model, these terms are zero. Q_{res} , the first term of Eq. (4.1), is the heat released due the body's respiration which can be found in Eq. (2.2). The second term represents the sensible heat transfer from the core to the skin, where K is effective conductance between the core node and the skin layer($W/(m^2\ K)$). The third term represents the heat transfer from the core to skin due to blood flow, where $c_{p,,bl}$ is specific heat of blood, 4.187 kJ/(kg K), m_{bl} is blood flow rate ($kg/(m^2 s)$) which can be expressed as,

$$m_{bl}=[(6.3+200\ WSIG_{cr})/(1+0.1\ CSIG_{sk})]/3600 \tag{4.3}$$

where $WSIG_{cr}$ and $CSIG_{sk}$ are the temperature signals for both core and skin nodes, which can be found as :

$$WSIG_{cr}=\max\ ((T_{cr} - T_{cr,n}),0) \tag{4.3a}$$

and,

$$CSIG_{sk}=\max\ ((T_{sk,n} - T_{sk}),0) \tag{4.3b}$$

where $T_{cr,n}$ is the thermal neutrality for body core, 36.8 ^{0}C. $T_{sk,n}$ is the thermal neutrality for body skin, 33.7 ^{0}C.

The last two terms in Eq. (4.2) include E_{sk} , the evaporative heat flux, Q_{cv} , the convective heat flux from the surface to the ambient, and Q_r , the radiation flux; which all can be found in Eq. (2.3).

4.3 The Algorithm of the Coupled Solution Procedure

As stated earlier, the primary objective of this study is to develop a combined numerical simulation methodology for determining the total (sensible+latent) heat transfer from of the human body, and to predict thermal comfort zone in the room for given vent conditions. The algorithm for the combined numerical analysis of human body and surrounding environment is illustrated in Fig. 4.2. The analysis is performed in two stages with the body skin surface being the interface between the body core and the surrounding air. In the first stage, the heat transfer inside the human body is calculated based on a human thermo-physiological model. A micro-climate (temperature and humidity) around the body is first guessed, and the two-node human body energy transport model is implemented to yield skin surface boundary conditions for sensible heat flux and water vapor concentration [6].

The second stage of the analysis involves prediction of heat and moisture transfer between the body surface and the surrounding environment by means of a coupled simulation of airflow, radiation and moisture transport. Using the computational fluid dynamics (CFD) code "FLUENT", the body skin temperature and humidity are calculated, and are used as an input to the two-node human body energy transport model. This process is continued until a converged solution is obtained.

The steps involved in the algorithm are summarized as follows:

Step 1: Input the metabolic heat production M. The value of M is based on the assumption of the activity of human body.

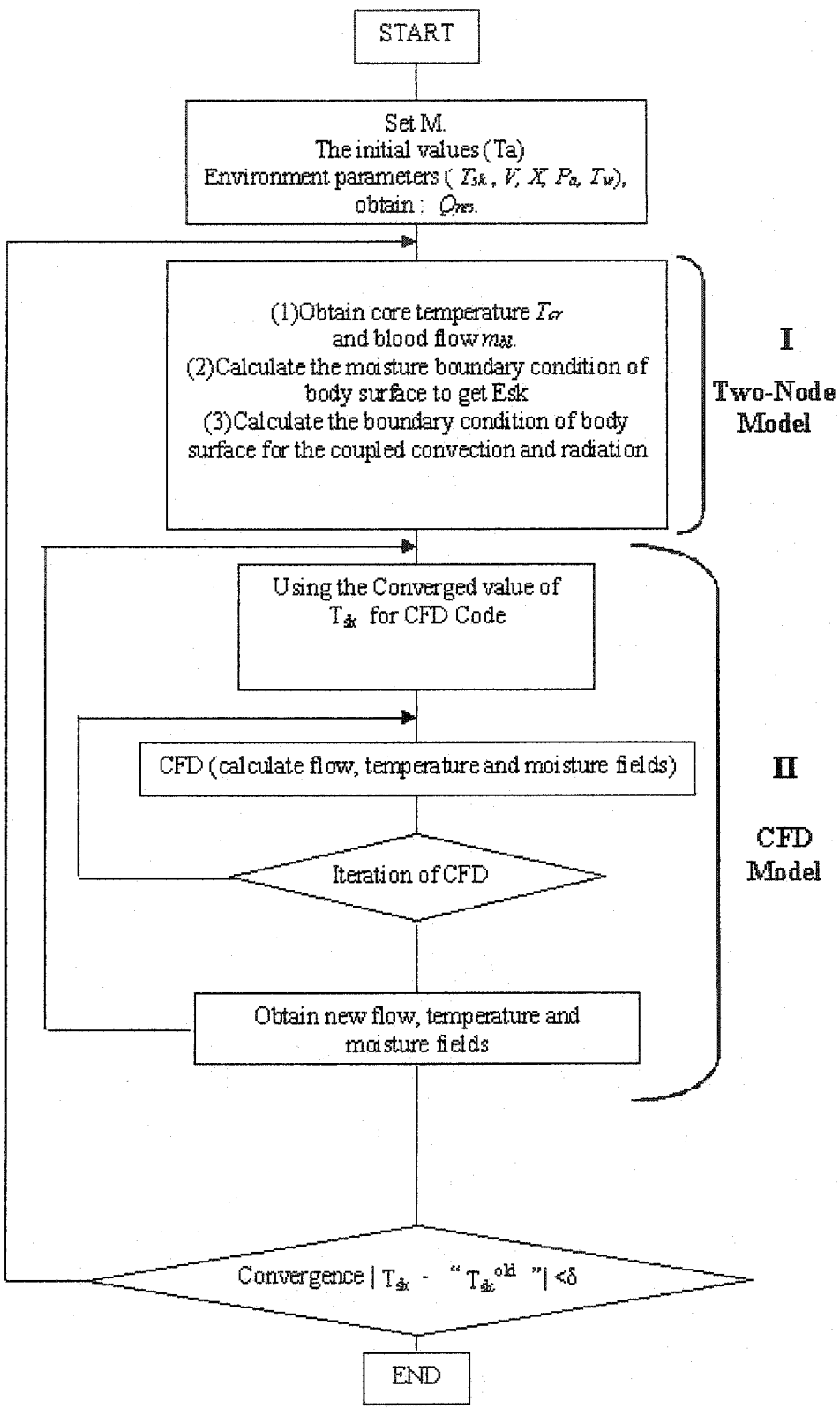

Figure 4.2 Flow chart of numerical methodology

Step 2: Assume the initial values (skin temperature T_{sk}, environment parameters (Ta, U, X, P_a and T_w).

Step 3: Obtain heat loss from respiration Q_{res}.

Step 4: Calculate the initial core temperature T_{cr} and the initial blood flow m_{bl} using the initial skin temperature T_{sk}.

Step 5: Calculate the moisture boundary condition of body surface to obtain the value of the evaporative heat E_{sk}.

Step 6: Obtain the boundary condition of body surface for the coupled convection and radiation heat loss from the skin.

Step 7: Using the converged value of skin temperature in the internal code as boundary condition of the CFD code.

Step 8: Calculate the flow, temperature and moisture fields in the CFD code.

Step 9: Solve for the thermal responses, such as temperature distribution, thermal load, etc. in the CFD code.

Step 10: Obtain new flow, temperature and moisture fields.

Step 11: New converged skin temperature T_{sk} is obtained, to be used in further solutions.

4.4 Model Geometry

The geometrical complexity of human body shape poses a modeling challenge. Also, the thermal properties and thermoregulatory variables change from one part of the body to another, making the analysis quite difficult, if not intractable. A growing number

of human body models have been proposed with the purpose of determining the human sensation and different thermal comfort indices for various indoor environments.

A review of literature dealing with human body geometric modeling indicates a variety of approaches have been used to develop a geometry model for human body. For instance, Dunnet [43] has used an elliptical cylinder to simulate a standing person. Niwa et al. [44] used rectangular box geometry to model a seated person. Davidson and Nielson [45] simulated the air flow in facial regions and nasal cavity by means of a two-dimensional isothermal simulation with detailed model of the human head. Heinsohn [46] has used unheated three-dimensional paralleled-pipe geometry to model a standing human body. Other researchers have used a three-dimensional, heated paralleled-pipe in rectangular geometry to model either a seated body [47] or a standing body [48-52]. Murakami et al. [53] and Kato et al. [54] have developed a model for human body in a generalized curvilinear geometry.

Most of above models have used a simplified body shape without modeling body parts such as legs and hands separately. Since the body geometry can affect heat and vapor transport processes, this study has developed a geometrical model for the human body that is more realistic compare to those developed by previous researchers. The three-dimensional model of a human body developed in this study is shown in Fig. 4.2. The body height, weight and surface areas are respectively 1.7 m, 70 kg and 1.82 m^2 for an average person, as recommended by ASHRAE [6]. In order to account for spatial variation of properties such as skin temperature, the human body is divided into nine eleven parts namely head, neck, two hands, two feet (cylindrical shape), two arms, two legs (cone shape), and the middle torso (elliptical shape).

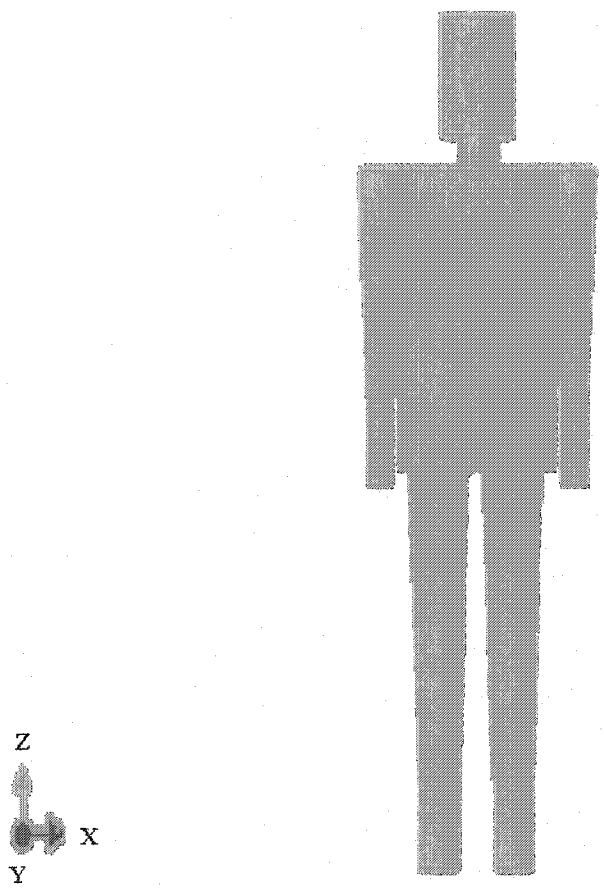

Figure 4.3 Human body model

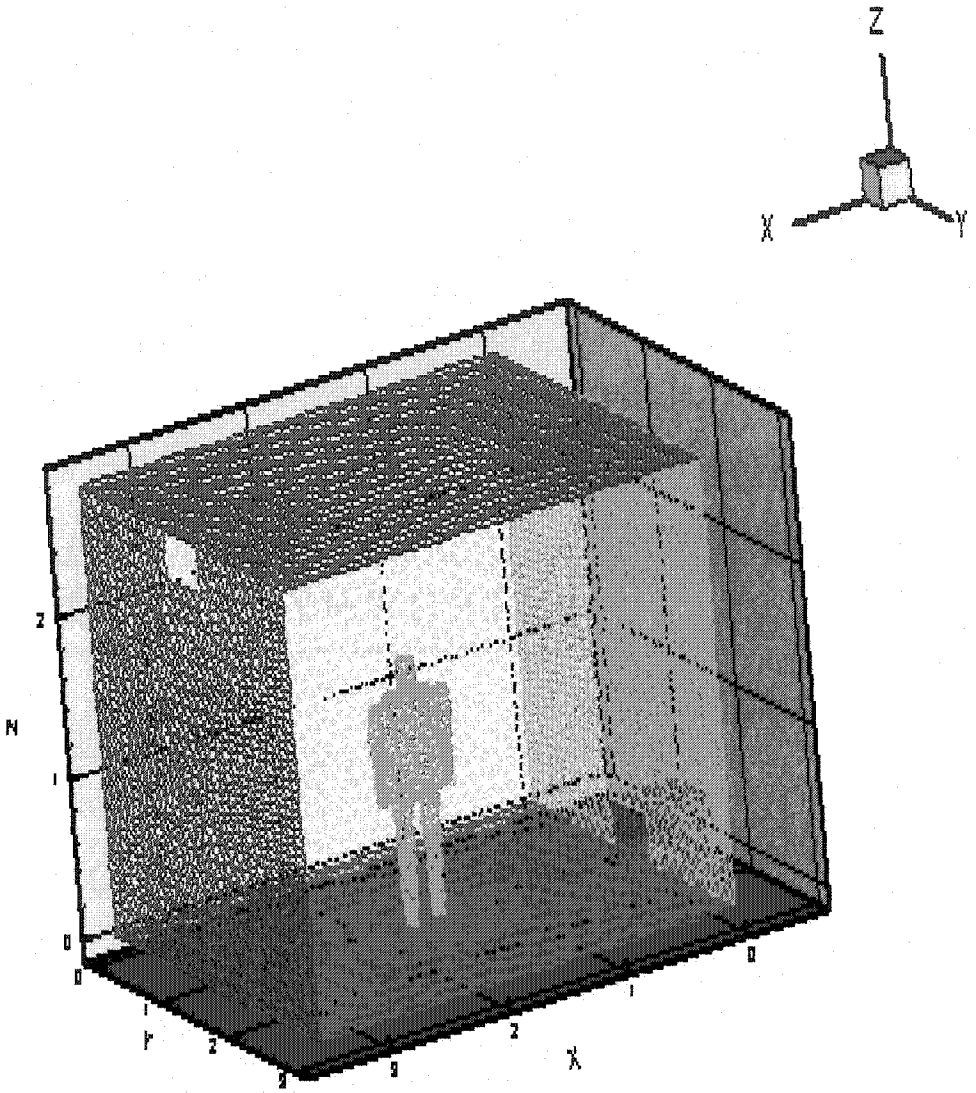

Figure 4.4 The occupied ventilated room

For simulation of room air flow a ventilated room, with dimensions of 3.5-meter length, 3-meter width and 2.8-meter height was chosen (Fig. 4.3). The room is air-conditioned in order to remove the heat and moisture production from the human body. The ventilation system uses a supply vent at the bottom of the left wall (Fig. 4.3) and a discharge vent at the top of the opposite wall. The vent opening is 0.45 meter by 0.3 meter in area. The air is supplied at different specified temperatures, relative humidity and air velocities. All surfaces in the room have varied specified temperatures, except the floor, which is kept insulated.

The simulations have been performed with Fluent V.6.0, a commercial CFD code. Four different unstructured grid sizes were used; 105,000, 197,000, 325,000 and 415,000 grids.

4.5 Boundary Conditions

The accuracy of numerical solution depends on the way boundary conditions are integrated within the numerical model. Therefore, this issue represents a crucial feature of a numerical model. In this study, three kinds of boundary conditions are applied, namely, supply inlet conditions, outlet conditions and wall boundary conditions. The specified quantities at the supply inlet are as follows: velocity, temperature and turbulent parameters (turbulence kinetic energy and its dissipation rate). The velocity and the temperature values are chosen based on a wide range of known indoor flow experimental data, their values being uniformly distributed across the inlet vent. The turbulence quantities, are imposed by means of two parameters: I, the turbulence intensity and L, the

length scale Assuming a fully developed flow upstream with velocity u [42], turbulence kinetic energy (k) and dissipation (ε) can be calculated as a function of I and L

$$k = \frac{3}{2}(uI)^2 \qquad \text{and} \qquad \varepsilon = C_{\mu}^{3/4}\frac{k^{3/2}}{L} \tag{4.1}$$

For the outlet conditions, the zero diffusion flux condition applied by the code (FLUENT) at outlet boundary is approached physically in fully-developed flows [42]. Moreover, the gradients normal to flow direction of the other variables are also set to zero at the exit plane. Finally, for the boundary conditions of wall surfaces, the classical no-slip boundary conditions are assigned to the walls. For thermal boundary conditions, fixed values of temperatures have been imposed at internal surfaces of walls. On the floor zero heat flux condition is applied which in turn leads to zero normal temperature gradient.

Initial conditions throughout the whole domain of the designed indoor flow model in this study are essential to initiate the numerical solution for the code. Initial conditions are obtained by imposing inlet conditions throughout the indoor space.

4.6 Model Validation

Before using the CFD code for detailed simulation of room air, it was validated by comparing computed results from the code with results from an independent experimental source.

Before validation of the CFD code, different grid sizes were used to establish grid independence first. The simulations were performed with 105,000, 197,000, 325,000 and

415,000 grid points. Figure 4.4 shows the vertical temperature distributions in the central plane of the room. Figure 4.5 shows the vertical velocities distributions in the same plane. Both figures shows that the results with 325,000 and 415,000 grid points are very close to each other, indicating that 415,000 grid can be used for obtaining grid independent solutions .

The first validation case involves an unoccupied ventilated room for which results were obtained from two different models for similar operating conditions. One was modeled by Wurtz [55] who has described a comparison he made between the experimental measurements and computer predictions using a CFD model. The room model dimensions were 3.6 m long, 2.6 m wide and 2.55 m high. The other model was implemented by Ren and Stewart [56] with another CFD code, with room dimensions as 3.1m long, 3.1m wide and 2.5m high. For both cases the inlet air is supplied at 19 °C temperature, 50% relative humidity and air velocity of 0.2 m/s. A turbulence intensity of 5% is used for the inlet air. All surfaces in the room have a specified temperature of 26 °C, except the floor which is adiabatic. A comparison of results from the two models and those obtained from the present CFD code is given in Fig. 4.6 that shows the temperature distribution in the central plane of the room for all models. Results in the figure clearly indicated that the present model simulates the experimental data much better than the other two CFD models.

The second CFD model validation case involved a room occupied by a human, a case analyzed by Murakami et al. [27]. In this case, the coupled heat transfer problem

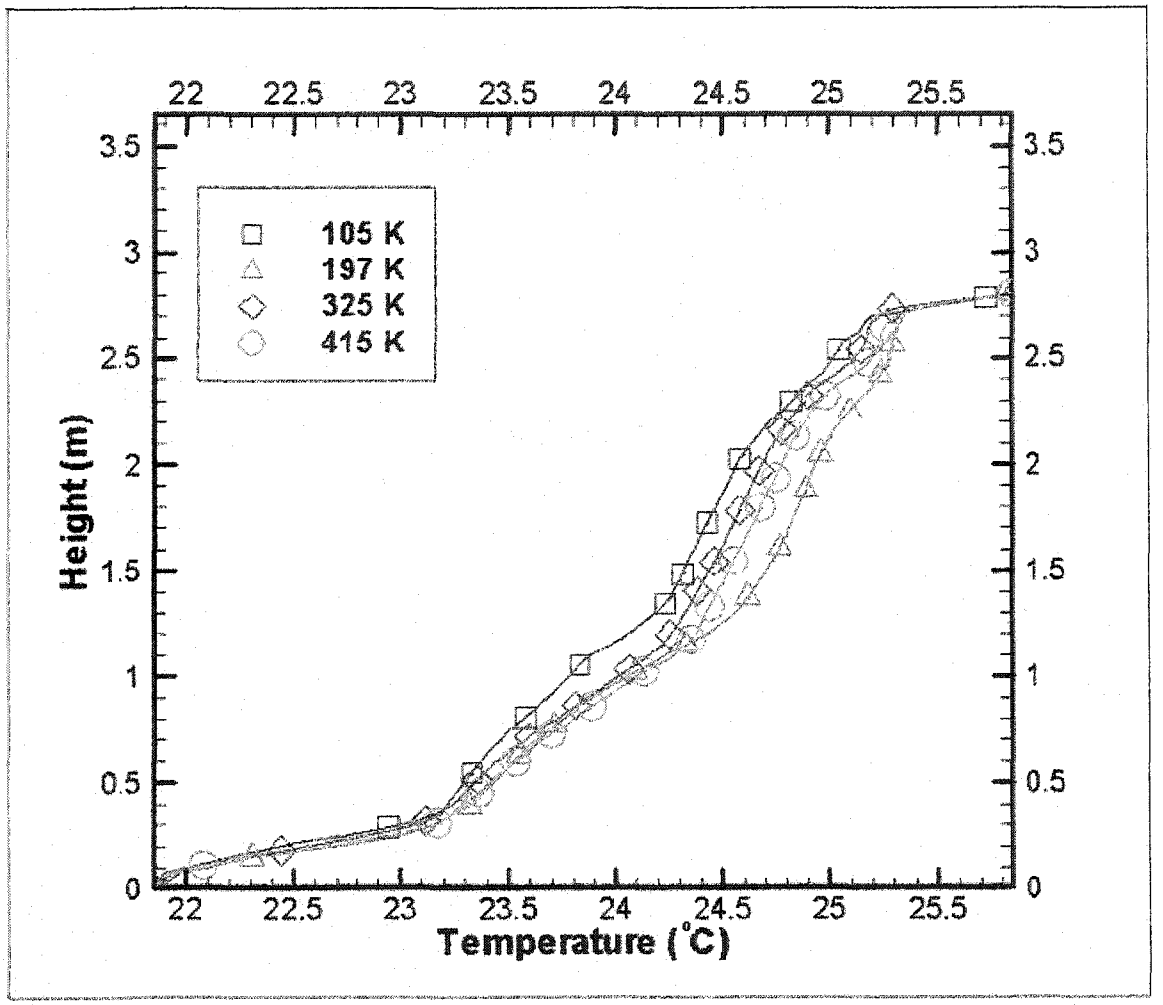

Figure 4.5 Grid independency by vertical temperature distribution

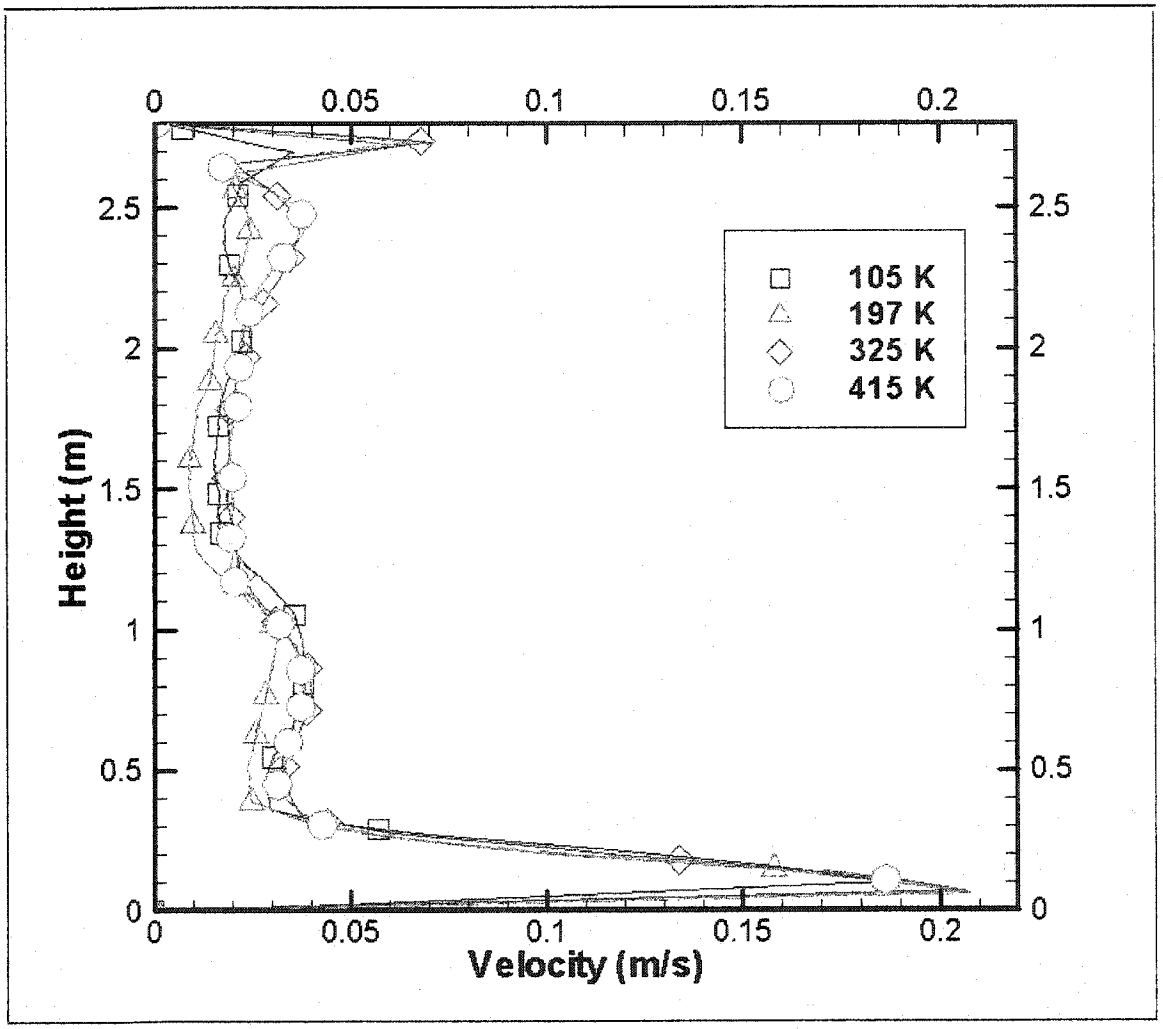

Figure 4.6 Grid independency by vertical velocity distribution

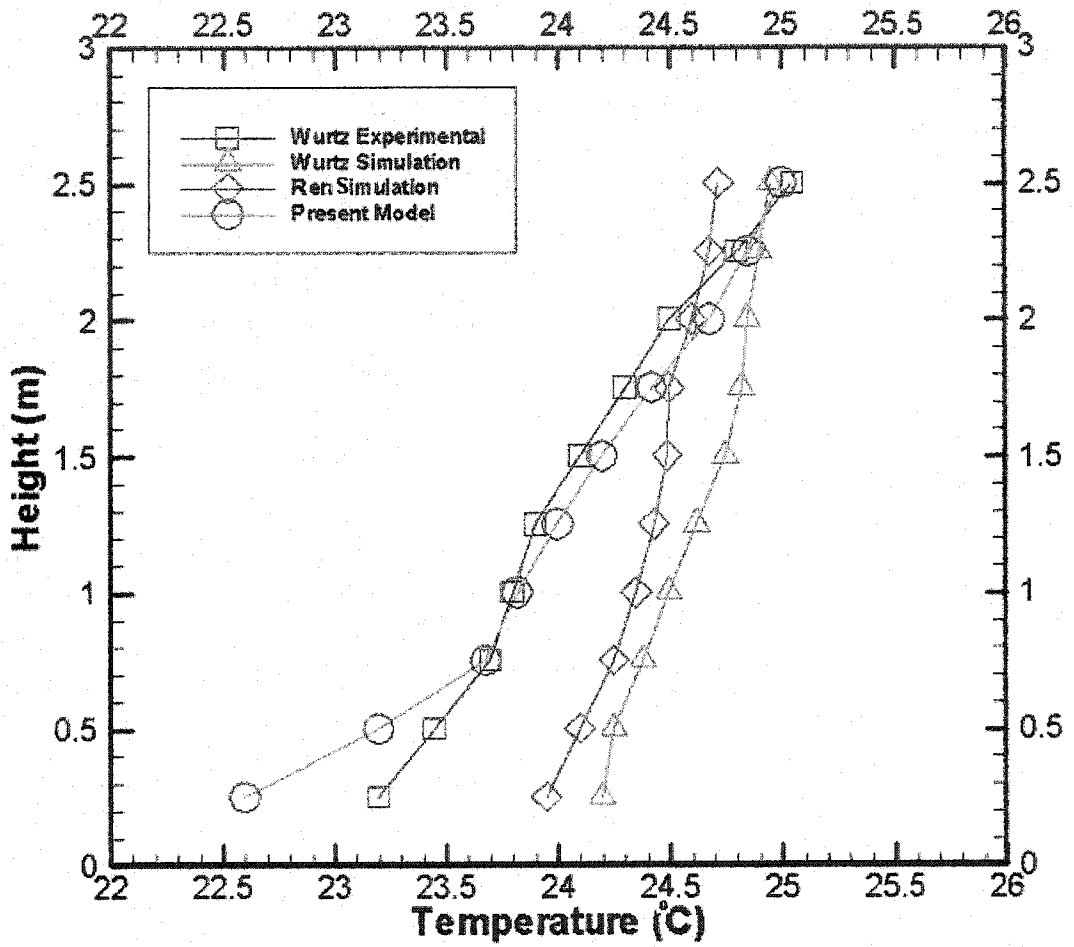

Figure 4.7 Comparison of predictions of vertical temperature with different models

involves human thermo-regulation and heat dispersed to room air is solved. The human body is assumed to be naked and is located in the center of the room.

The air is supplied at 21 °C temperature, 50% relative humidity and air velocity of 0.2 m/s. A turbulence intensity of 5% is used for the inlet air. The floor is adiabatic, while the other surfaces in the room have a specified temperature of 27 °C.

Table 4.1 Comparison of heat release from human body with Murakami Model

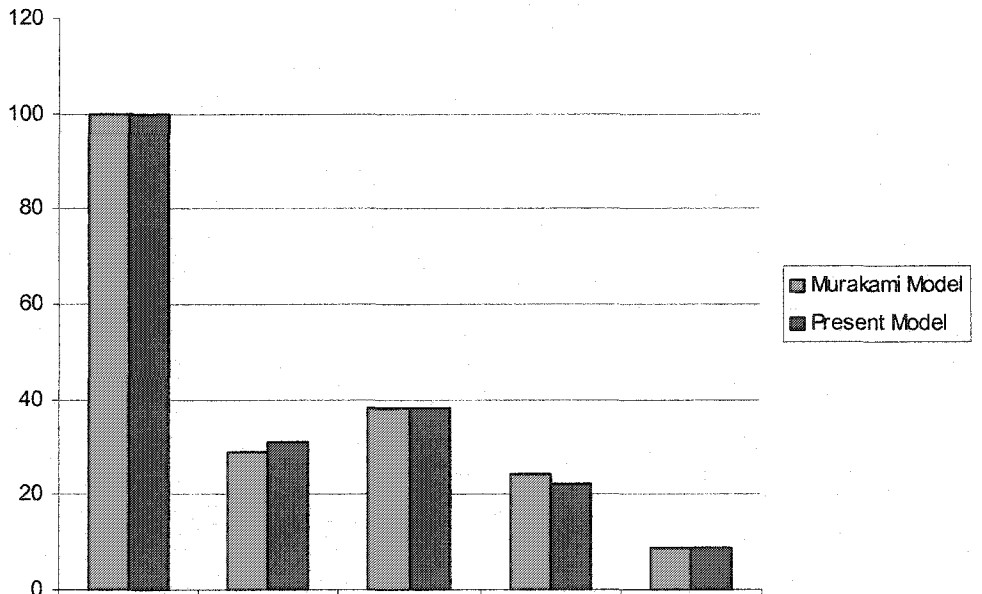

	M	Qcv	Qr	Esk	Qres
Murakami Model	100	29.1	38.3	24.3	8.7
Present Model	100	31	38.2	22.1	8.7

The metabolic rate is assumed to be 1.7 Met (100 W/m^2), which roughly corresponds to a person standing still. The converged results yielded various fluxes as: 56.42 W (31 W/m^2) by convection, 69.52 W (38.2 W/m^2) by radiation, 40.22 W (22.1 W/m^2) by evaporation and 15.83 W (8.7 W/m^2) by respiration. Table 4.1 shows a reasonable agreement between the present study and the one by Murakami et al. [27].

The cases described earlier establish "Fluent" CFD code as a reliable tool for calculation of room air motion and heat transfer from the human body. The next chapter describes results obtained from the validated CFD code for a variety of boundary conditions and cases.

CHAPTER V

RESULTS AND DISCUSSION

5.1 Introduction

Human thermal comfort in a conditioned room is investigated using the coupled model described in Chap. 4. Heat transfer inside the human body is calculated for a given level of activity (metabolic rate), using the two node human thermo-regulation model. Prediction of metabolic heat dispersal to the surrounding is accomplished by a CFD code. Results for different cases with varying supply air velocity, temperature and turbulence intensity as well as human metabolic rate are obtained to predict thermal comfort conditions in the room, using several comfort indices.

First, the occupancy effect is analyzed to compare thermal comfort zones that result when the room is occupied or unoccupied. Subsequently, results pertaining to effects of varying supply air conditions and physical activity are presented. Finally, the results from the segmented body model are presented to incorporate effects of varying human body properties.

5.2 Effect of Occupation in Conditioned Room

Results are obtained for both empty and occupied room cases to show the effect of human occupation in ventilated room on parameters such as temperature, relative humidity and thermal comfort indices. All results are presented in the vertical plane in the center of the room containing the two vents.

The room geometry considered in this study is shown in Fig. 4.3. The two vents are located in the middle of the two opposing walls, with the inlet vent being at the ground level and the exit vent being located at the ceiling level. The size of vents have been stated earlier in Chap. 4. In the empty room case, the same boundary conditions as in the occupied room case are applied except that there is no human body present in the room. The air inlet temperature is 19 ^{0}C; inlet velocity is 0.2 m/s and air relative humidity is 50% for both cases while the metabolic rate is assumed to be 100 W/m^2 in the occupied case.

5.2.1 Room Temperature and Relative Humidity

The effect of presence of human body on the room micro-climate is illustrated using this case. Figure 5.1 shows the room air temperature contours for the empty room. The room temperature increases from the ground to ceiling by a magnitude of about 7 ^{0}C, representing a substantial temperature stratification in the room. The average room air temperature is 24.40 ^{0}C for this case. Figure 5.2 shows the room temperature contours for the occupied room case for the same operating conditions. The magnitude of temperature

variation is 7.7 ^{0}C from the inlet (19 ^{0}C) to the ceiling (27.7 ^{0}C). The average room temperature for the occupied case is 24.85 ^{0}C. For this case, the occupancy in the room increases slightly the temperature stratification as well as the average air temperature by 0.45 ^{0}C, primarily due to metabolic heat generation. It is also noted that the human body is engulfed in a thin thermal boundary layer across which temperatures change significantly from the skin temperature to the temperature of the air next to the body.

Figure 5.3 presents the spatial variation of relative humidity for the empty room case. It shows that relative humidity varies from 50 % at the inlet to 33 % at the ceiling level. The average relative humidity in the room is 36.7 % for this case. Figure 5.4 shows the variation of relative humidity in the occupied room, indicating a variation from 50 % to 31 %, with an average value of 35.9 % for the room. In this case, the occupancy in the room results in lower average relative humidity primarily due to increasing value of saturation vapor pressure. It rises because of increase in air temperature due to metabolic heat generation.

5.2.2 Thermal Comfort Indices

The computed values of air temperature, velocity and humidity are used to calculate thermal comfort indices. In this study, three indices namely, Effective Draft Temperature (EDT), Predicted Mean Vote (PMV) and Percentage of People Dissatisfied (PPD) have been used. These indices have been described in Chap. 2. It should be noted that the PMV and PPD indices are not independent but related to one another.

The EDT index, as discussed earlier, combines the effect of dry bulb temperature and air velocity to describe zones of thermal comfort and discomfort. The values $-1.7 \leq$ EDT ≤ 1.1 indicate the zone of thermal comfort. A value lower than -1.7, indicates discomfort due to coolness while a value greater than $+1.1$, indicates thermal discomfort due to warm sensation. The region of thermal discomfort, as predicted by EDT, is shown by white color in the illustrated figures.

Figure 5.5 shows the thermal comfort zone for the empty room case as indicated by the EDT index. The thermal comfort zone is indicated by shaded color region in Fig. 5.5, with the index ranging from -1.7 in the floor region to $+1.1$ in the upper region of the room. The EDT comfort index indicates that the comfort zone for this case extends from the floor to a height of nearly 2.75 meters. Figure 5.6 shows the comfort zone for the occupied case. It is noted that there is a shift towards higher values of the index in the occupied case due to release of metabolic heat into the surrounding air.

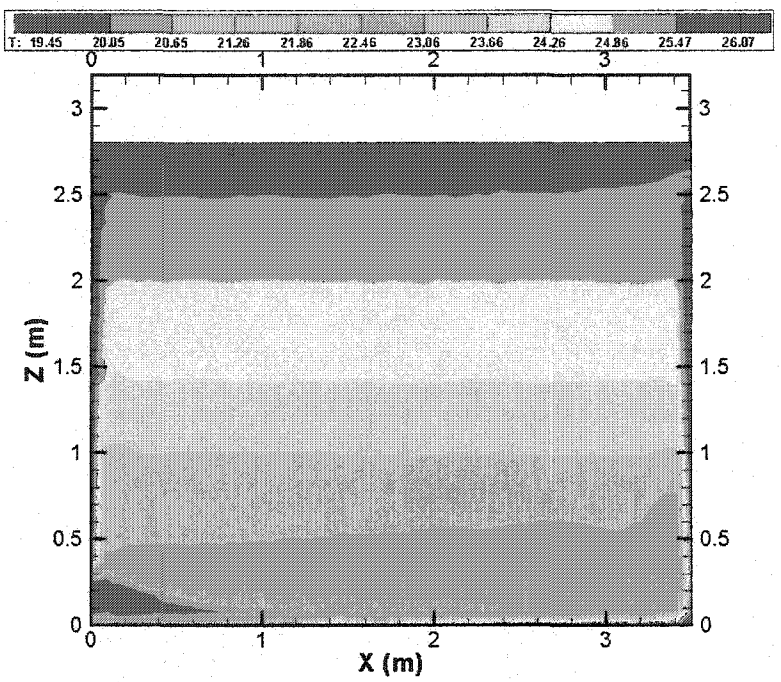

Figure 5.1 Temperature contours for the empty room

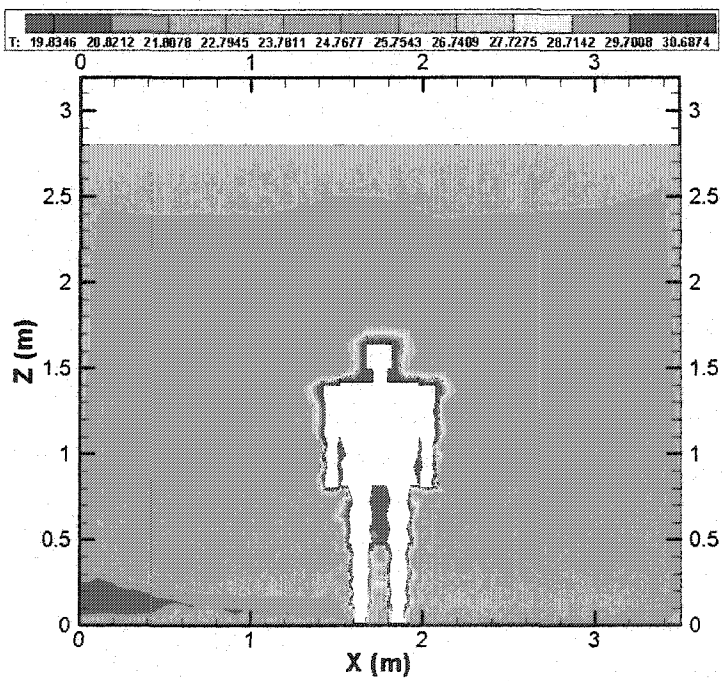

Figure 5.2 Temperature contours for the occupied room

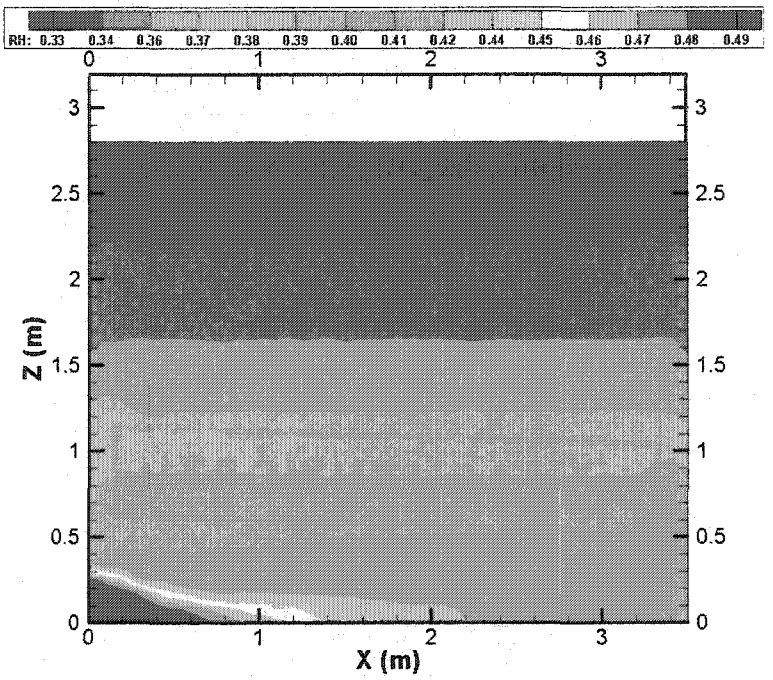

Figure 5.3 Relative humidity contours for the empty room

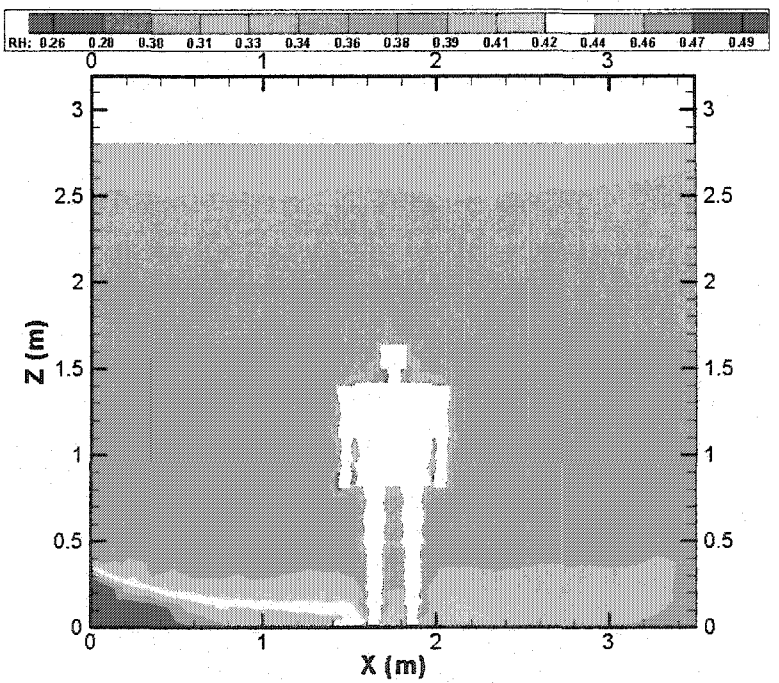

Figure 5.4 Relative humidity contours for the occupied room

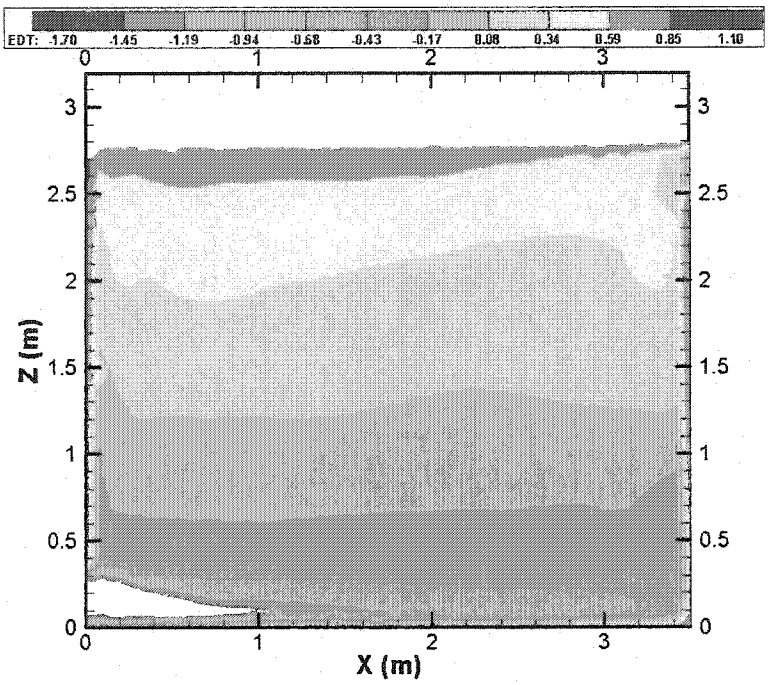

Figure 5.5 EDT index for the empty room

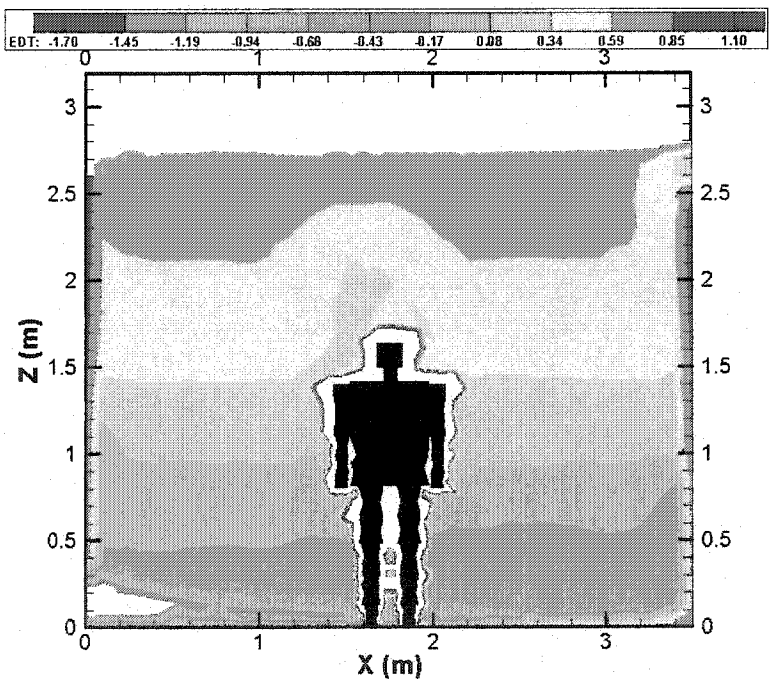

Figure 5.6 EDT index for the occupied room

5.3 Effect of Physical Variables on Thermal Comfort

Physical variables which affect overall human thermal comfort include both environmental and personal or life style factors. There are four environmental factors affecting human thermal comfort: air temperature, air velocity, relative humidity, and mean radiant temperature. The life style factors are the activity level and clothing.

As stated previously the present study models only a naked human and as a result clothing effects are neglected. This has been done primarily to simplify the modeling, and to focus on factors such as activity level. However, it should be emphasized that clothing does have an important influence on comfort considerations but it has not been considered in the present study. Also, since calculation of the mean radiant temperature (T_{mrt}) is a complicated process, a conservative assumption of $T_{mrt} = T_{ambient}$ is made for simplicity. Consequently, in this section, effects of remaining four variables are studied to predict thermal comfort. For all these cases a turbulence intensity of 5% is used for the inlet air. The floor is assumed to be adiabatic, while all other surfaces in the room have a specified temperature of 27 °C.

5.3.1 Effect of Air Temperature

Four cases were studied in which the supply air temperature to the conditioned room is varied from a low value of 10 ^{0}C to a high value of 30 ^{0}C. Other parameters were assumed to be fixed with inlet velocity at 0.2 m/s, relative humidity at 50 %, and metabolic activity at 100 W/m^2.

Figure 5.7(a)-(b) shows isotherms for the occupied room for different supply air temperature. One can observe that for the lower temperature cases, Fig. 5.9-(a)-(b), the room exhibits stable temperature stratification, and the air temperature increases in layers from the floor to the ceiling. Also, the inlet air jet stays attached to the floor, and decays slowly over the floor. In the higher temperature cases, the effect of buoyancy becomes more pronounced, and the resultant mixing tends to make temperature stratification effect weaker, and nearly disappear for the highest supply air temperature case (Fig. 5.7(d)). In fact, this case is dominated by the supply air jet lift-off and its merging with the plume emanating from the human body.

The velocity fields generated by the incoming jet are illustrated in Fig. 5.10(a)-(d) for the four inlet temperature cases ranging from 10 ^{0}C to 30 ^{0}C. The inlet jet velocity is 0.2 m/s for all four cases. Several interesting features of the air flow patterns can be discerned. For instance, Fig. 5.10(a) shows that the inlet air jet dips slightly towards the floor. This is because cooler air sinks due to the negative buoyancy effect. The cool air jet eventually decays before it reaches the opposite wall of the room. The inlet air jet motion creates air velocity in the range of 4 to 8 cm/sec up to the knee level. Also, the air plume generated by the human body is quite weak and has velocity in the range of 6 to 10 cm/sec. With increasing inlet air temperature, as shown in Fig. 5.10(c) the body plume becomes stronger. For the 30 ^{0}C inlet air temperature case, the air supply jet lifts off due to buoyancy action and it merges with the body plume. This creates a higher velocity draft near the upstream part of the upper body while the downstream side of the room shows weaker air flow patterns.

The PMV scale ranges from –3 (cold) to +3 (hot) with zero value indicating the fact that occupant feels neither hot or cold. This corresponds to a value of 95% for the PPD index, a value indicating that 95% of the occupants are satisfied with the comfort level. In order to compare PMV with other indices such as EDT, it is important that we abandon the single point PMV criterion and adopt a range of PMV over which one can deem room conditions as comfortable. The range $-0.5 \leq$ PMV ≤ 0.5 has been chosen as defining thermal comfort. The value 0.5 corresponds to a PPD value of 10%, indicating that 90% of occupants feel satisfied. For PMV > +0.5, the room conditions are designated as uncomfortably warm. For PMV < -0.5, the room conditions can be described as uncomfortably cool.

Figure 5.8(a)-(d) shows the thermal comfort region as predicted by the PMV index for the four air inlet temperatures (10°C, 15°C, 25° and 30°C). It is noted from Fig. 5.9 (a) that the PMV index predicts a region of thermal discomfort due to coolness of air (PMV < –0.5) that extends from the floor to about 2.2 meter height, engulfing the entire human body. Similar trends are also seen in Fig. 5-9 (b) for the 15°C inlet air temperature case. The point of neutral sensation (zero PMV value) identified as neither warm nor cool sensation is at an elevation of 2.0 meters for the 10°C inlet temperature case. For the inlet air temperature of 25°C (Fig. 5-9(c)), the entire body is in the zone of thermal comfort (PMV value ranging between –0.5 and +0.5). For the inlet temperature of 30°C, the upstream side of the body, including shoulder, neck and head regions are subjected to warm sensation due to PMV exceeding +0.5 value. The backside of the body is subjected to relatively cooler as determined by the PMV criterion.

Figure 5.10(a) to (d) shows the thermal comfort zone as mapped by the EDT index. It is noted that thermal comfort region is indicated by $-1.7 \leq EDT \leq +1.1$. The central white region indicates the human body profile while the white regions elsewhere represent the region of discomfort. For the 10°C and 15°C air inlet temperature cases, the regions of discomfort are mostly confined to the lower (floor) region of the room. The 25°C inlet air temperature case indicates a much bigger zone of discomfort especially on the downstream side of the body.

Figure 5.11 shows the variation of the room averaged values of PMV and the corresponding PPD values as a function of supply air temperature. The results show that the average PMV value rises from -0.8 to about 1.1 as the air inlet temperature is increased from 10 ^{0}C to 30 ^{0}C. Since the zero value of PMV indicates neutral (best comfort) sensation, it is clear from this diagram that an inlet air temperature of about 19 ^{0}C will provide the optimal comfort condition with the PPD index showing a minimum value of 5 percent. This indicates that 95 percent of occupants will find condition resulting from 19 ^{0}C supply air temperature as comfortable.

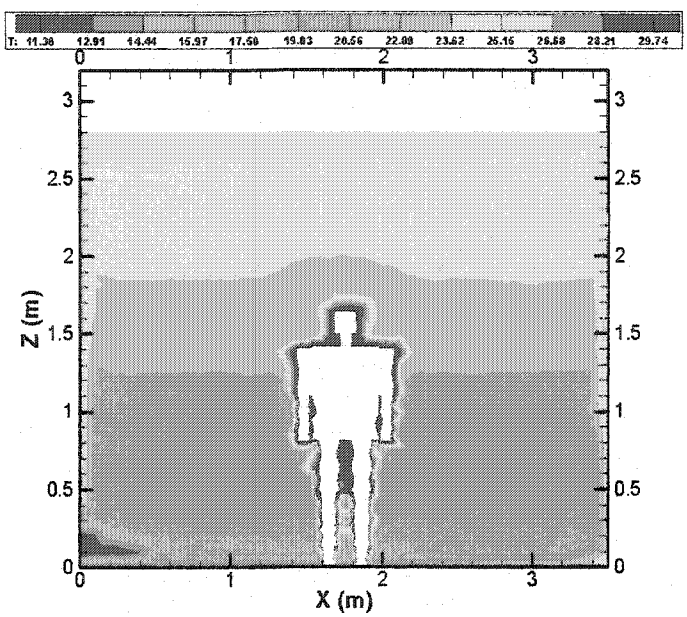

a) Inlet temperature = 10 ^{0}C

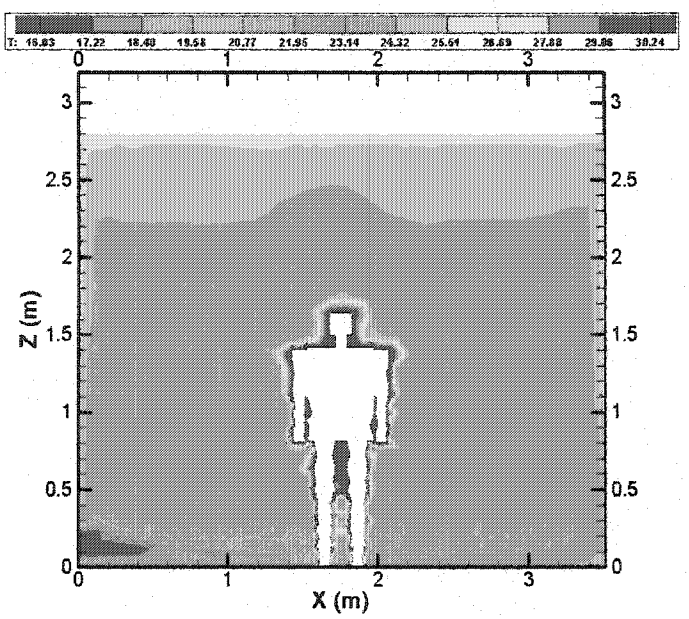

b) Inlet temperature = 15 ^{0}C

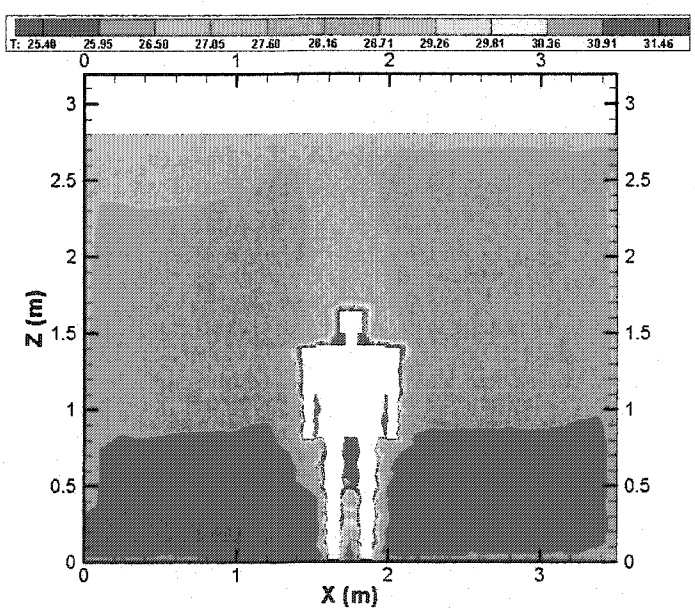

c) Inlet temperature = 25 ^{0}C

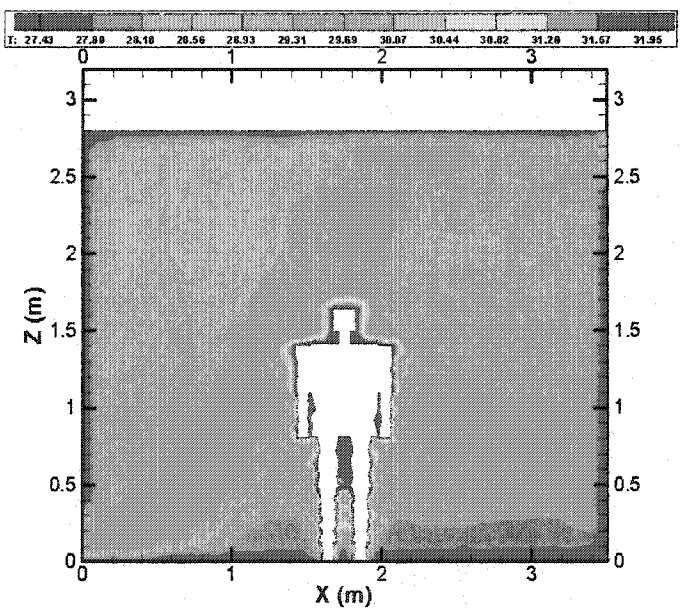

d) Inlet temperature = 30 ^{0}C

Figure 5.7 Temperature contours for different inlet temperatures

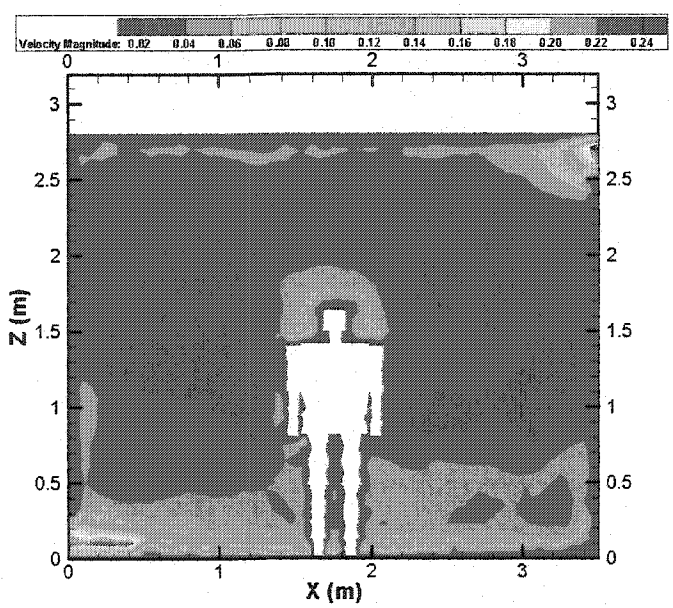

a) Inlet temperature = 10 ^{0}C

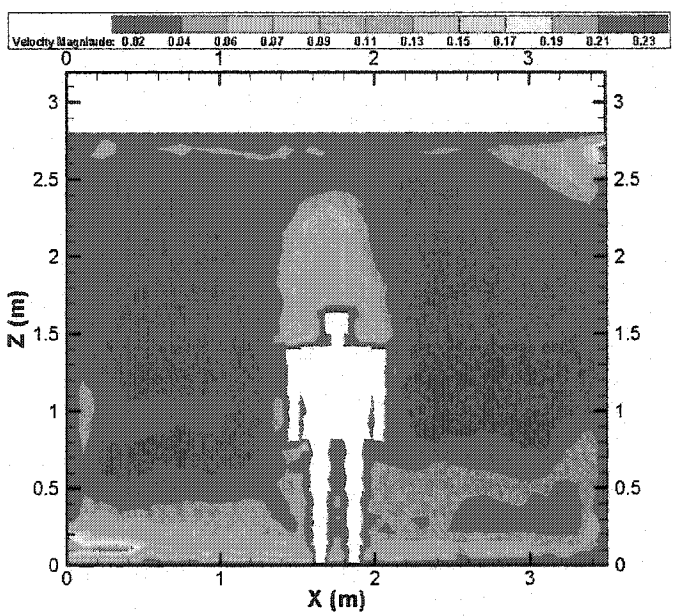

b) Inlet temperature = 15 ^{0}C

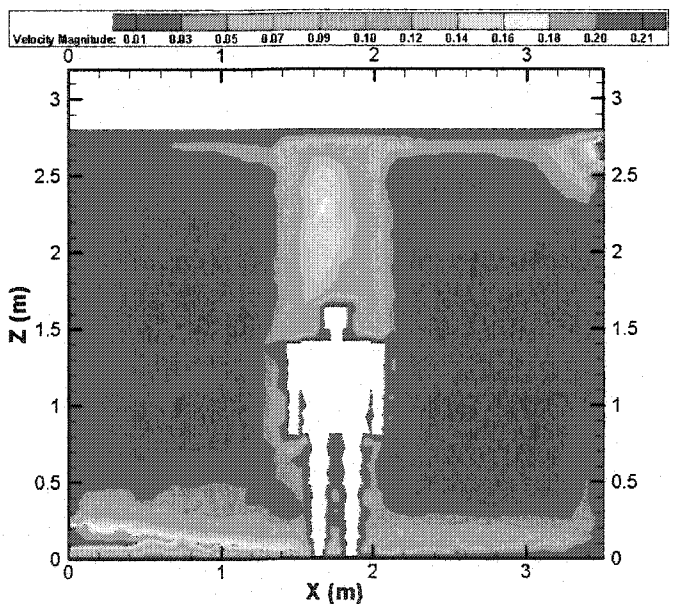

c) Inlet temperature = 25 ^{0}C

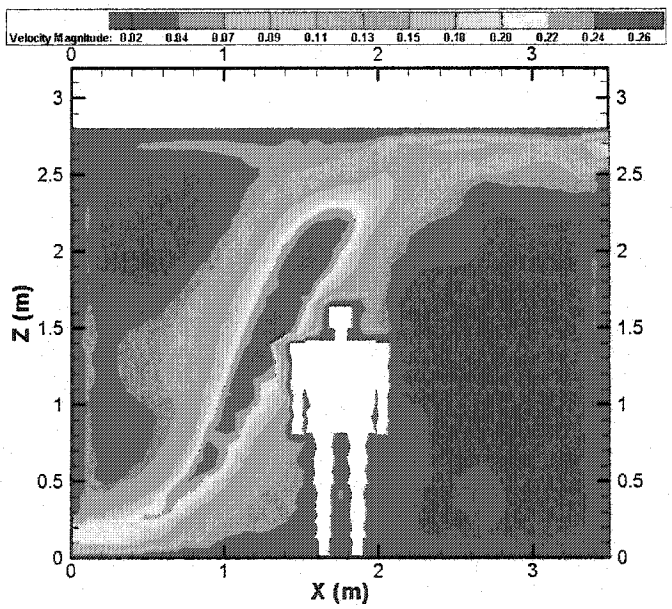

d) Inlet temperature = 30 ^{0}C

Figure 5.8 Velocity contours for different inlet temperatures

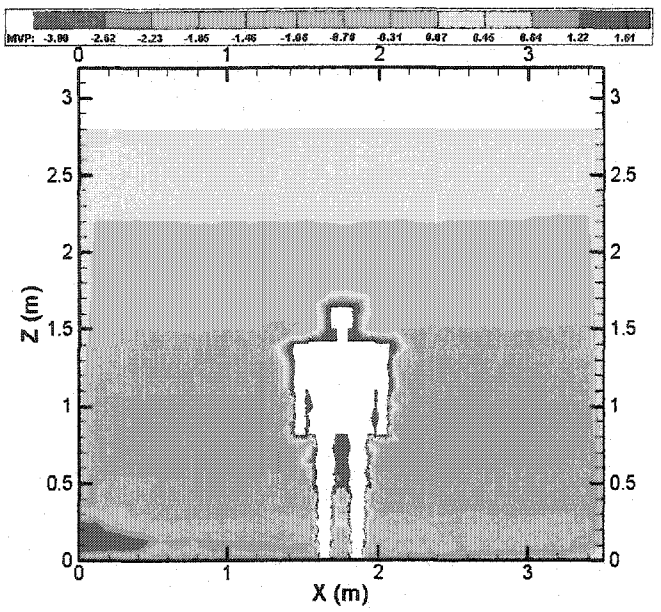

a) Inlet temperature = 10 ^{0}C

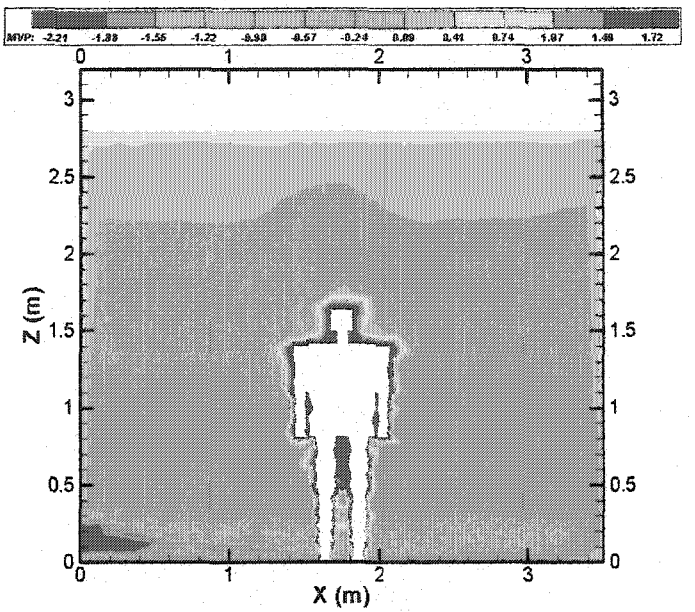

b) Inlet temperature = 15 ^{0}C

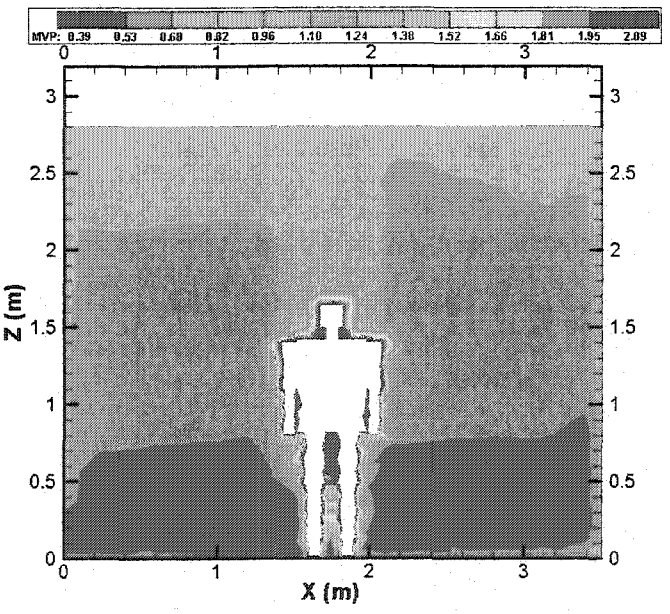

c) Inlet temperature = 25 ^{0}C

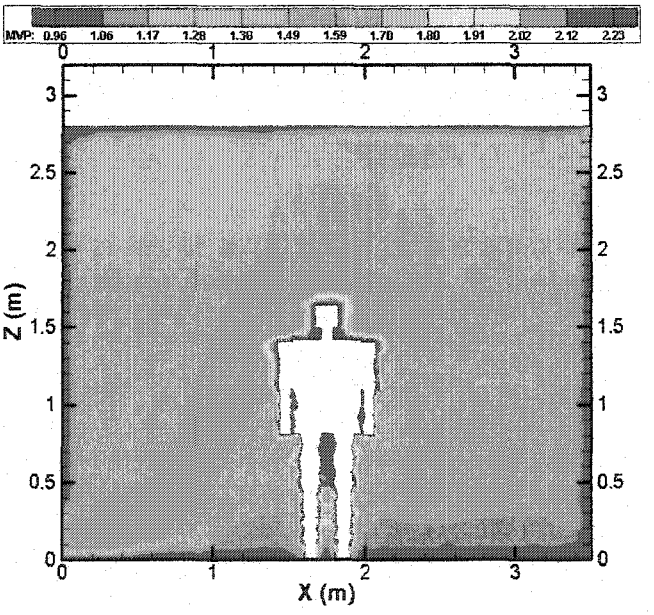

d) Inlet temperature = 30 ^{0}C

Figure 5.9 PMV index for different inlet temperatures

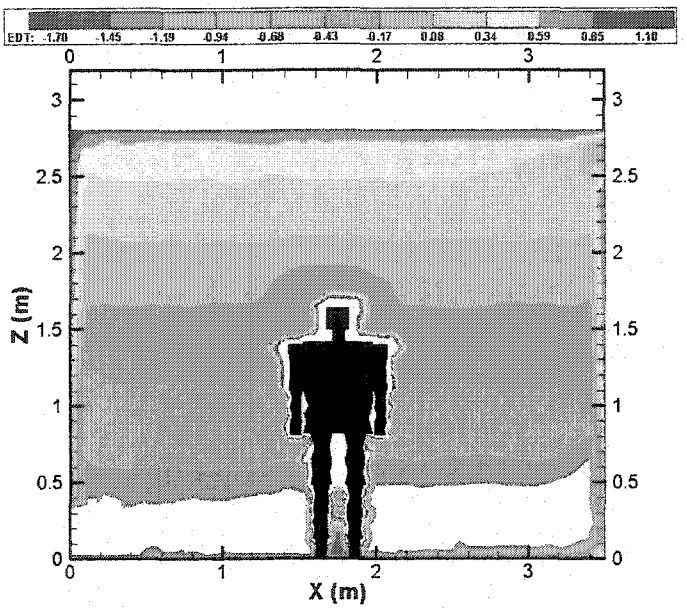

a) Inlet temperature = 10 ^{0}C

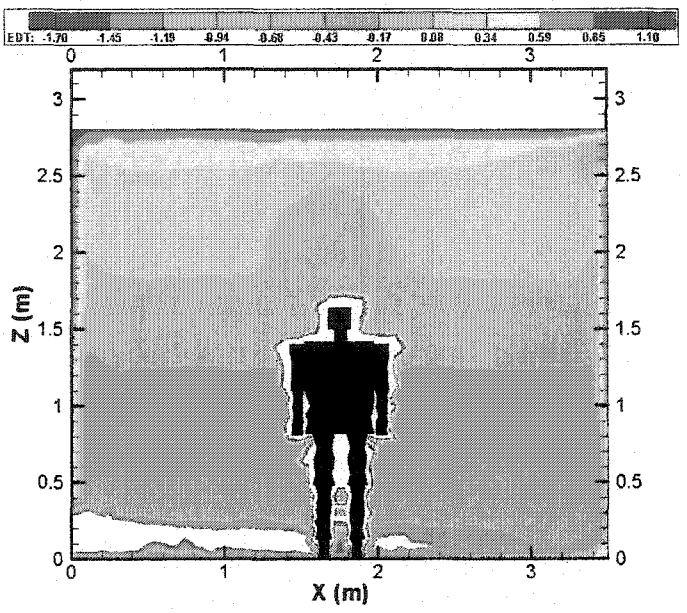

b) Inlet temperature = 15 ^{0}C

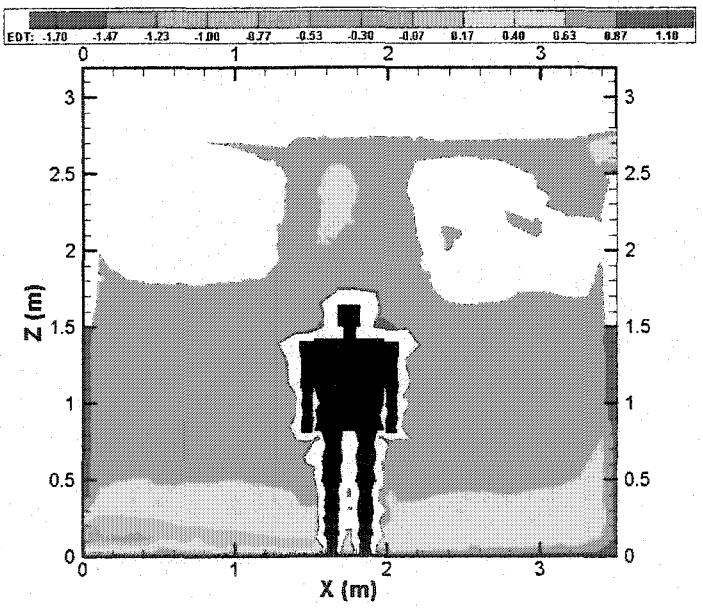

c) Inlet temperature = 25 ^{0}C

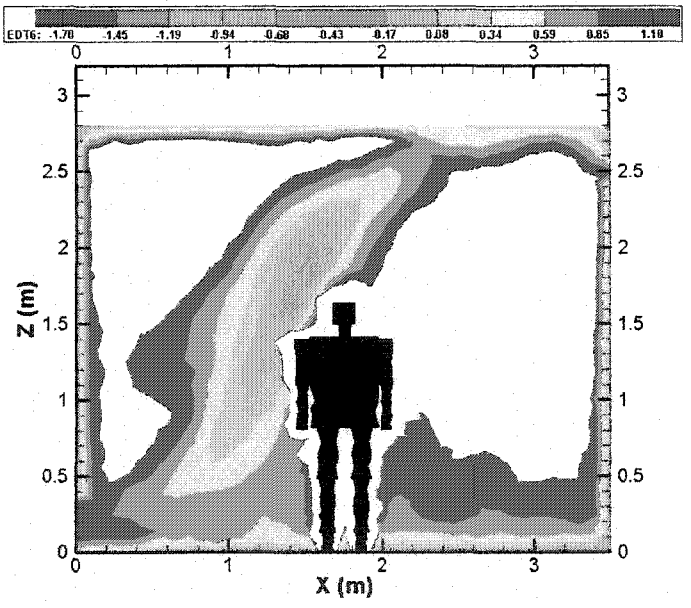

d) Inlet temperature = 30 ^{0}C

Figure 5.10 EDT index for different inlet temperatures

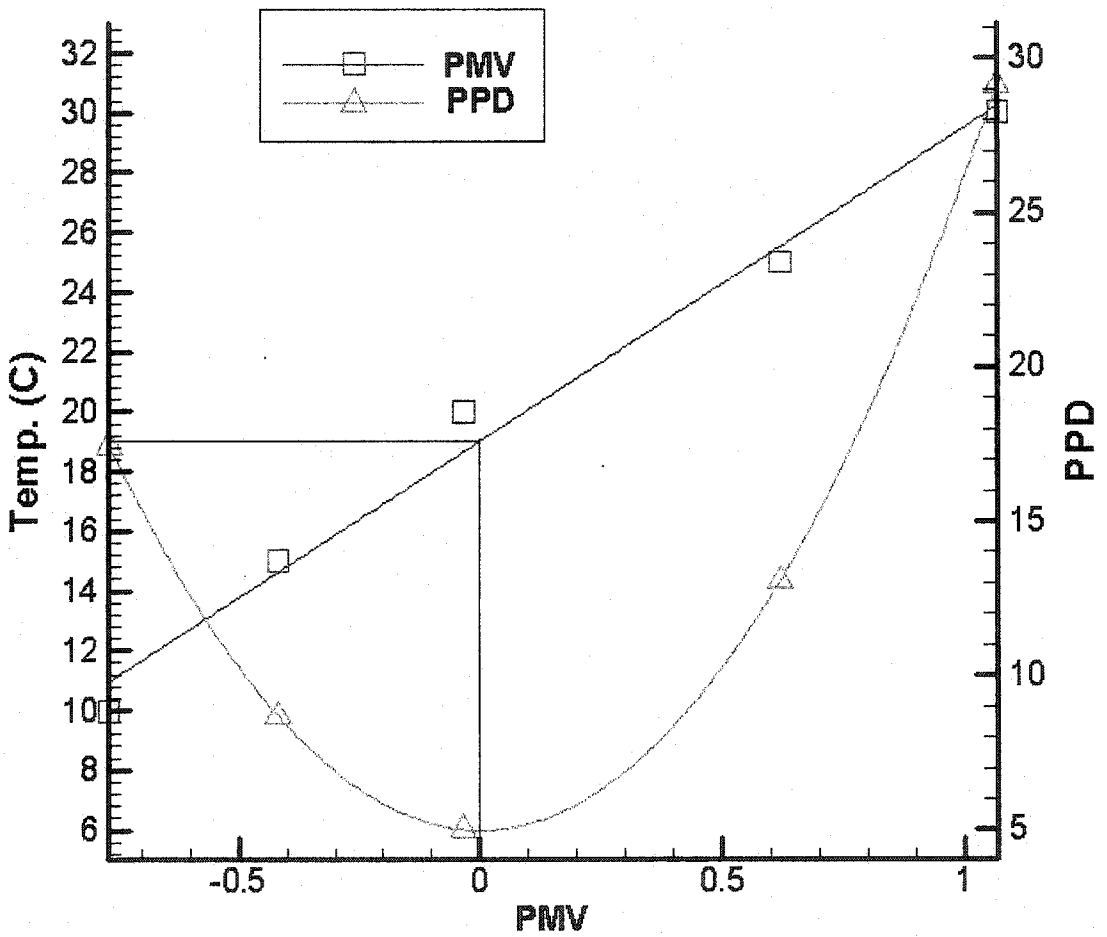

Figure 5.11 Inlet temperatures vs. PMV & PPD

5.3.2 Supply Air Velocity Effect

In order to investigate the effect of the supply air velocity on thermal comfort condition, the air velocity is changed from 0.05 m/s to 0.35 m/s in steps of 0.10 m/s. For all these four velocity cases (0.05, 0.15, 0.25 and 0.35 m/s) it is assumed that the inlet air temperature is maintained at 19 °C, the optimal value obtained earlier, and relative humidity and metabolic activity rate are maintained at 50 %, and 100 W/m² respectively.

Figure 5.12(a)-(d) shows the room air temperature contours for different inlet velocities. The lowest velocity case (0.05 m/s) shows that the room temperature changes very little from the floor to the ceiling level. As the velocity increases, flow entrainment and mixing cause the inlet air temperature effect to spread to higher elevations. For instance, for the case of 0.35 m/s one observes from Fig. 5.12(d) that air temperature varies from 19 °C at the floor level to about 28 °C at the ceiling level. The temperature variation (stratification effect) is quite pronounced from the floor to body mid-height level.

The corresponding velocity contours are shown in Fig. 5.13(a)-(d). The results indicate that the body plume is quite strong for the low air inlet velocity cases, since buoyancy effect due to metabolic heat generation dominates in absence of strong forced convection effect. However, this effect weakens for the highest velocity case (Fig. 5-13 (d)) due to dominance of room convective motion over buoyancy.

Figure 5.14(a)-(d) shows the PMV index for different velocities. It is noted that at a low velocity of 0.05 m/s, the comfort zone extends from the floor to the shoulder level. The neck and head region are clearly in the region of discomfort characterized by the PMV index. The cases involving 0.15 and 0.25 m/s inlet air velocity indicate that the

entire body is in the region of comfort. The final case with the velocity of 0.35 m/s indicates that while the body from knee to head region is in the region of the comfort, region below the knee is characterized by a cooler sensation.

Figure 5.15 (a)-(b) shows the EDT index for different velocity cases. Once again, the EDT index for 0.05 m/s inlet velocity shows that the floor to the upper waist region, lies in the region of comfort but upper extremity of the body including neck and head are in the discomfort region. These conclusions are similar to the ones indicated by the PMV index. The EDT index for 0.15 and 0.25 m/s cases, like the PMV criterion, indicates that the entire body is in the zone of thermal comfort. The inlet velocity case of 0.35 m/s parallels the conclusion drawn for the PMV index, indicating that except for the floor to knee region, the entire body experiences thermal comfort.

Figure 5.16 shows the variation of average PMV index and the corresponding PPD values with air inlet velocity. It is noted for instance at inlet velocity of 0.35 m/s, the average PMV is about -0.45 while the value of PPD is about 9, indicating that about 9 percent people in the room are not satisfied with maintained comfort conditions. Likewise, the inlet velocity of 0.05 m/s indicates a PPD value of about 13 which implies that about 13 percent of the occupants are not satisfied. The PMV value of zero represents the minimum value for the PPD index and it represents the fact that 95 percent of the occupants are satisfied while 5 percent occupants are dissatisfied. From Fig 5.16, this corresponds to an optimum value of inlet air velocity of about 0.225 m/s.

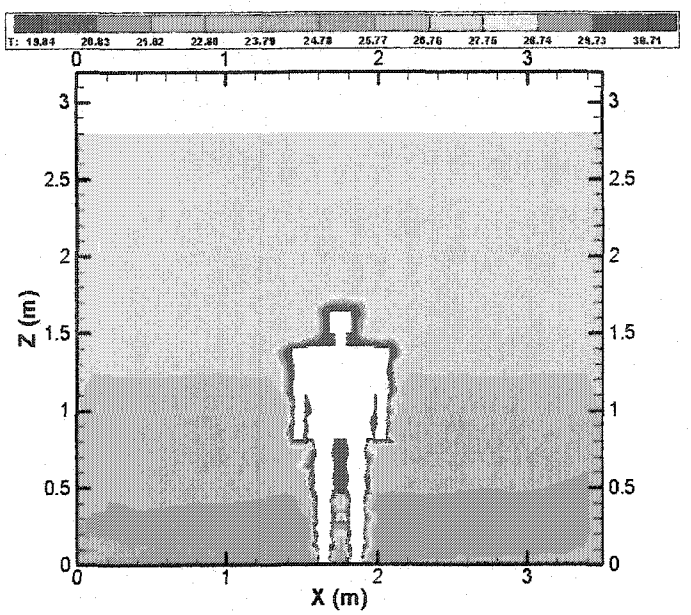

a) Inlet velocity = 0.05 m/s

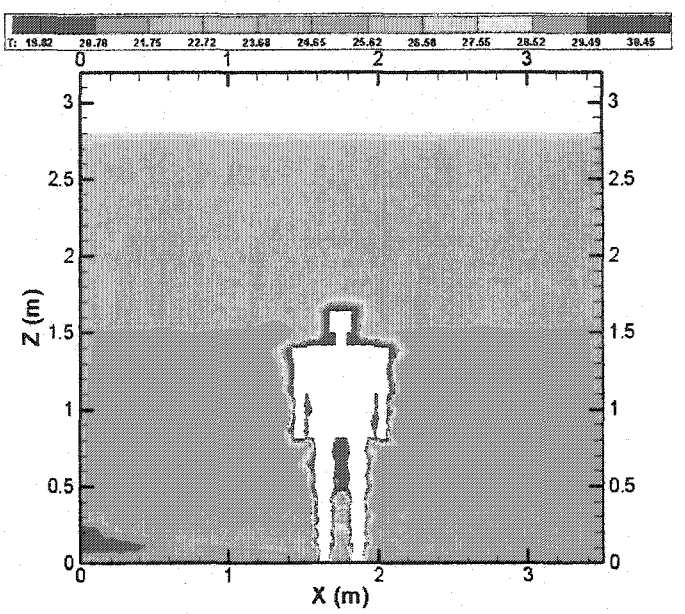

b) Inlet velocity = 0.15 m/s

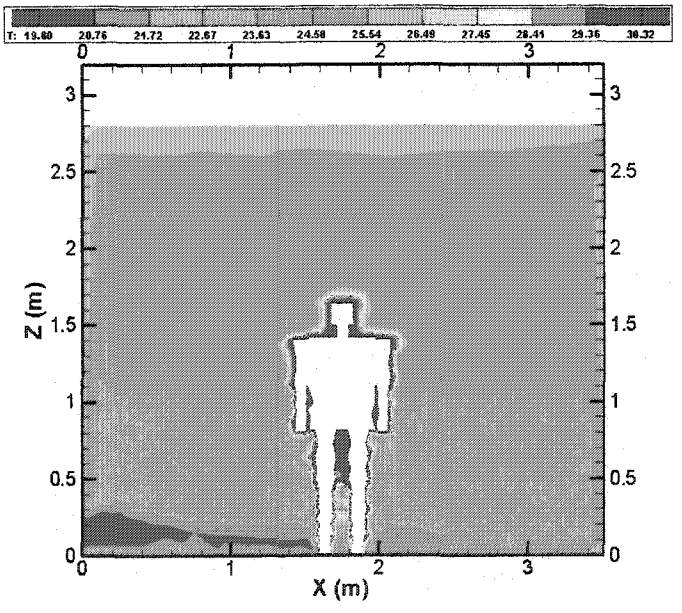

c) Inlet velocity = 0.25 m/s

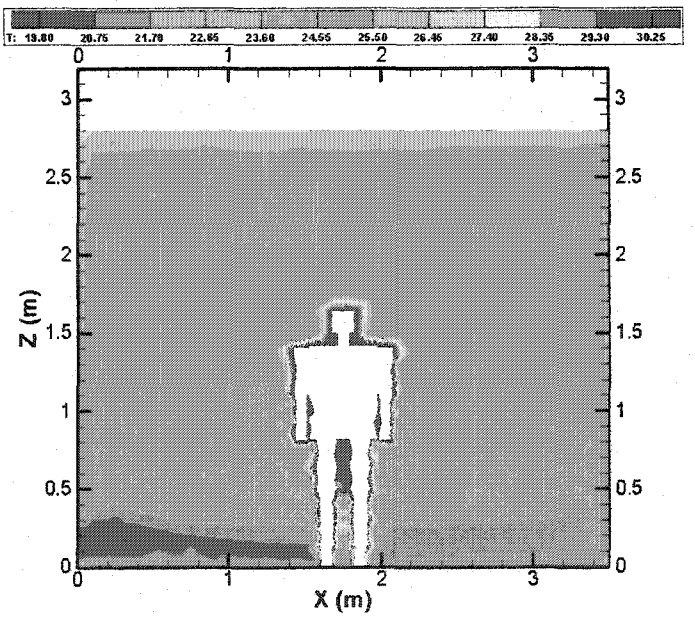

d) Inlet velocity = 0.35 m/s

Figure 5.12 Temperature contours for different Inlet velocities

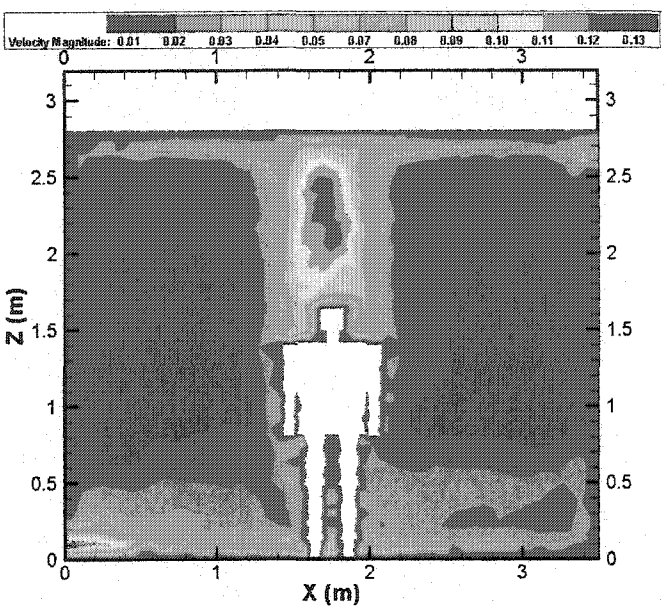

a) Inlet velocity = 0.05 m/s

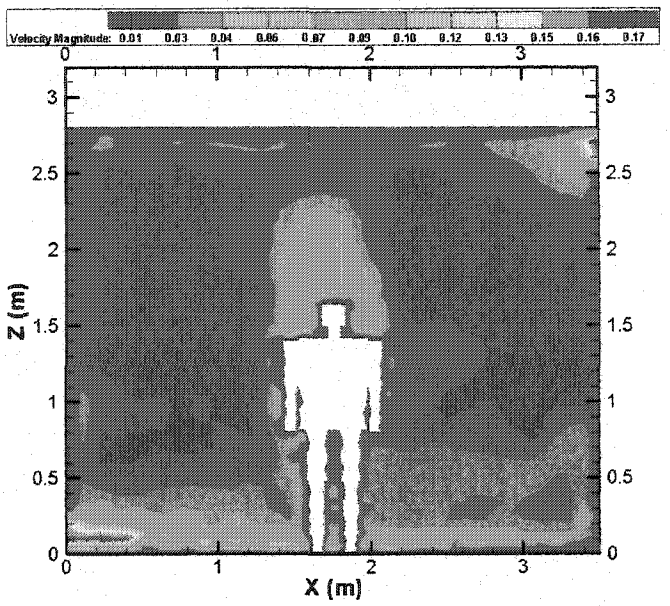

b) Inlet velocity = 0.15 m/s

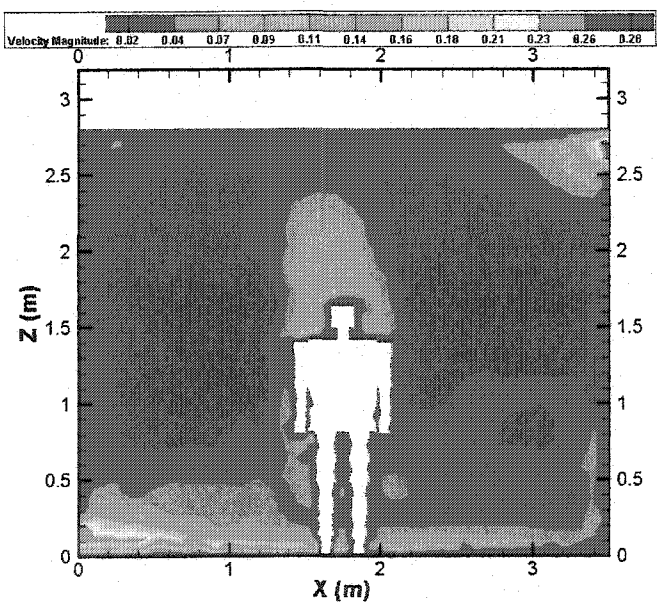

c) Inlet velocity = 0.25 m/s

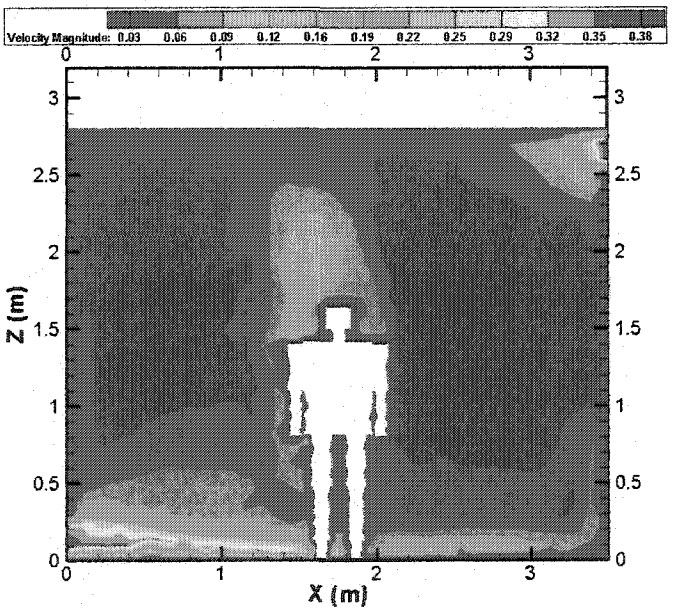

d) Inlet velocity = 0.35 m/s

Figure 5.13 Velocity contours for different inlet velocities

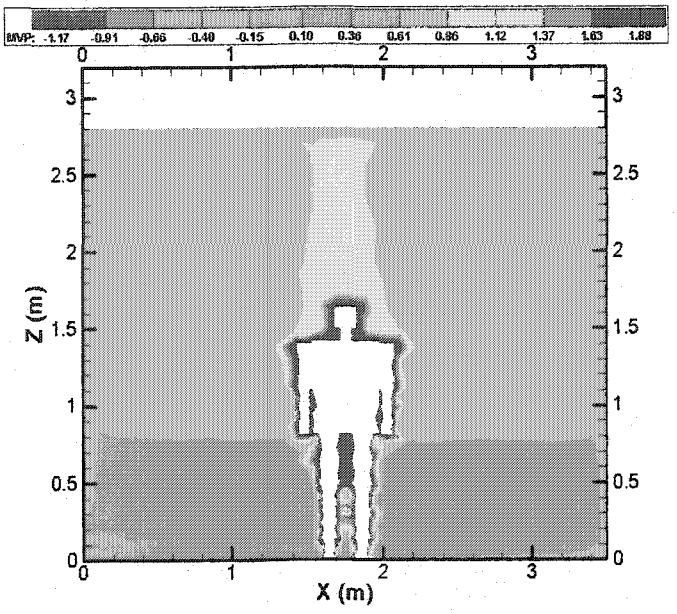

a) Inlet velocity = 0.05 m/s

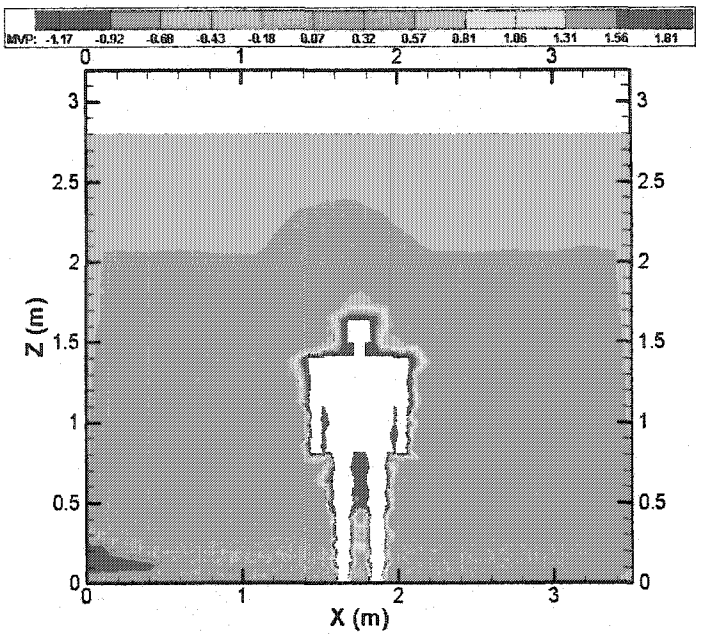

b) Inlet velocity = 0.15 m/s

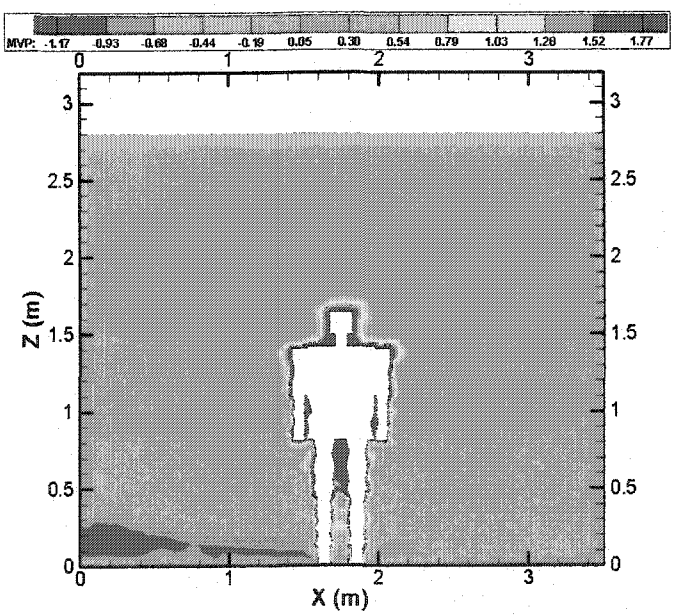

c) Inlet velocity = 0.25 m/s

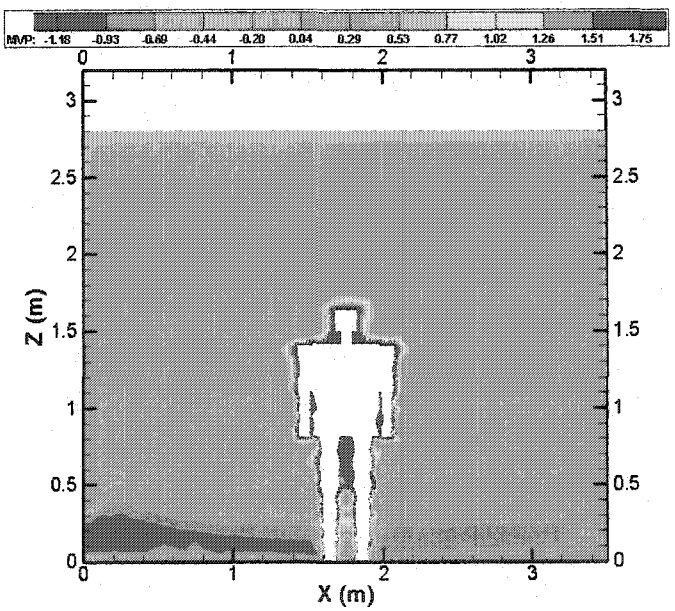

d) Inlet velocity = 0.35 m/s

Figure 5.14 PMV index for different inlet velocities

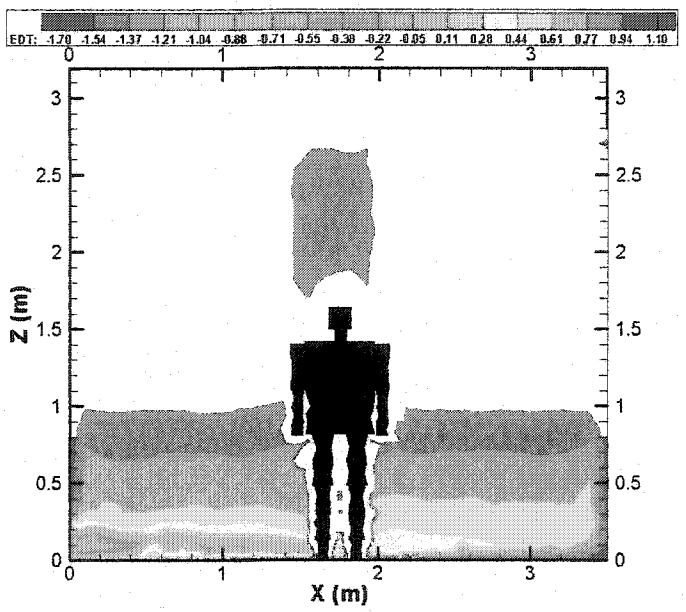

a) Inlet velocity = 0.05 m/s

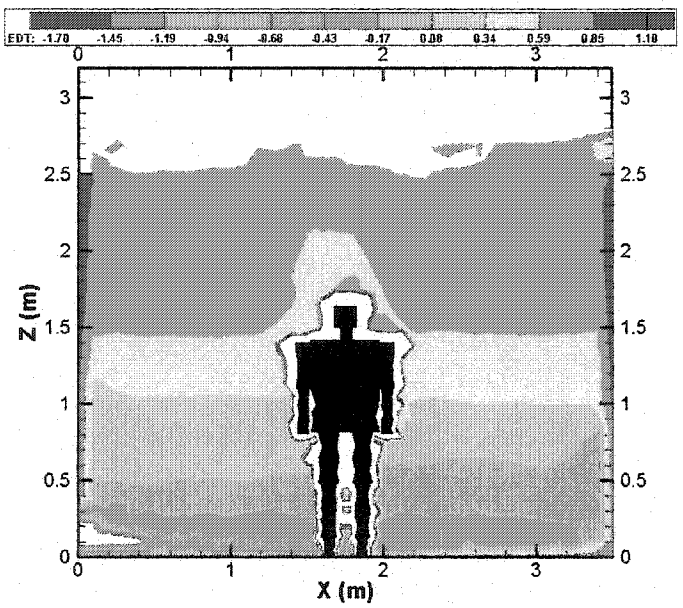

b) Inlet velocity = 0.15 m/s

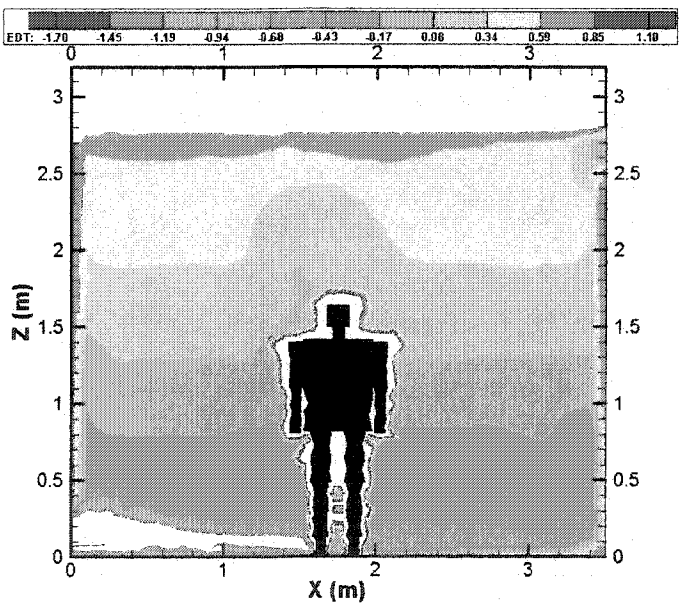

c) Inlet velocity = 0.25 m/s

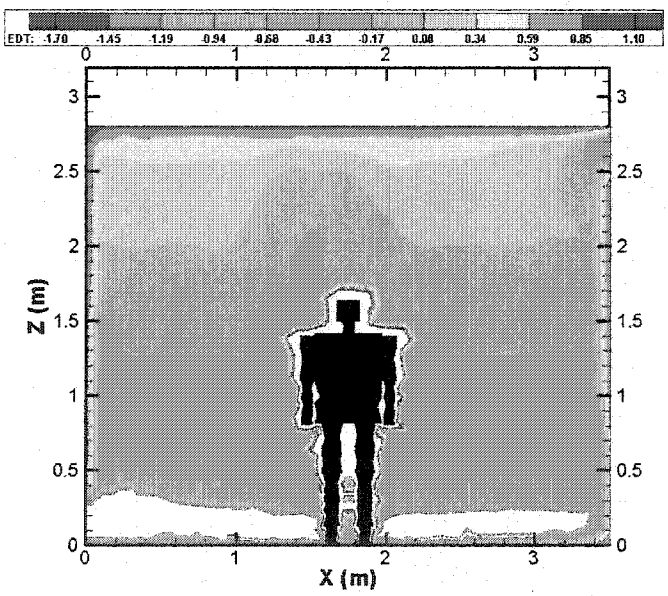

d) Inlet velocity = 0.35 m/s

Figure 5.15 EDT index for different inlet velocities

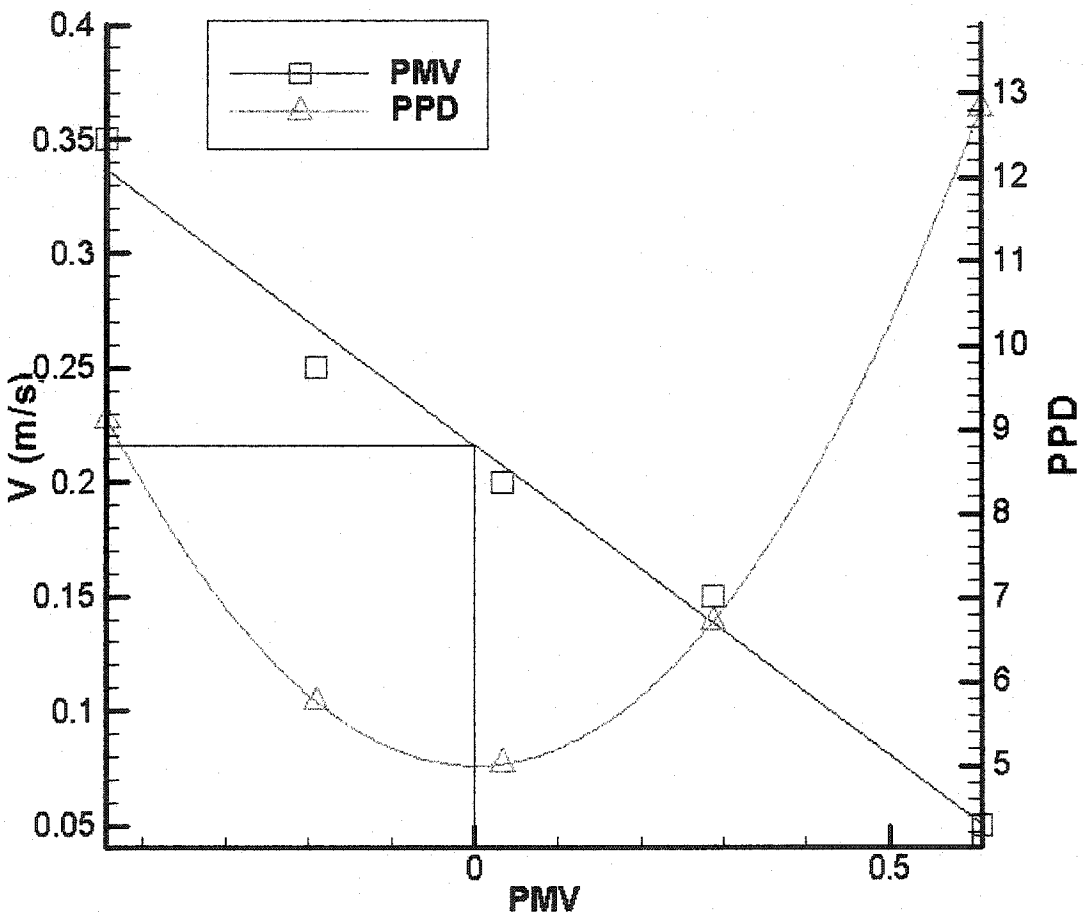

Figure 5.16 inlet velocity vs. PMV & PPD

5.3.3 Effect of Relative Humidity

The effect of inlet air relative humidity on human thermal comfort is evaluated by varying it from 20 percent to 80 percent in the steps of 20 percent. For all these cases the inlet air temperature, velocity and occupant metabolic rate are fixed at 19°C, 0.2 m/s and 100 W/m^2 respectively. The calculated room air temperature and velocity variations are shown in Figs. 5.17 and 5.18. Figure 5.19(a)-(d) shows the PMV index computed from the calculated room air temperature and velocity field in the room. Results show that for the lowest humidity, the average PMV index is –0.24, indicating thermal comfort. For 40 % and 60 % relative humidity cases, the average PMV values are -0.1 and 0.18 respectively, indicating near neutral conditions. In the final case, at 80 % relative humidity, the average index value is 0.34, again implying thermal comfort. It is noted that increasing humidity while keeping inlet dry bulb temperature fixed, results in the PMV value changing from -0.24 to +0.34. According to the PMV scale the sensation shifts from one of slight coolness to slight warm, but overall still staying in the comfort zone.

Figure 5.20 shows the variation of the EDT index in the room. One observes, that like the PMV index for this case, the EDT index also predicts that for all four cases the thermal comfort condition prevails throughout the room.

Figure 5.21 shows the variation of PMV and PPD as a function of the supply air relative humidity. The optimal value of inlet relative humidity which leads to zero PMV value and minimum value of PPD is about 48 %. This value represents the best comfort.

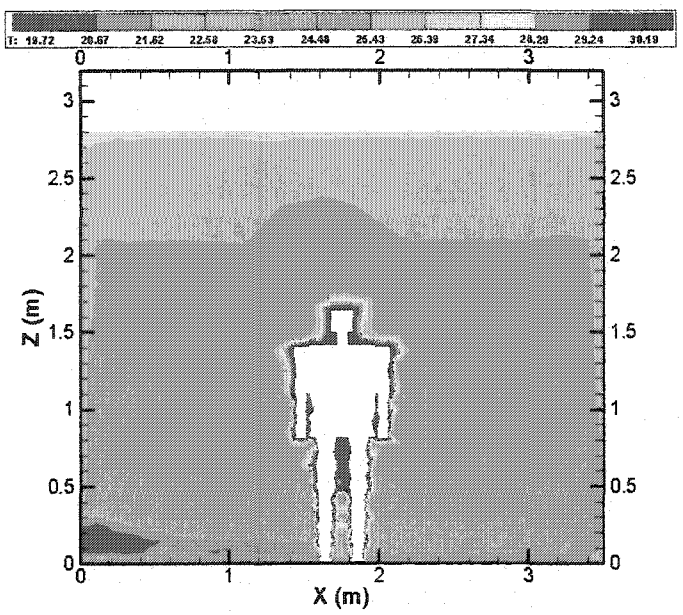

a) Relative humidity = 20 %

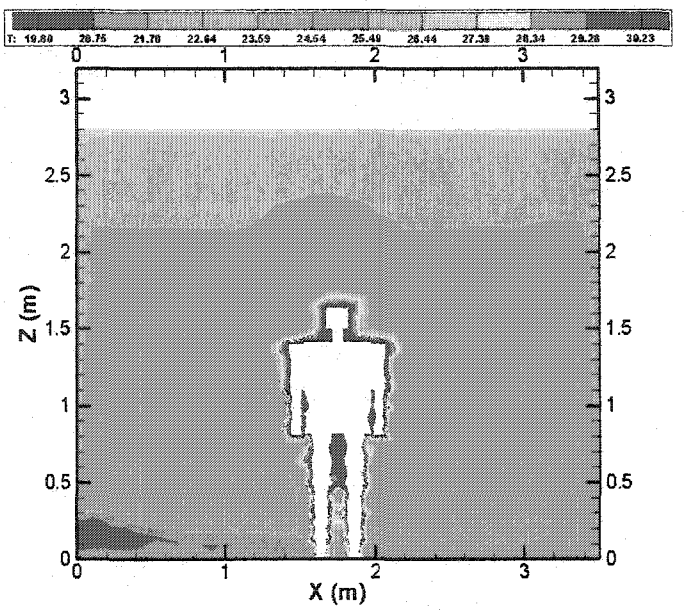

b) Relative humidity = 40 %

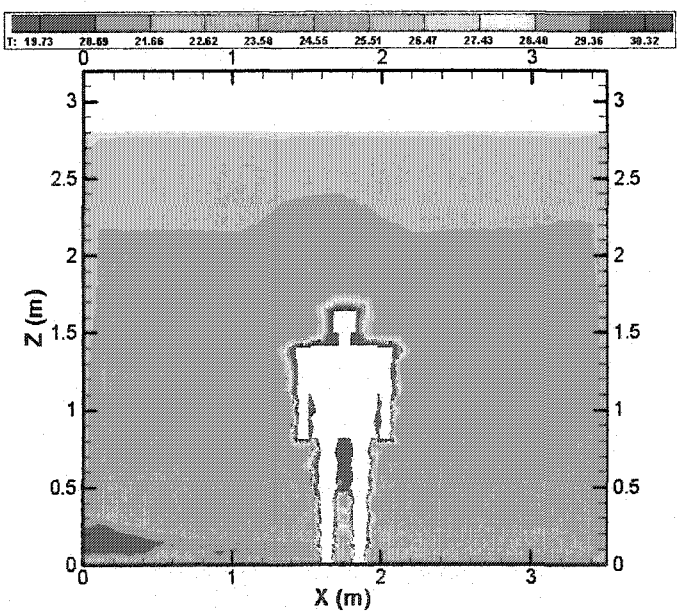

c) Relative humidity = 60 %

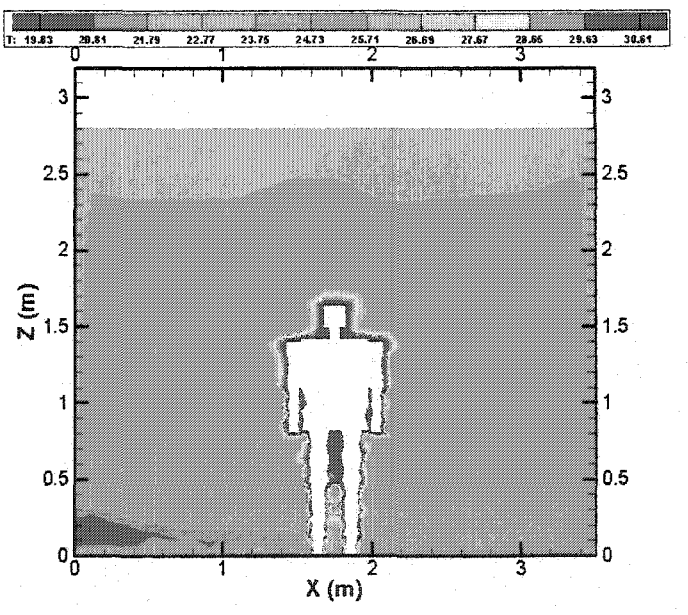

d) Relative humidity = 80 %

Figure 5.17 Temperature contours for different relative humidity

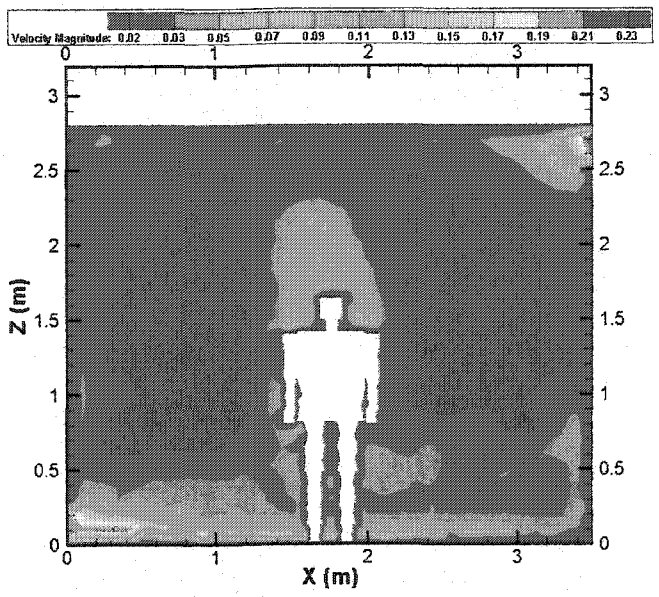

a) Relative humidity = 20 %

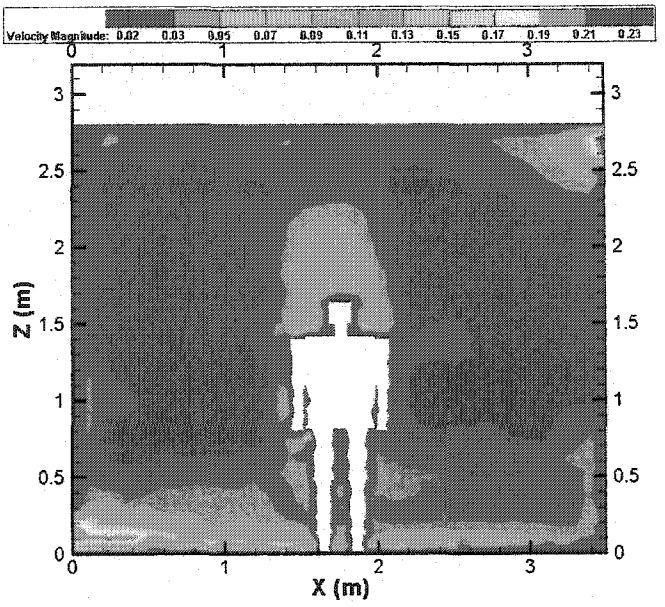

b) Relative humidity = 40 %

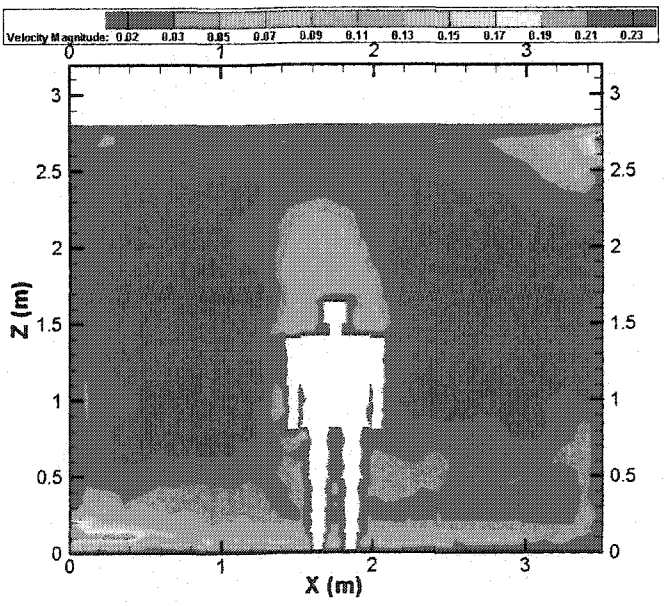

c) Relative humidity = 60 %

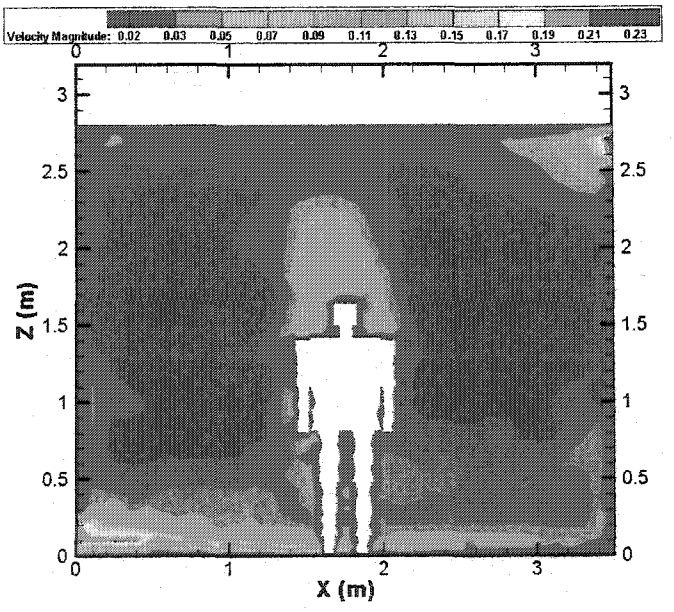

d) Relative humidity = 80 %

Figure 5.18 Velocity contours for different relative humidity

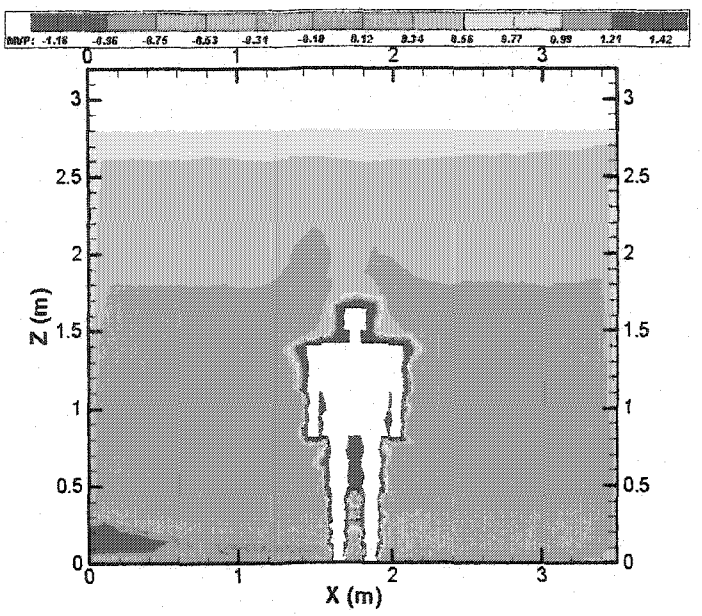

a) Relative humidity = 20 %

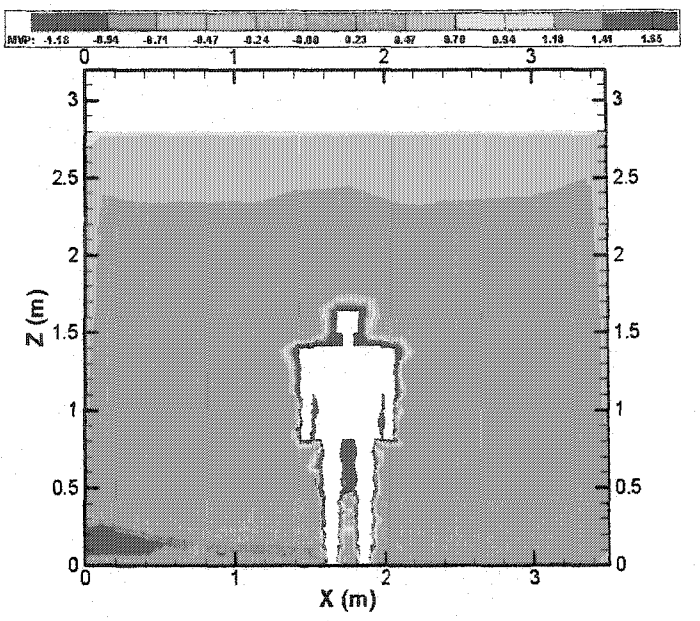

b) Relative humidity = 40 %

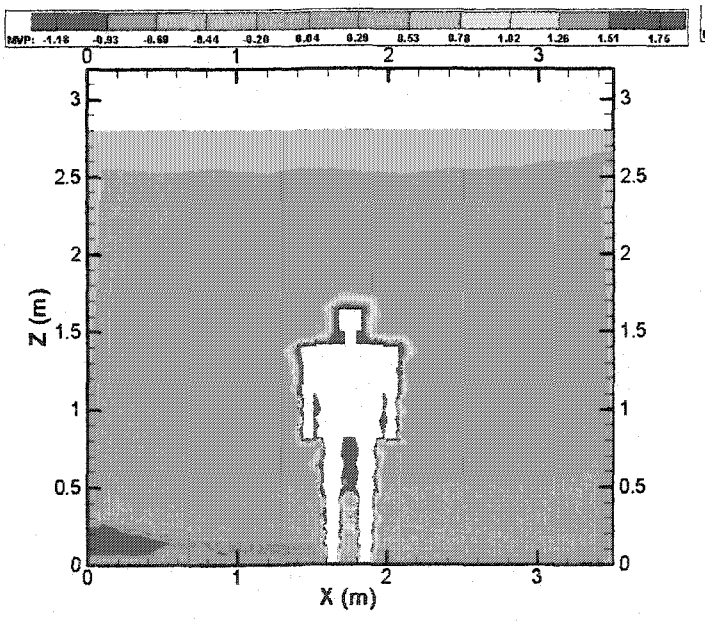

c) Relative humidity = 60 %

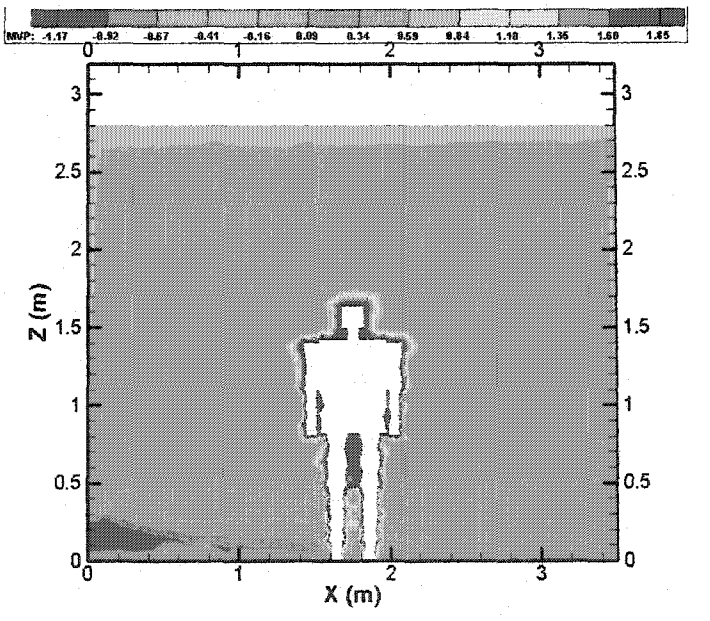

d) Relative humidity = 80 %

Figure 5.19 PMV index for different relative humidity

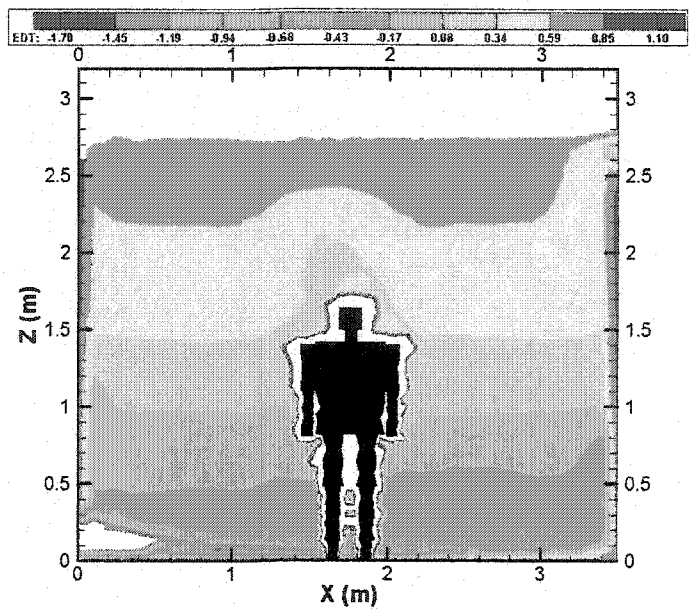

a) Relative humidity = 20 %

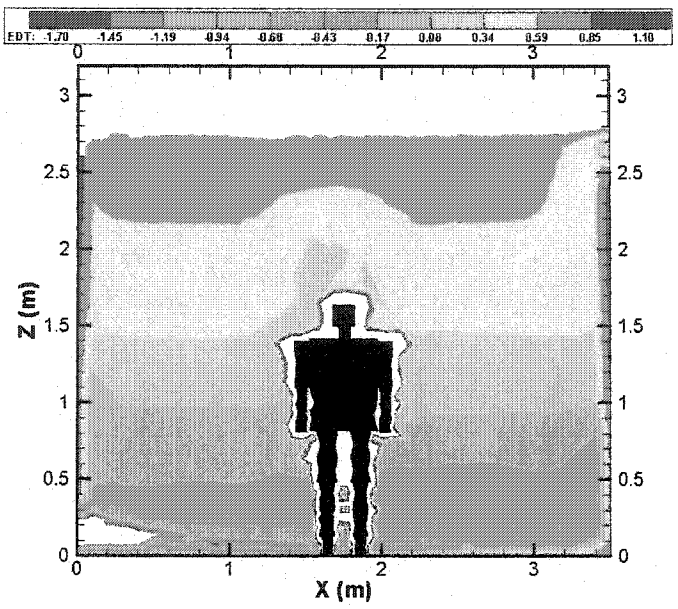

b) Relative humidity = 40 %

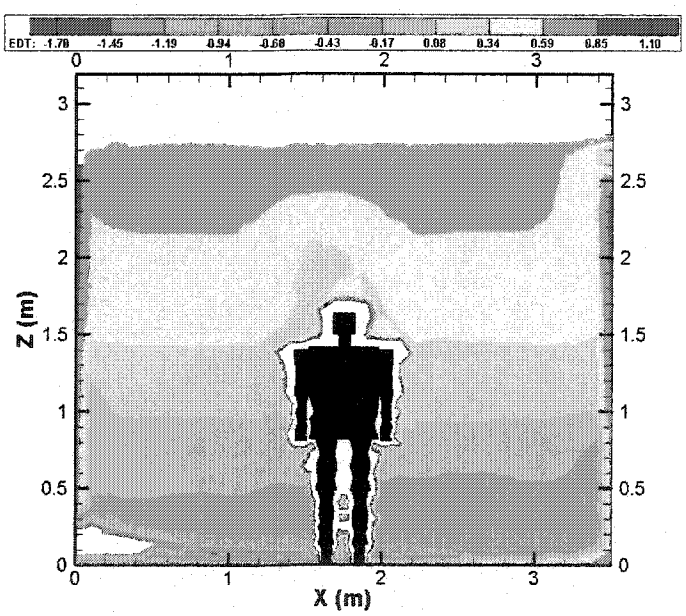

c) Relative humidity = 60 %

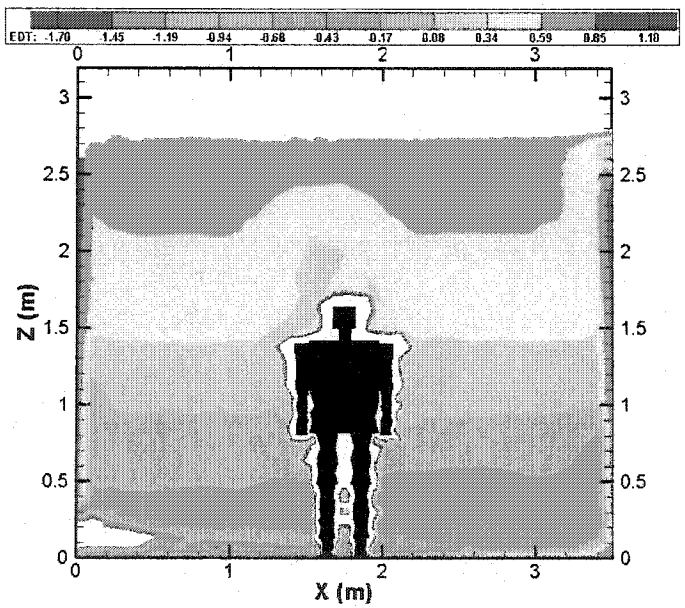

d) Relative humidity = 80 %

Figure 5.20 EDT index for different relative humidity

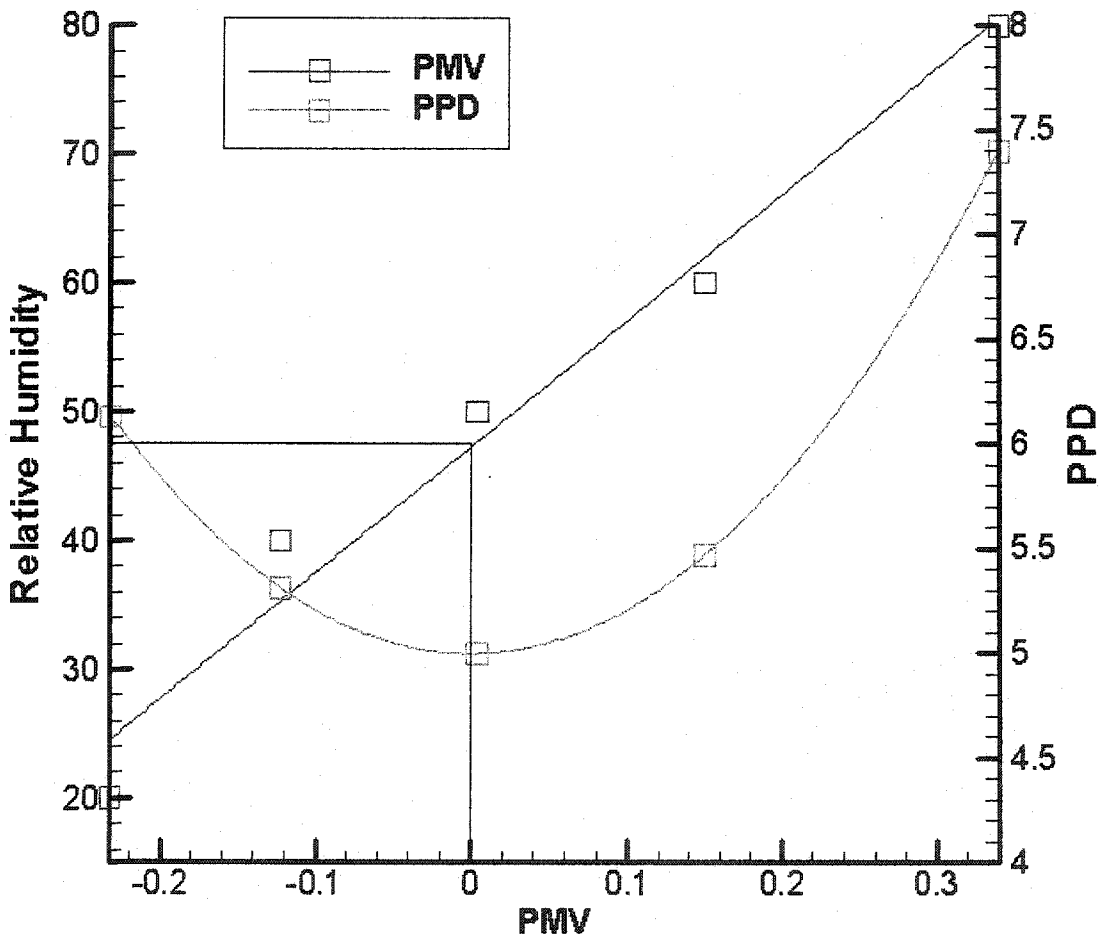

Figure 5.21 Relative humidity vs. PMV & PPD

5.3.4 Effect of Metabolic Activity

It has been noted earlier that the human metabolic activity can affect the thermal comfort condition in a ventilated room due to heat generation and dispersal. To assess this effect, four metabolic activity levels namely 50, 90, 170, and 210 W/m^2 are considered. The supply air conditions for all theses cases have been fixed at 19°C dry bulb temperature, 0.2 m/s air velocity and 50% relative humidity.

Figure 5.22(a)-(d) illustrates the effect of metabolic rate on room air temperature. In the first case with 50 W/m^2 metabolic rate, the average room air temperature is 24.74°C, and the temperature variation ranges from 19°C at floor level to 26.26°C near the ceiling. For the second case (M=90 W/m^2), the average room air temperature is 24.85 ^{0}C as compared to 24.97 ^{0}C temperature for the third case (M=170 W/m^2). For the highest metabolic rate (M=210 W/m^2), the average room air temperature is 25.12 ^{0}C. The rise in room air temperature is primarily due to addition of metabolic heat to the room air by the process of convection and radiation. Figure 5.23(a)-(d) shows the velocity contours for different metabolic rates. One can observe from this figure that as metabolic heat generation increases, the body heat generated plume intensifies. The region above the shoulder and head, extending all the way to ceiling shows high velocity field, with maximum velocity around 0.15 m/s.

Figure 5.24 (a)-(d) shows the maps of PMV index for different metabolic rates. For the first case (M=50 W/m^2), the lower two thirds of room tends to provide slightly cool sensation. In the second case (M=90 W/m^2), the calculated PMV values place the room in the comfort zone. For the third case (M=170 W/m^2), the upper part of

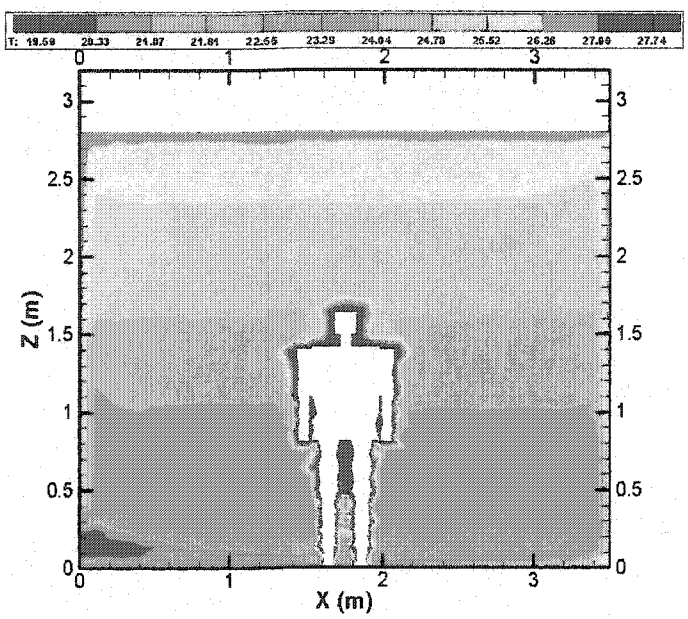

a) M = 50 W/ m^2

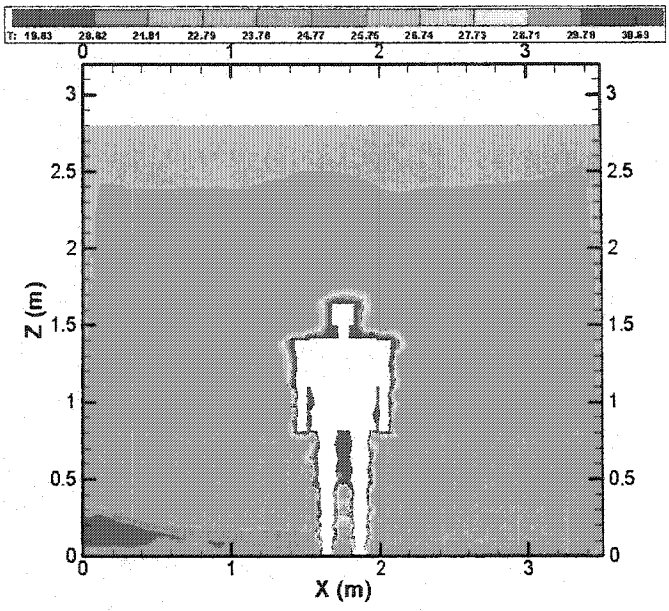

b) M = 100 W/ m^2

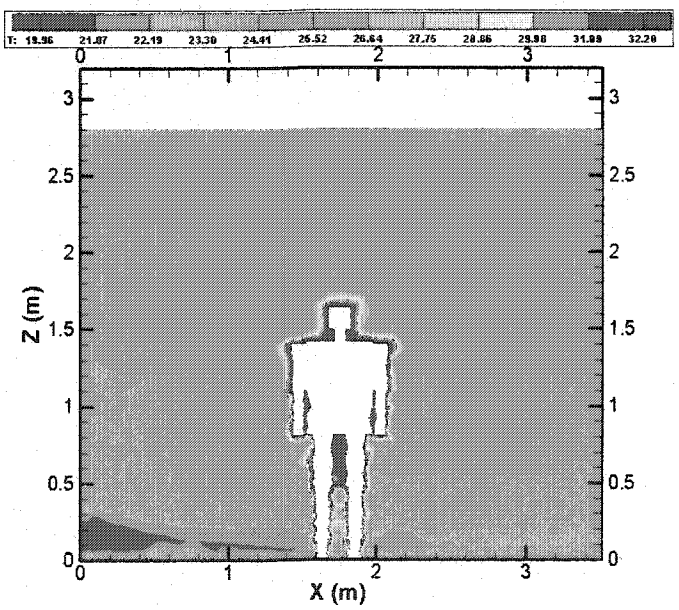

c) M = 150 W/ m^2

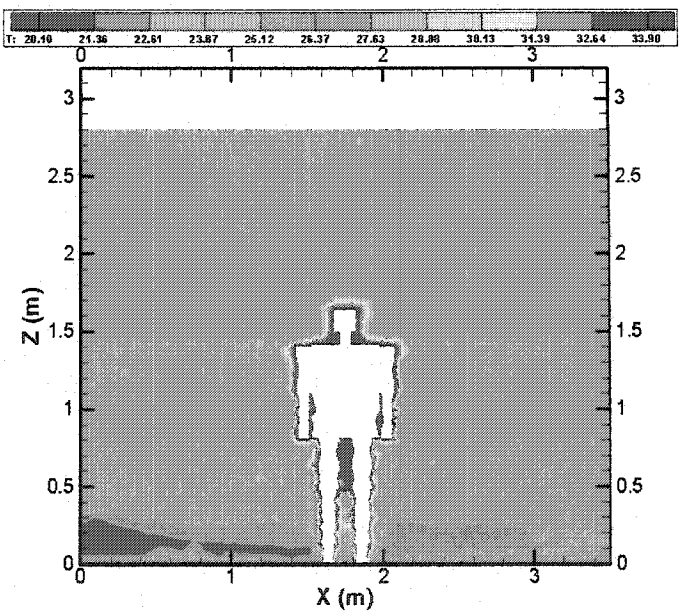

d) M = 200 W/ m^2

Figure 5.22 Temperature contours for different metabolic activity

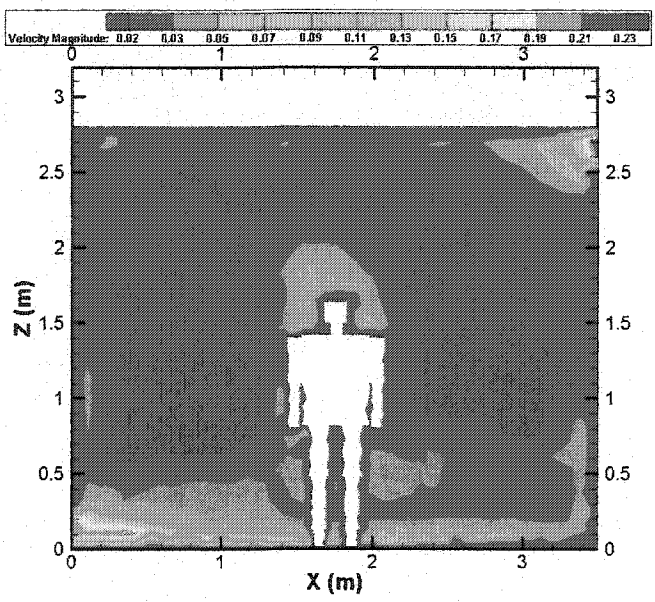

a) M = 50 W/ m^2

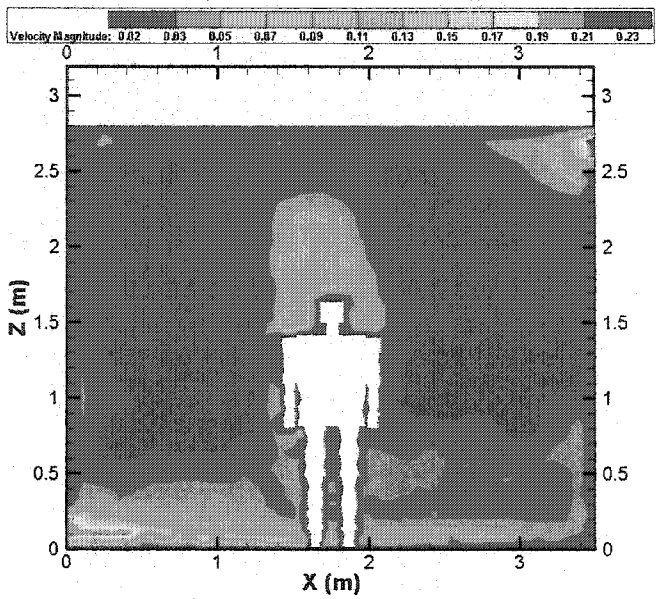

b) M = 100 W/ m^2

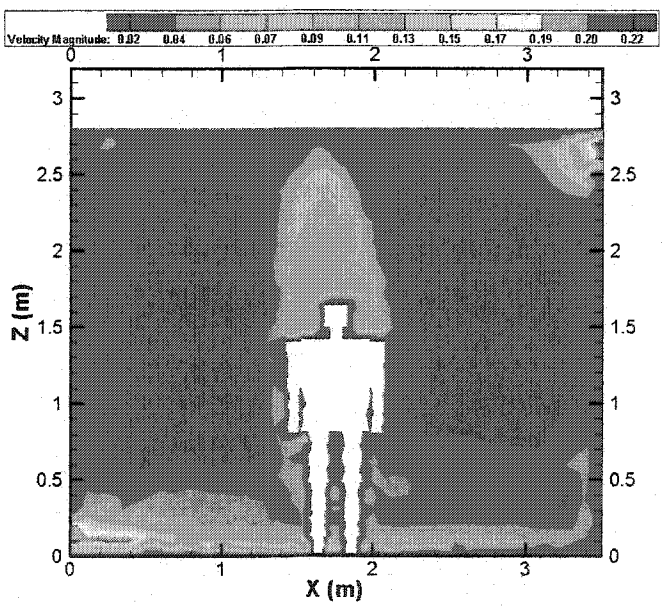

c) M = 150 W/ m^2

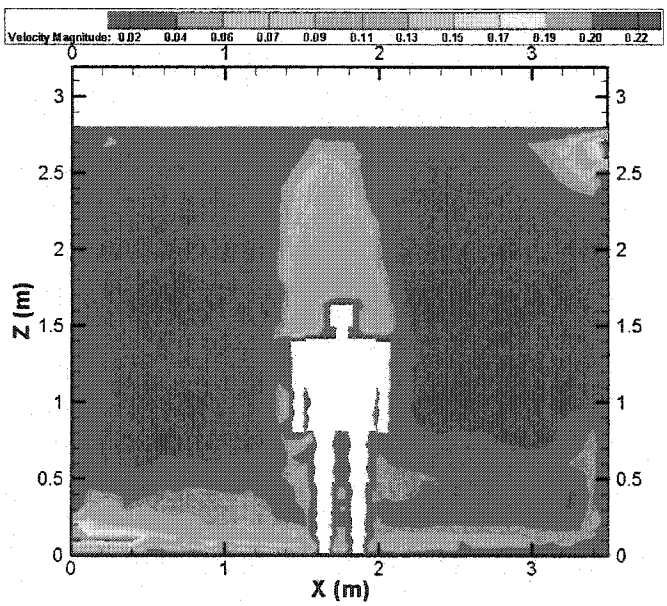

d) M = 200 W/ m^2

Figure 5.23 Velocity contours for different metabolic activity

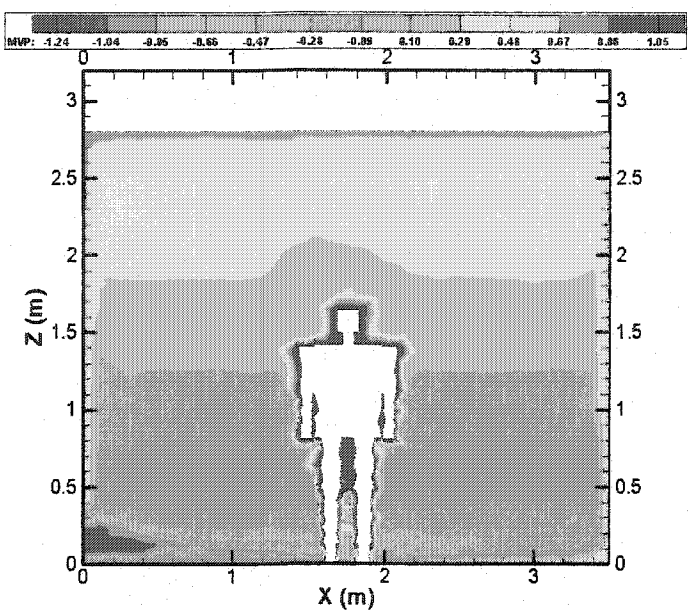

a) M = 50 W/ m^2

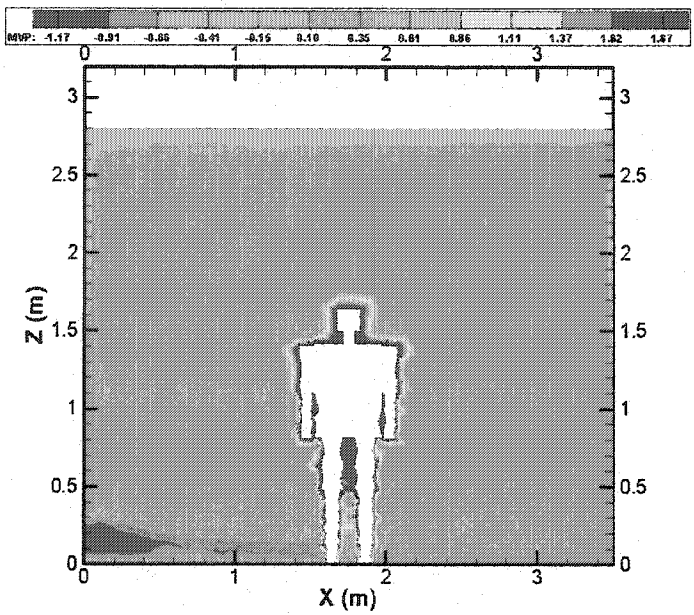

b) M = 100 W/ m^2

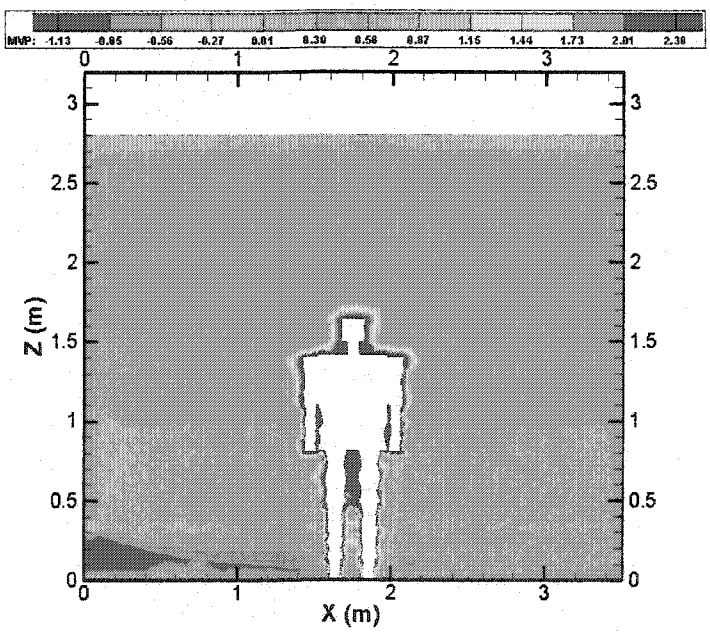

c) M = 150 W/ m^2

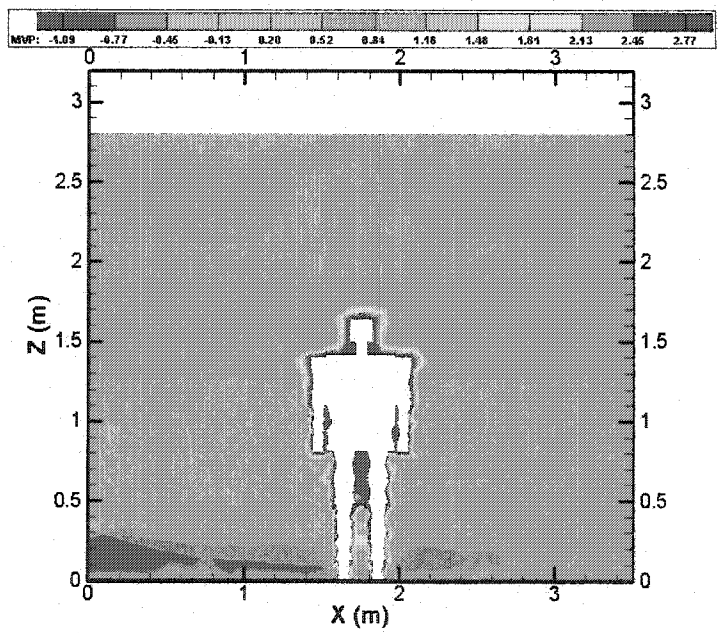

d) M = 200 W/ m^2

Figure 5.24 PMV index for different metabolic activity

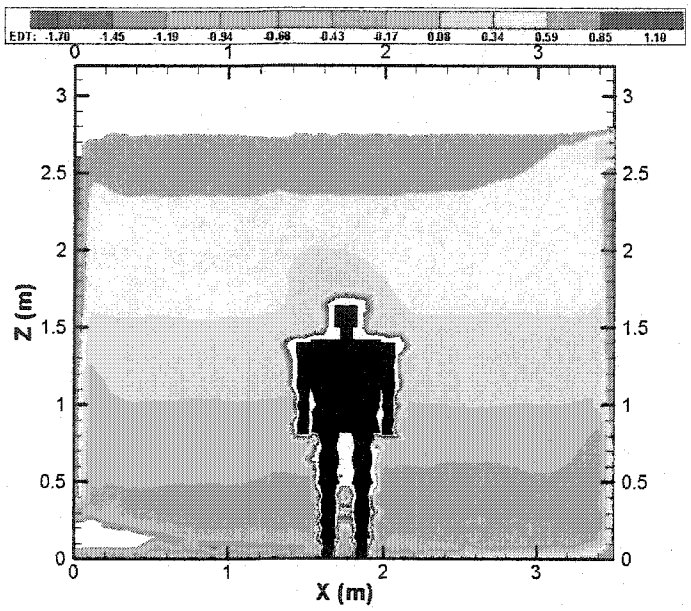

a) M = 50 W/ m^2

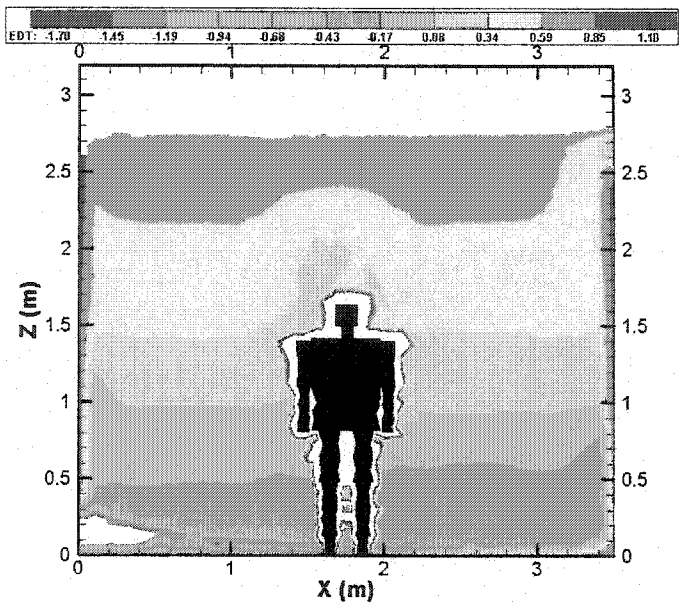

b) M = 100 W/ m^2

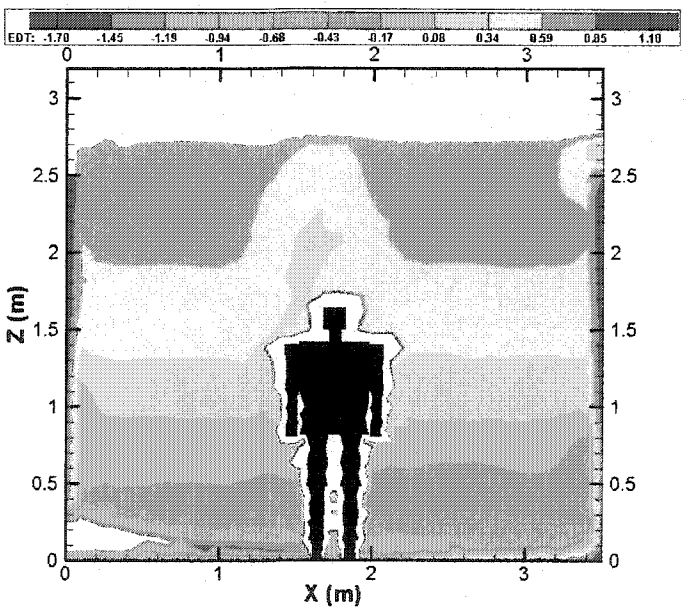

c) M = 150 W/ m^2

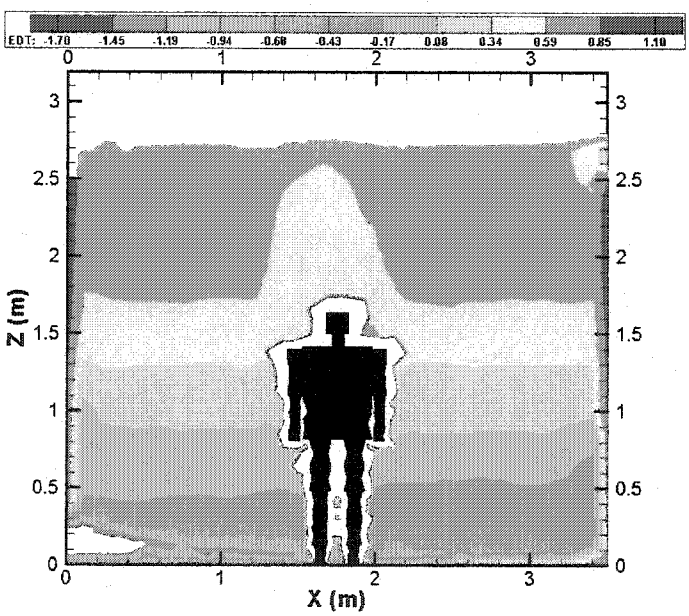

d) M = 200 W/ m^2

Figure 5.25 EDT index for different metabolic activity

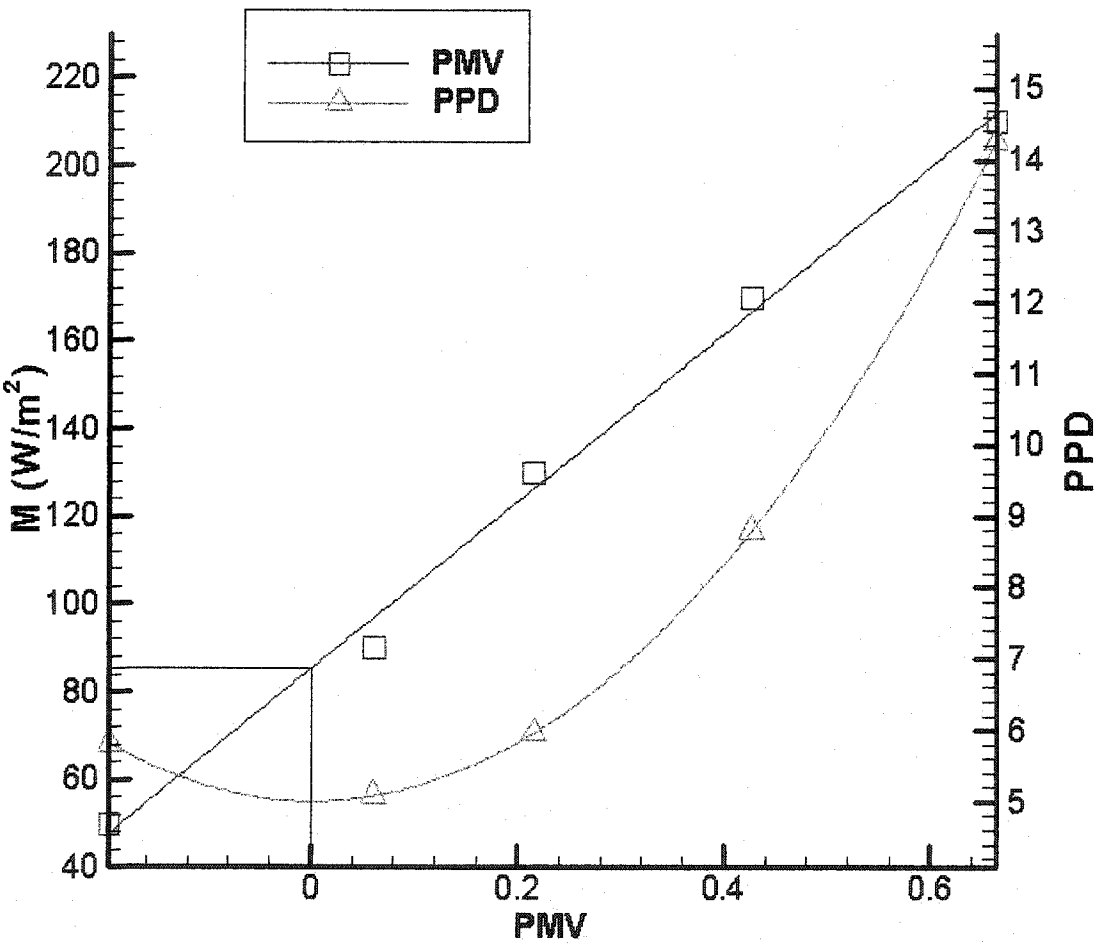

Figure 5.26 Metabolic activity rate vs. PMV & PPD

The room tends to provide warm sensation. At the highest activity level case, the PMV index gives an indication of thermal discomfort. The body is exposed to an environment which gives cool sensation in the lower part of the body and warm sensation in the upper part of the body.

Figure 5.25(a)-(d) presents the EDT index. It is noted that despite changing activity level, one observes that almost all levels in the room are in comfort zone. As metabolic rate increases, the region of warm sensation grows while the region of cool sensation shrinks in size.

In Fig. 5.26, a relationship between the metabolic activity level and the average PMV and PPD is presented. This figure indicates that a minimum value of PPD equal to 5 percent is achieved for a value of M=85 W/m^2 . This indicates that 95 percent of the occupants will be satisfied with supply conditions of T=19 ^0C, V=0.2 m/s and RH=50 %.

5.4 Effect of the Turbulence Intensity Level

As stated previously, the accepted turbulence intensity in the indoor airflow simulation is between 1 and 10 %. To evaluate effect of turbulence intensity, three different levels namely 2.5 %, 5 % and 7.5 % have been chosen for simulation. For all three cases, the metabolic activity is assumed to be 100 W/m^2 and supply conditions are maintained at 19 ^0C dry bulb temperature, 0.2 m/s air inlet velocity and 50 percent relative humidity.

Figures 5.27, 5.28 and 5.29 show the variation of room air temperature, velocity

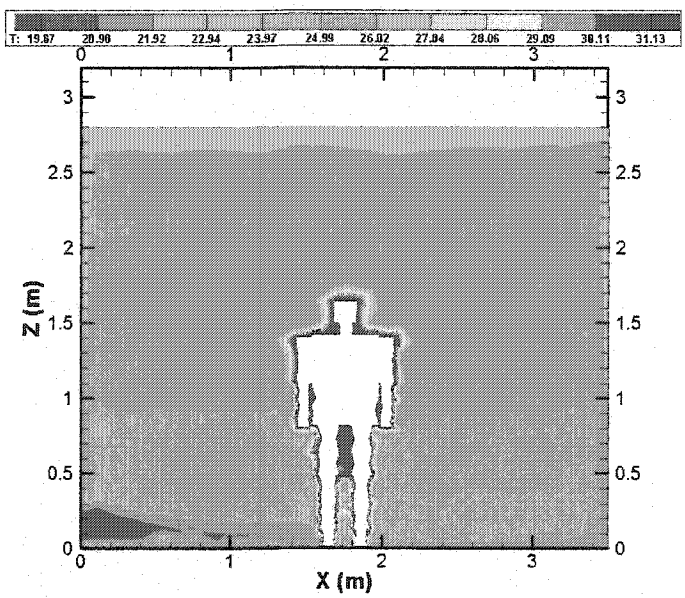

a) Intensity level = 2.5 %

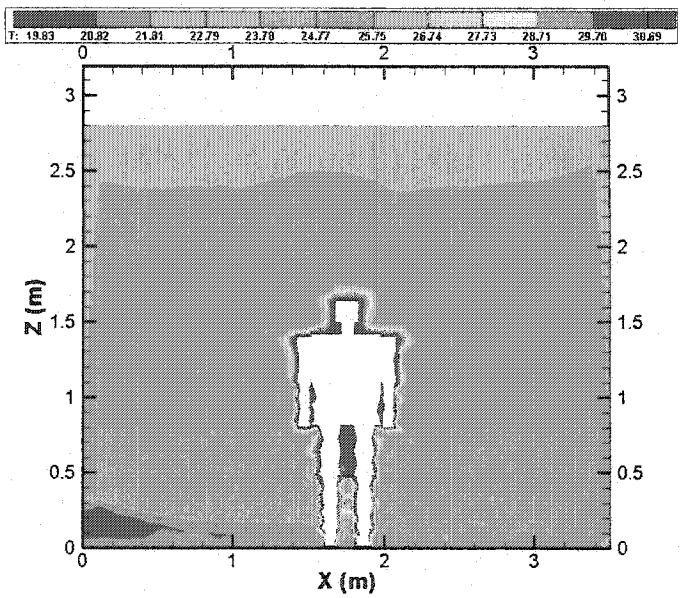

b) Intensity level = 5 %

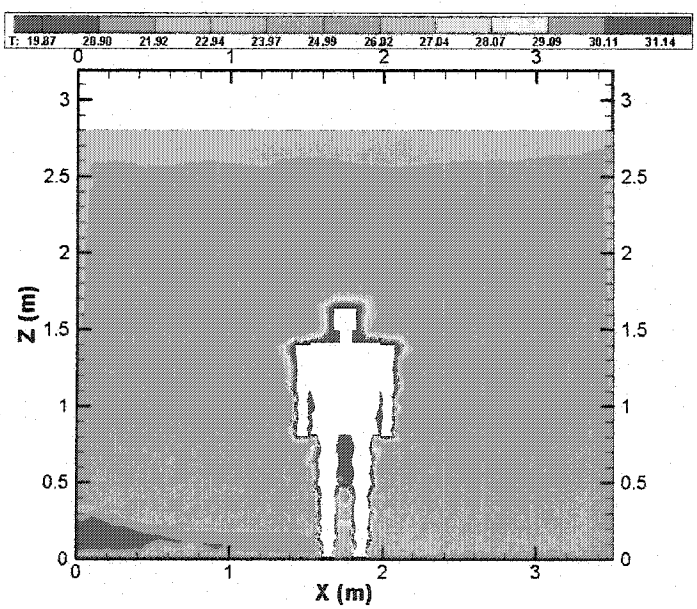

c) Intensity level = 7.5 %

Figure 5.27 Temperature contours for different intensity levels

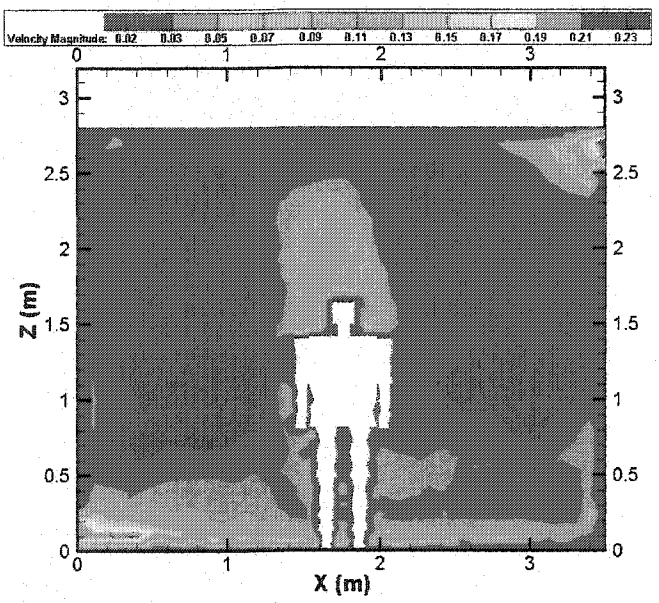

a) Intensity level = 2.5 %

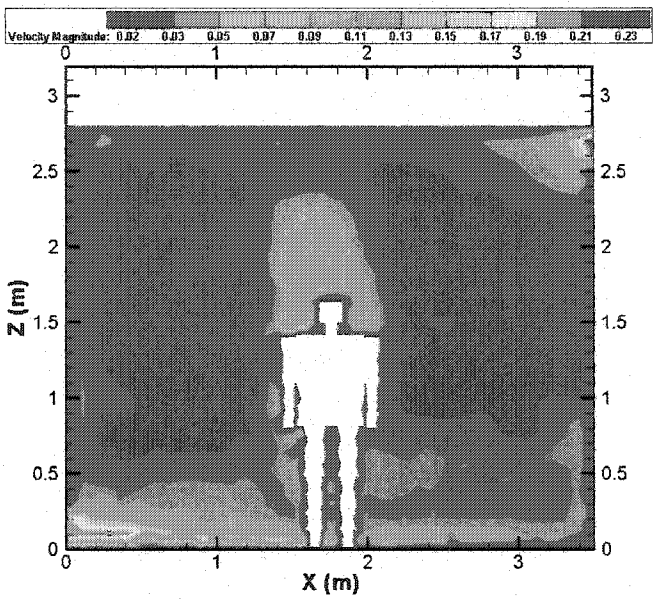

b) Intensity level = 5 %

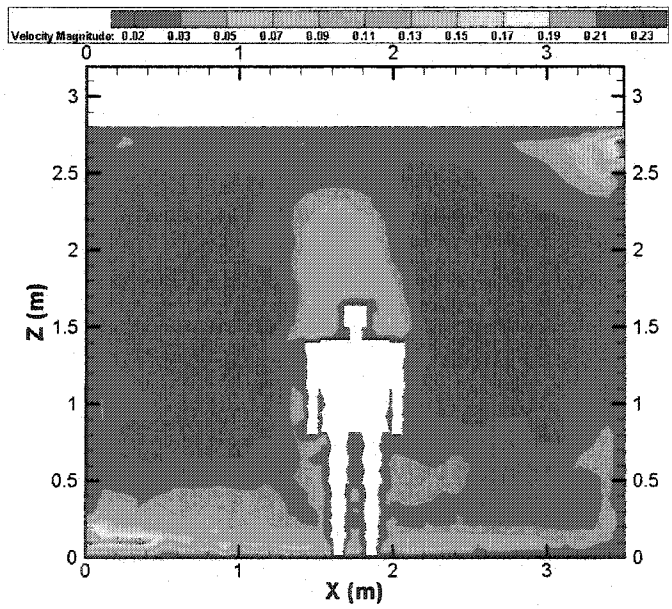

c) Intensity level = 7.5 %

Figure 5.28 Velocity contours for different intensity levels

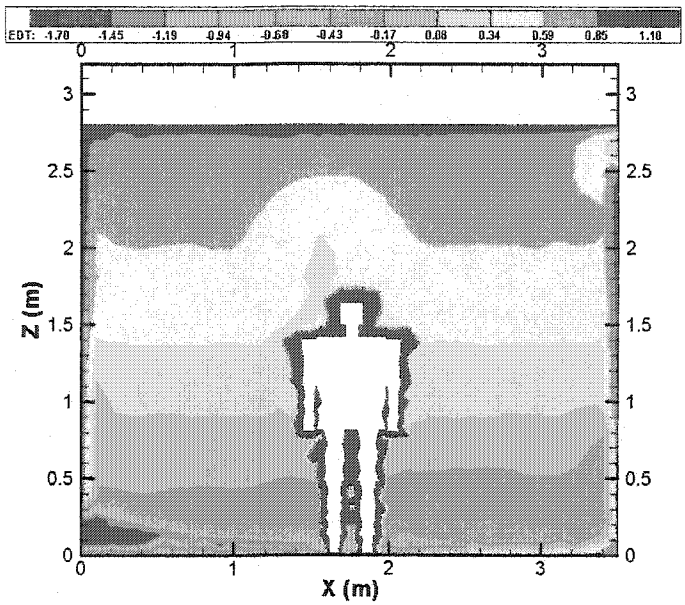

a) Intensity level = 2.5 %

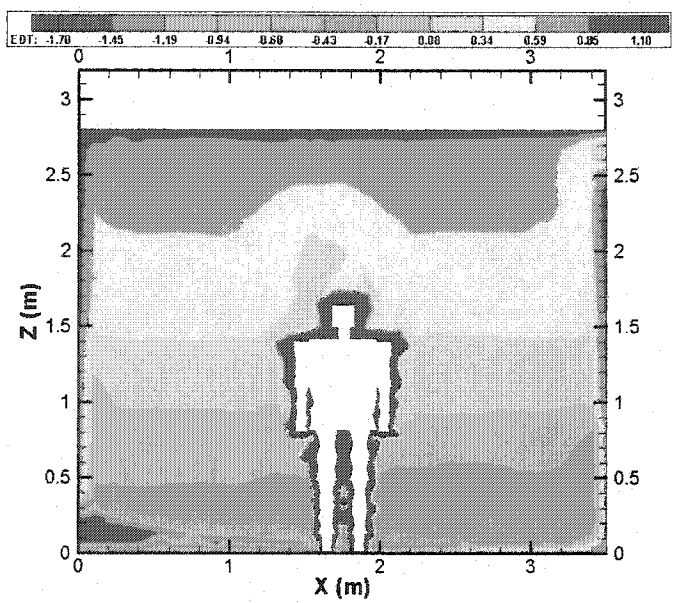

b) Intensity level = 5 %

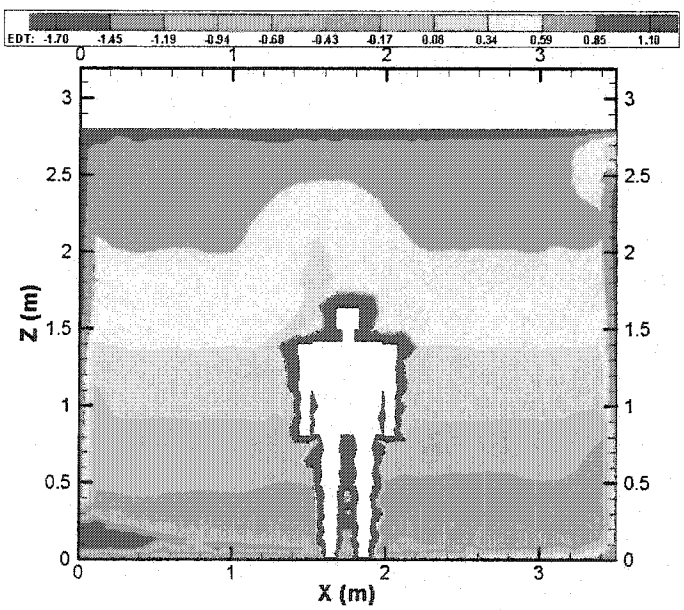

c) Intensity level = 7.5 %

Figure 5.29 EDT index for different intensity levels

and the EDT index. Results shown in these figures indicate that effects of inlet air turbulence intensity are minimal on the variation of these parameters in the room.

5.5 Segmented Body Model

One of the objectives of this study is to develop a segmented body model that uses different segments to model corresponding human body parts. The total number of segments included in the present model is nine including; the head, neck, two arms, two hands, two legs, two feet and the main middle part of the human body. The purpose of the segmented body model is to incorporate the varying properties of human body parts to predict varying skin temperature and to analyze its effect on the micro-environment variables and the overall thermal human comfort.

5.5.1 Variation of Skin Temperature and Convective Heat Transfer Coefficient

In order to achieve above objectives, variation of skin temperature, convective heat transfer and the heat transfer coefficient were analyzed by implementing the segmented body model. The details of the model are given in Appendix A. These results are presented below.

Figure 5.30 shows the skin temperature variation for the human body. The skin temperature increases from 31.2 °C at the bottom of the right foot that is closer to supply vent, to 34.8 °C near the head region. The average skin temperature is 33.6 °C for the conditions chosen for the present case. Figure 5.31 illustrates the calculated convective

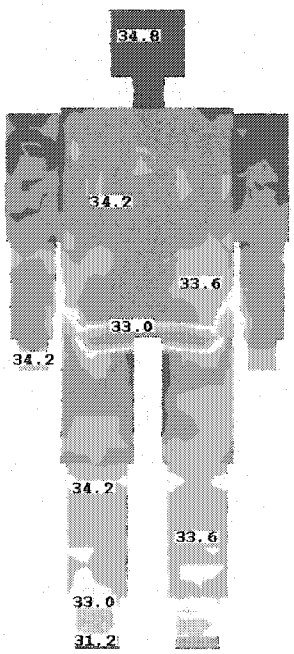

Figure 5.30 Body skin temperatures

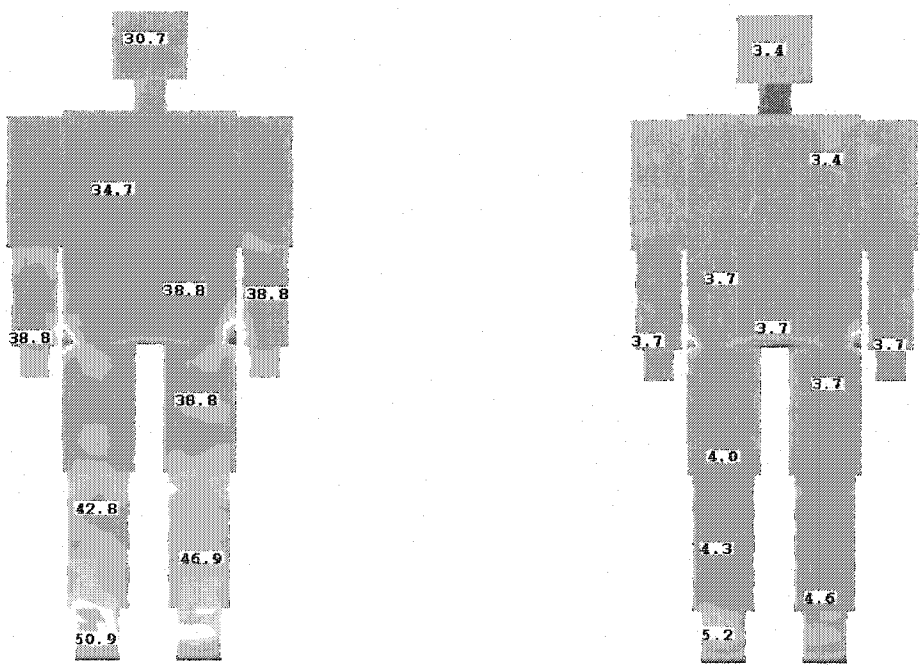

Figure 5.31 Convective heat transfer & coefficient

heat transfer rate and convective heat transfer coefficient variations on the human body surface. The convective heat transfer rate value ranges from 50.7 W/m^2 at bottom right foot to a value of 30.7 W/m^2 in the upper region of the body, with the average rate being 41 W/m^2. As shown in Fig. 5.31, higher values of convective heat transfer coefficient are predicted around leg and feet regions as 5.2 W/m^2 K. In contrast, lower values of convective heat transfer coefficient 3.4 W/m^2 K, prevailed in the upper chest and the head regions. The average value of convective heat transfer coefficient is predicted as 4.1 W/m^2 K for the entire body. This is comparable to values cited in the literature [36].

5.5.2 Thermal Comfort Using Segmented Model

Four main cases have been studied for different human metabolic activity levels: 50 W/m^2, 90 W/m^2, 170 W/m^2 and 210 W/m^2. All other parameters for the supply air in the room are kept at air temperature 19 ^{0}C, air velocity 0.2 m/s and the relative humidity 50 %.

Figure 5.32(a)-(d) presents temperature contours. The results show that increasing the metabolic activity level leads to increase in the average air temperature in the room which changes from 24.62 ^{0}C to 25.05 ^{0}C as the metabolic rate increases from 50 W/m^2 to 210 W/m^2.

Figure 5.33(a)-(d) shows velocity contours for different activity levels. The changing activity level creates higher velocity fields (human body plume) particularly

near the shoulder and head region of the body, because of the buoyancy effect. The higher the metabolic activity level, the higher is air velocity magnitude above the body.

Figure 5.34(a)-(d) shows the thermal comfort zone predicted from the PMV index. The first case shows that the entire body is in the zone of cool sensation. The second case gives a better sensation of thermal comfort. The third case indicates a little warmth sensation in the room. The final case shows a warmer sensation inside the room.

Figure 5.35(a)-(d) shows thermal comfort zone indicated by the EDT index. It is clear that the higher of activity rate, wider the region of warm sensation and narrower the region of cool sensation.

Figure 5.36 illustrates the relationship between the metabolic activity level and the average values of the two comfort indices PMV and PPD in the room. The figure gives the best activity level for the thermal comfort as 78 W/m^2 as compared to the uniform skin temperature model that yielded an optimal value of 87 W/m^2.

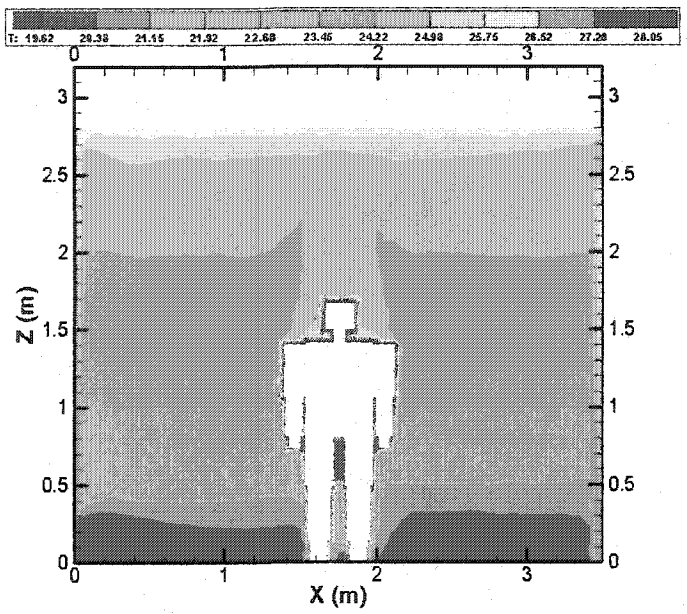

a) M = 50 W/ m^2

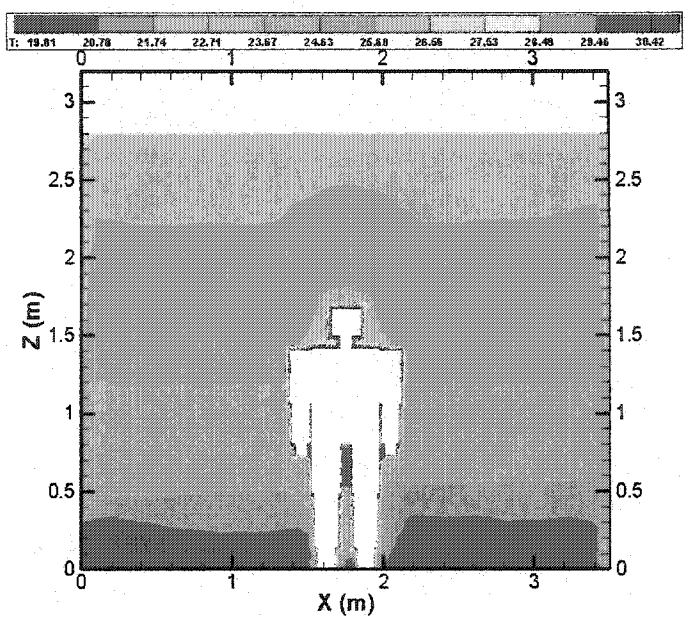

b) M = 100 W/ m^2

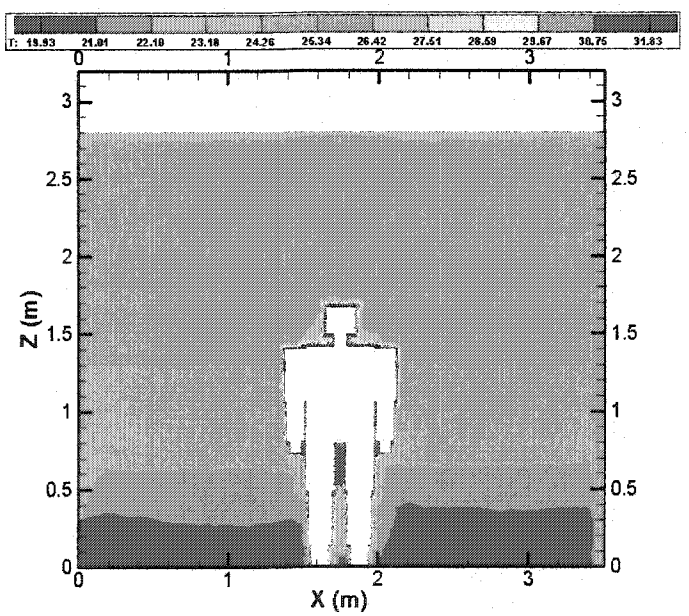

c) M = 150 W/ m^2

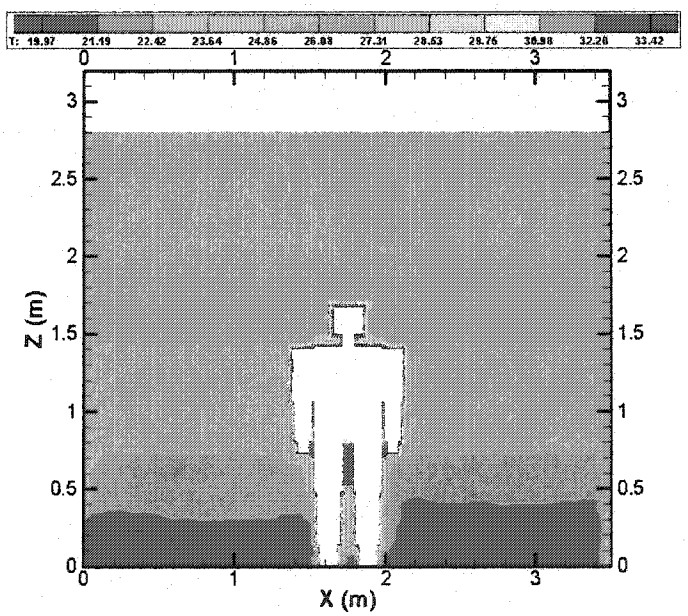

d) M = 200 W/ m^2

Figure 5.32 Temperature contours for different metabolic activity

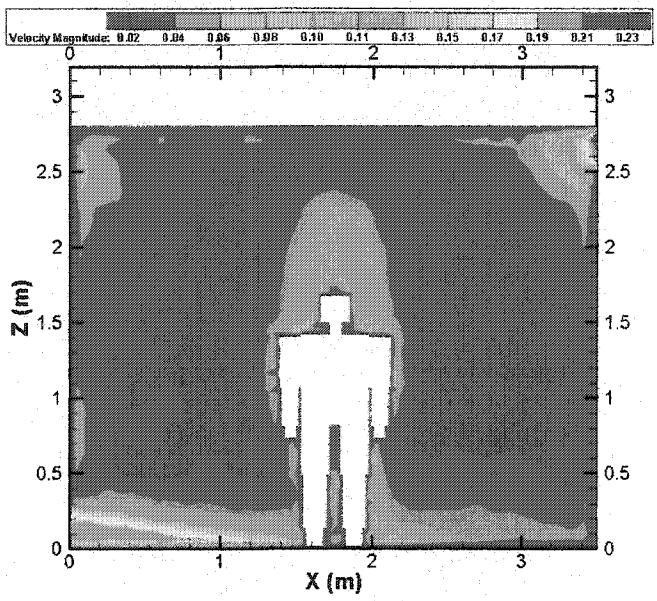

a) M = 50 W/ m^2

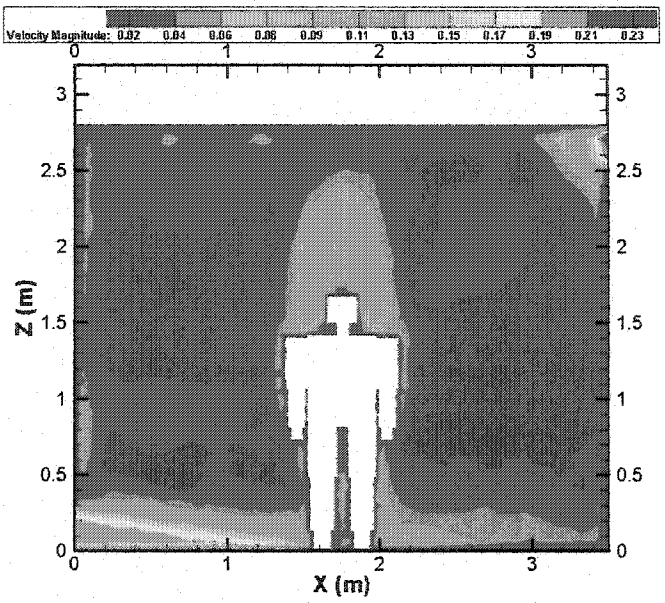

b) M = 100 W/ m^2

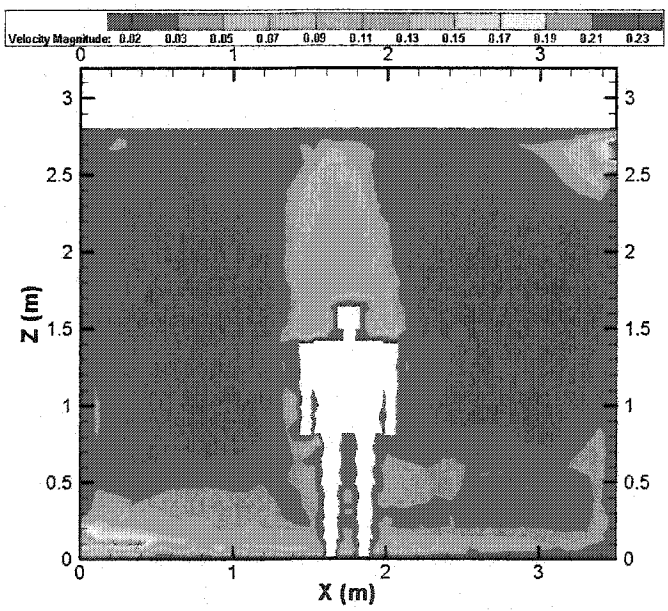

c) M = 150 W/ m^2

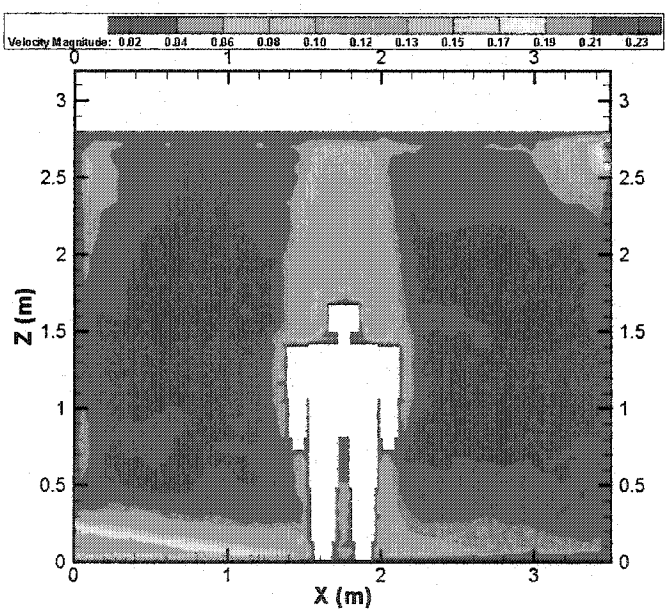

d) M = 200 W/ m^2

Figure 5.33 Velocity contours for different metabolic activity

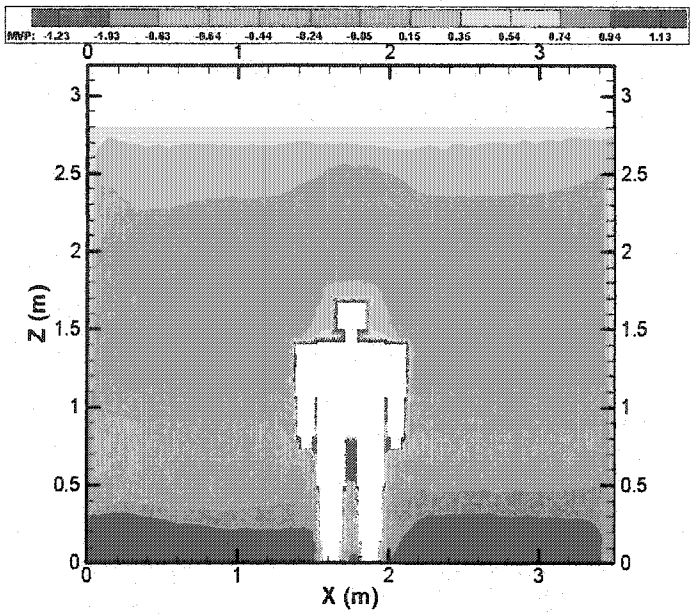

a) M = 50 W/ m^2

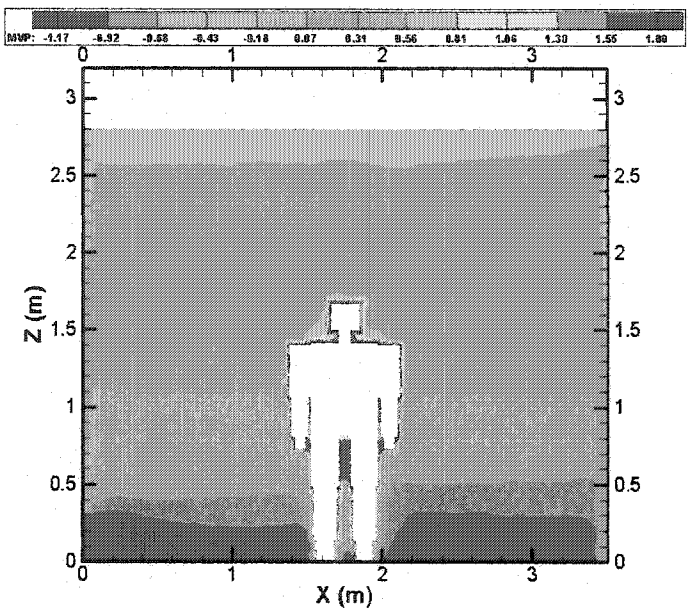

b) M = 100 W/ m^2

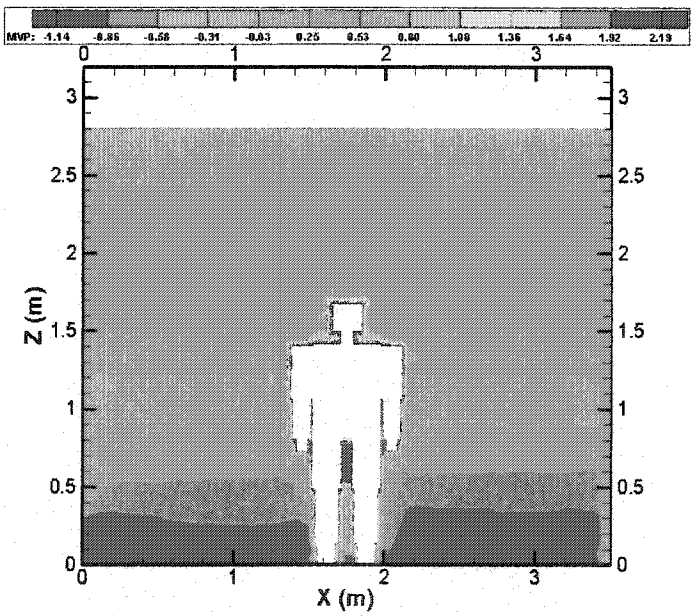

c) M = 150 W/ m^2

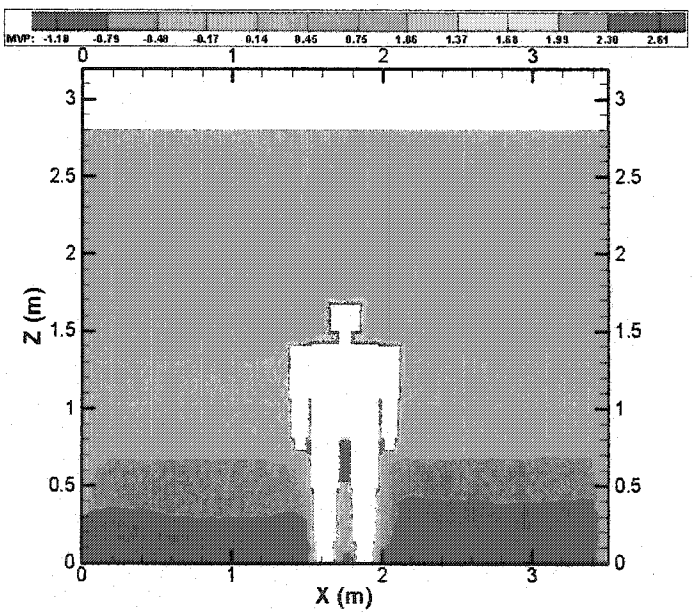

d) M = 200 W/ m^2

Figure 5.34 PMV index for different metabolic activity

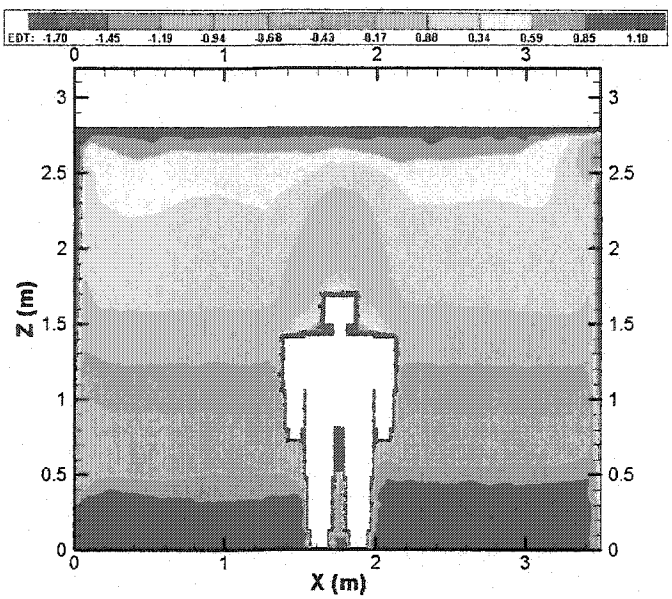

a) M = 50 W/ m^2

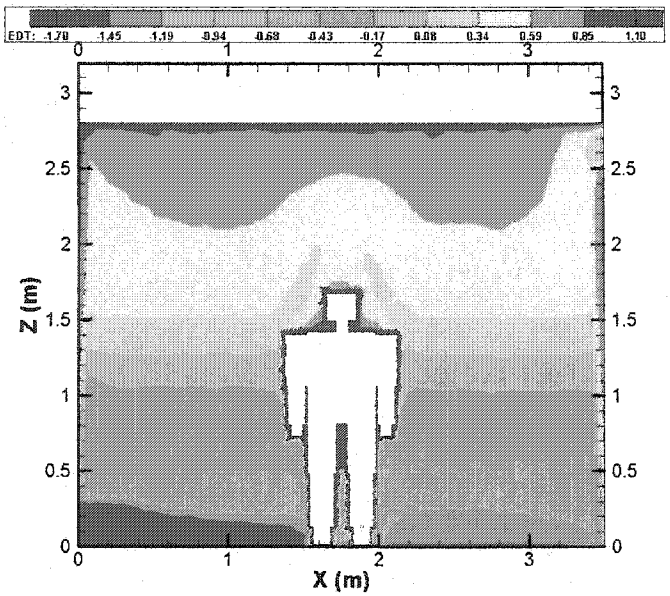

b) M = 100 W/ m^2

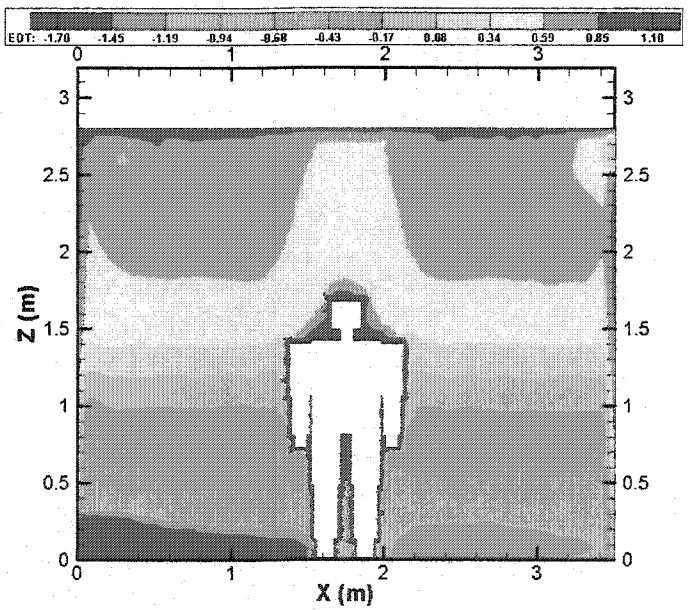

c) M = 150 W/ m^2

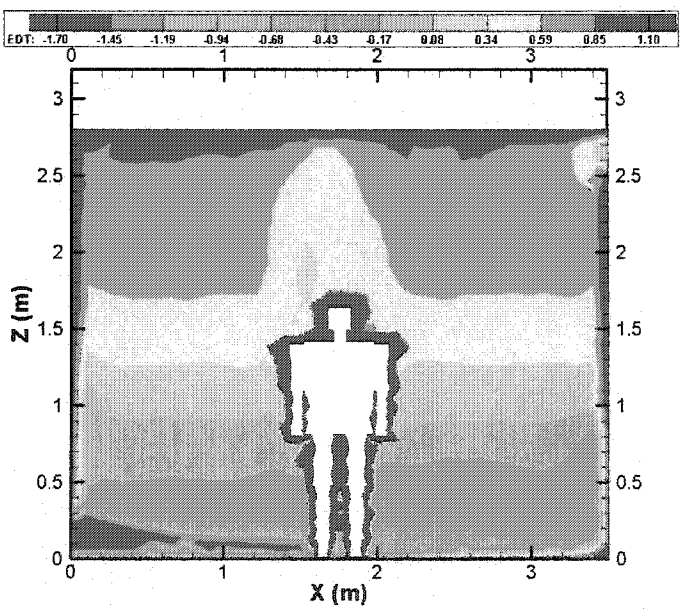

d) M = 200 W/ m^2

Figure 5.35 EDT index for different metabolic activity

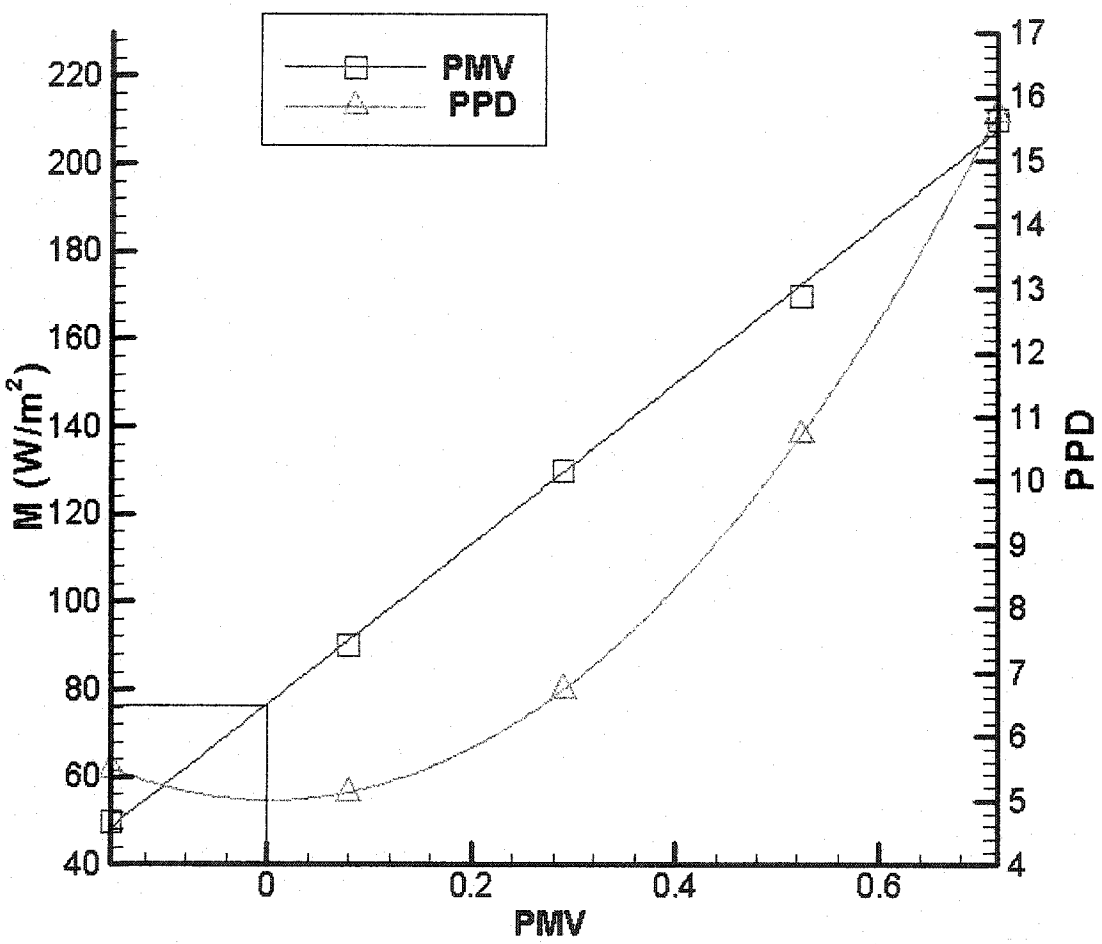

Figure 5.36 Metabolic activities vs. PMV & PPD

5.6 Effect of Environmental and Physical Parameters on the Skin and Core Temperatures

Figures 5.37-5.40 show the relationship between the body core and skin temperatures as a function of air temperature, velocity and relative humidity, and metabolic heat generation rate. These temperatures are predicted from the coupled human thermo-regulation model and the CFD model. Figure 5.37 indicates that as the supply air temperature increase from 10°C to 30°C, the body core temperature increases in a very narrow range from 36.7°C to 37.1°C, a rise of about 0.4°C. The core temperature is regulated in a very narrow range by human thermal regulation process. However, skin temperature is much more sensitive to the supply air temperature. Figure 5.37 shows that it increases from 32.85°C to 34.75°C, a rise of 1.9°C.

The effect of supply air velocity is shown in Fig. 5.38. It is noted that there is a very slight decrease of 0.17 °C in the core temperature as the supply air velocity increases from 0.05 to 0.35 m/s. On the other hand, the skin temperature decreases from nearly 34°C to 33°C. This is physically reasonable and expected behavior since increased flow velocity results in higher convective heat loss from the body.

Figure 5.39 shows that relative humidity has barely perceptible effect on core temperature, and insignificant effect on the skin temperature. The effect of metabolic rate is shown in Fig. 5.40. As expected, one observes that both core and skin temperatures are strongly influenced by metabolic heat generation rate. This is because metabolic heat generation term appears explicitly in the two node human body model, and consequently it directly affects the two nodal temperatures, namely skin and

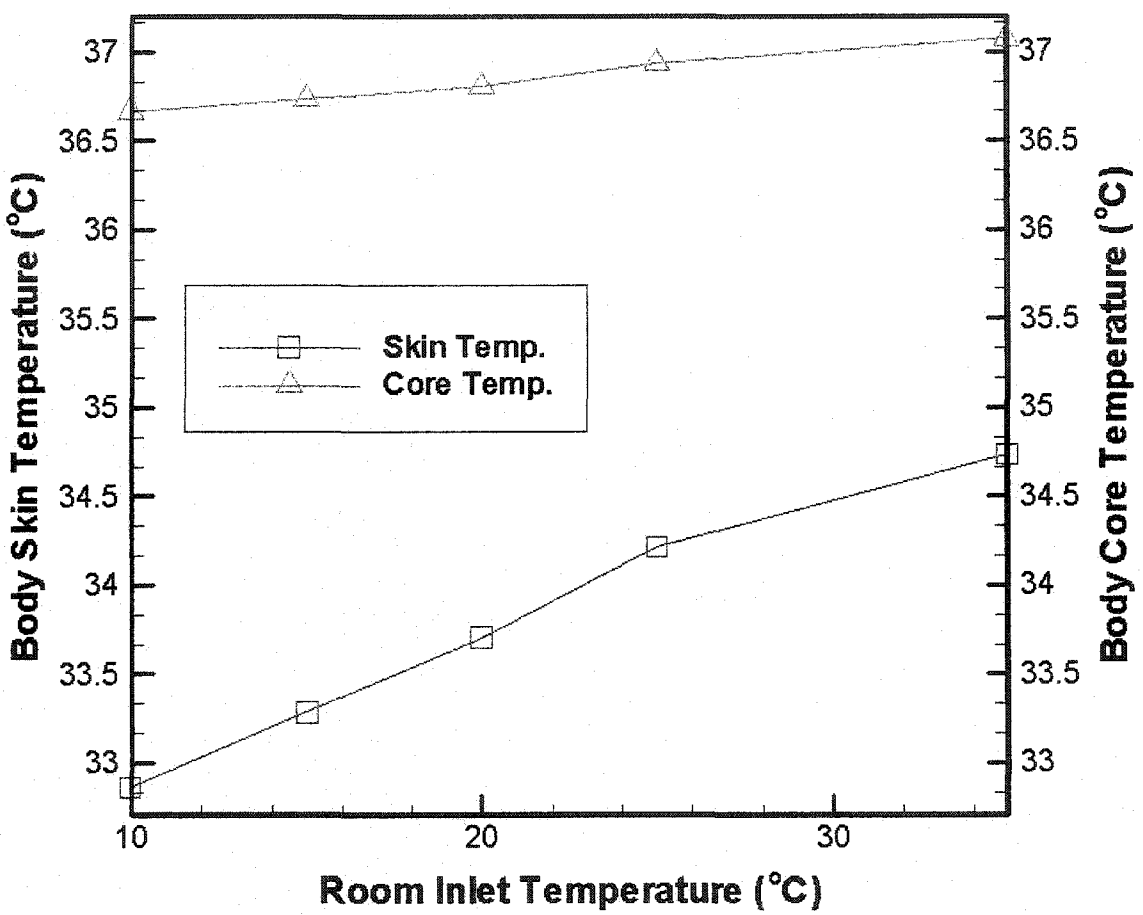

Figure 5.37 Core and skin temperatures as function of room inlet air temperature

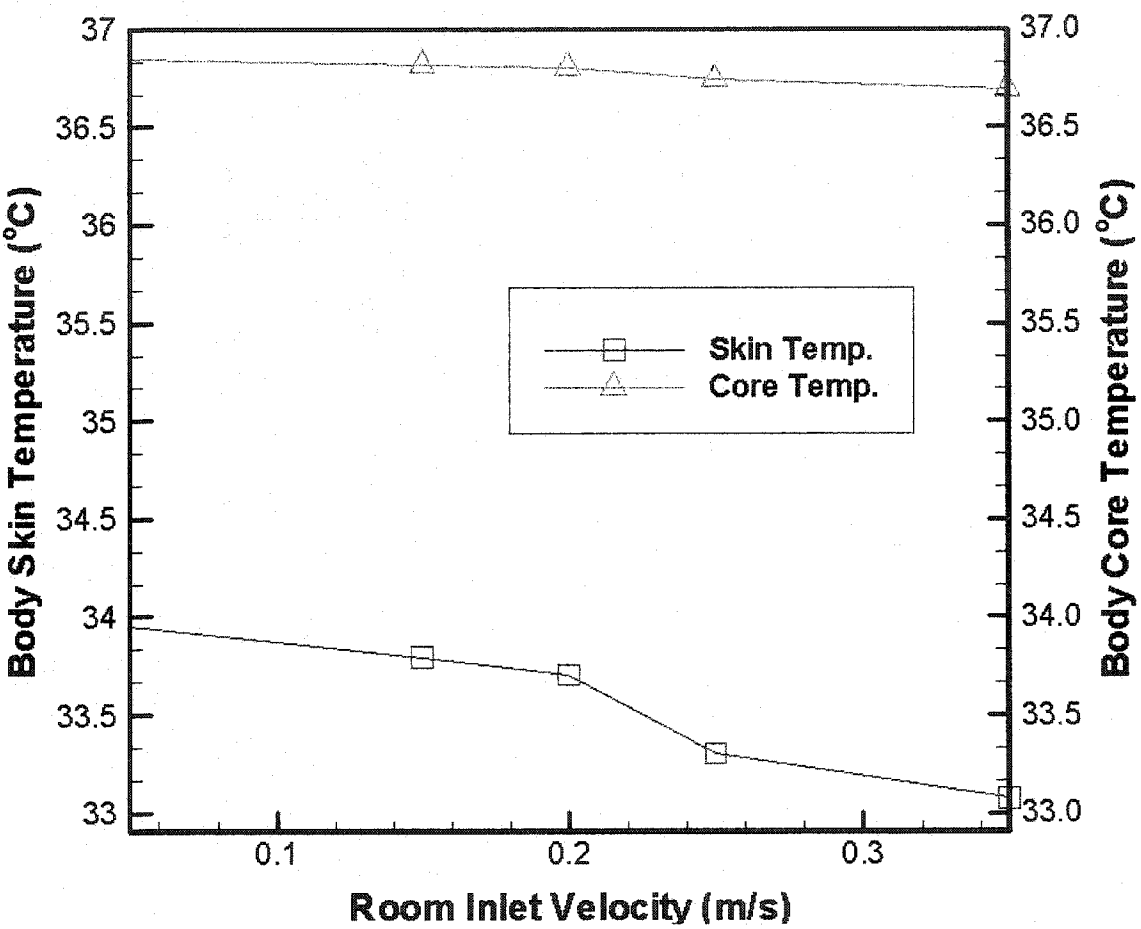

Figure 5.38 Core and skin temperatures as function of air velocity

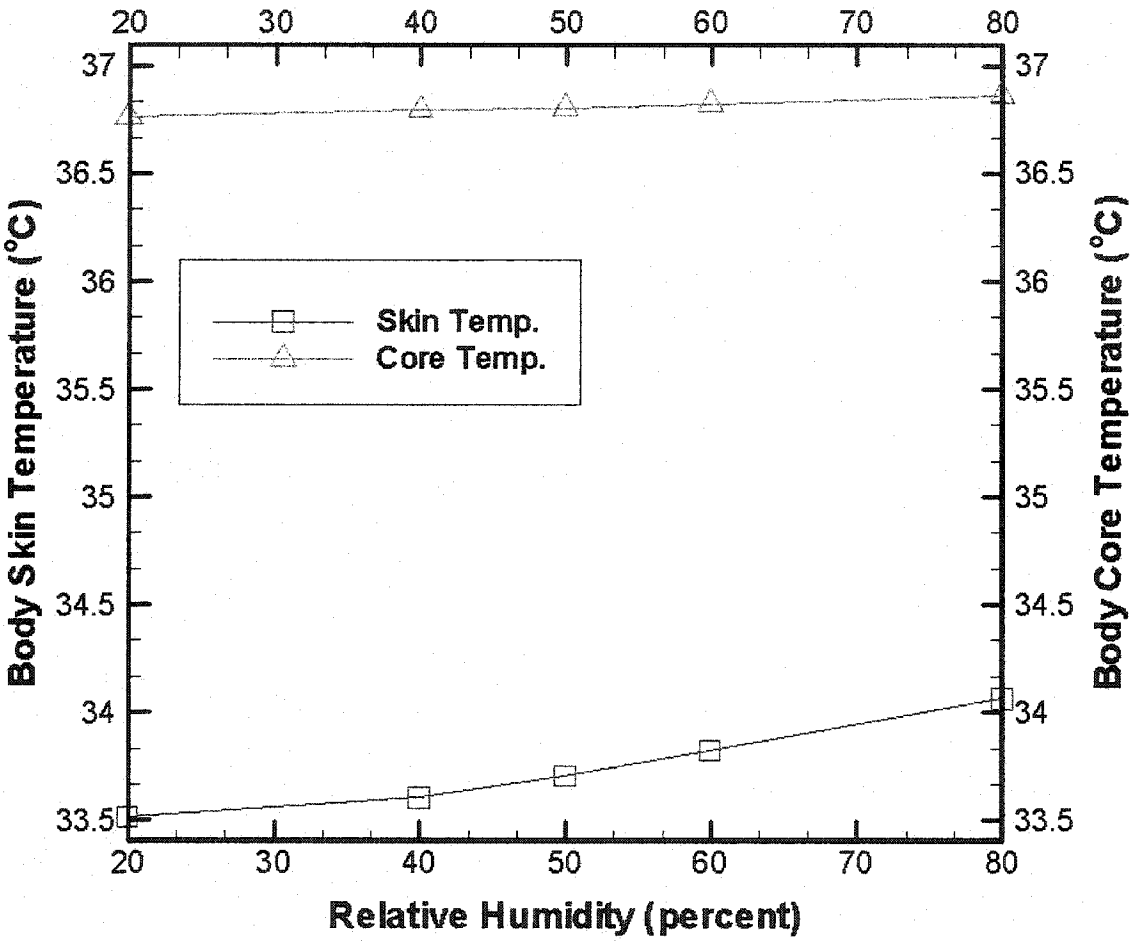

Figure 5.39 Core and skin temperatures as function of relative humidity

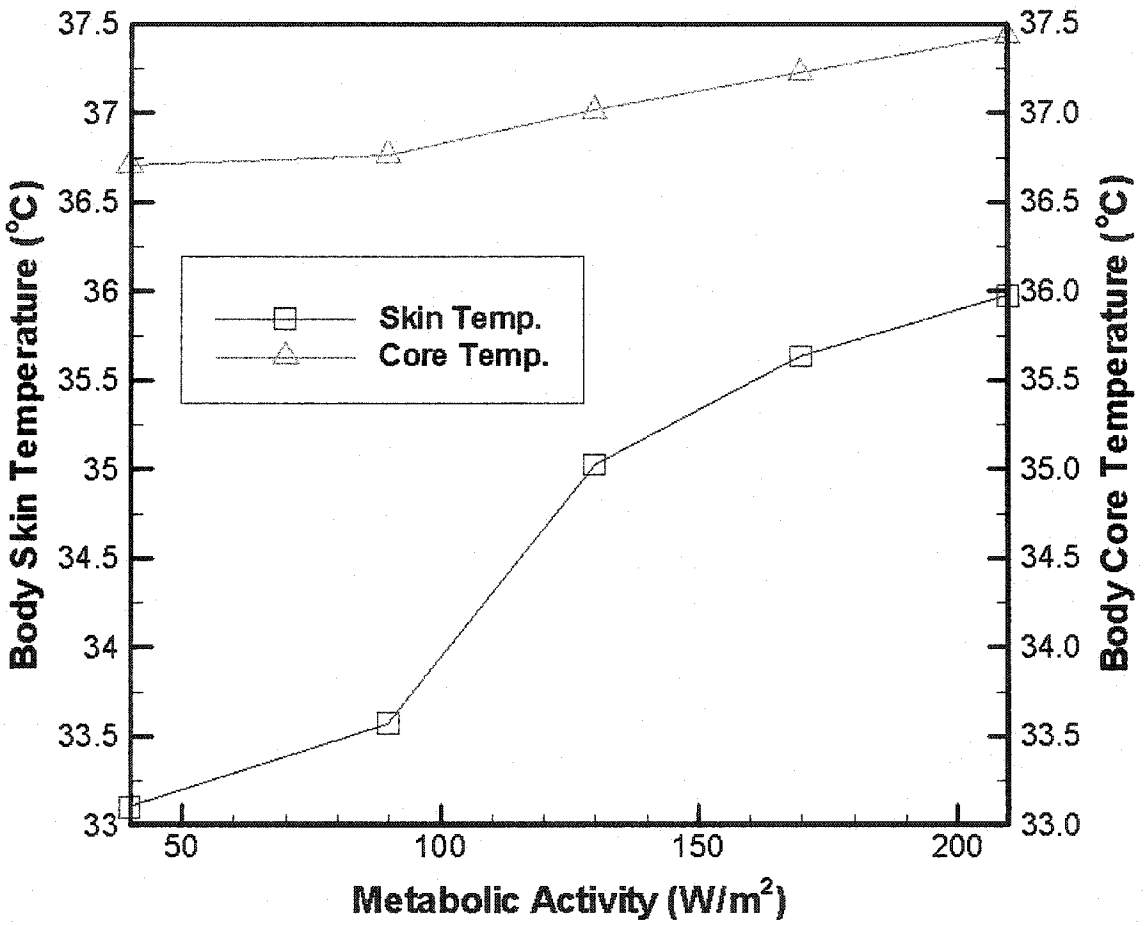

Figure 5.40 Core and skin temperatures as function of metabolic rate

core. As the metabolic rate increases nearly four fold, the core temperature increases from 36.65 °C to about 37.45 °C a rise of 1.8 °C. The skin temperature increases from about 33 °C to about36 °C, a 3 °C temperature rise.

5.7 The EDT-PMV Comfort Map

Figures 5.41-5.45 show EDT-PMV maps illustrating regions of thermal comfort, as predicted by respective indices. All values of indices are averaged over the entire room. The shaded region ($-0.5 \leq PMV \leq 0.5$) shows thermal comfort region as indicated by the PMV index (parallel vertical lines). The unshaded region confined by the parallel horizontal line gives the thermal comfort zone an indicated by the EDT index.

Figure 5.41 shows the effect of variation of supply air temperature as it increases from 10°C to 30°C. It is noted that where as according to the EDT index all supply air temperatures except the 30°C case indicate comfort zone, the PMV index shows that the only 15°C and 20°C supply temperature cases lie in the comfort zone while three other air temperatures 10°C, 25°C and 30°C fall outside the comfort zone.

Figure 5.42 shows the EDT-PMV comfort zone map for different supply air velocities. It is noted that both EDT and PMV are in agreement for all air velocity cases. The lowest four velocity cases lie in the thermal comfort zone while the highest velocity case is shown to lie in the thermal discomfort zone by both EDT and PMV indices. From Fig. 5.43 it is evident that all five relative humidity cases (20 to 80%) lie in the thermal comfort zone, thus indicating full agreement between EDT and PMV indices.

Figure 5.44 shows the effect of metabolic rate as shown on the EDT- PMV map. As the metabolic rate increases from 50 to 210 W/m^2 the EDT index indicates that all cases point to thermal comfort. The PMV index shows that while the highest metabolic rate case lies just outside the thermal comfort boundary, all other four conditions fall inside the comfort zone. Figure 5.45 shows the EDT-PMV comfort map for the segmented model. The variable in this case is the metabolic rate. Comparing with Fig 5.44 (uniform skin temperature model) one notes that only first three metabolic rates (50, 90, 130 W/m^2) lie in the thermal comfort zone as indicated by the PMV index, while two cases (170 and 210 W/m^2) lie outside the comfort zone. In that sense the segmented model produces conservative results, although, the differences between the two models are marginal.

In summary, it is noted that the PMV model predictions are conservative (fewer comfort conditions). Of all the 20 cases considered, the PMV model predicts 15 cases as comfort conditions and five cases as discomfort conditions. In contrast, the EDT index predicts 18 cases as comfort conditions and two cases as discomfort conditions.

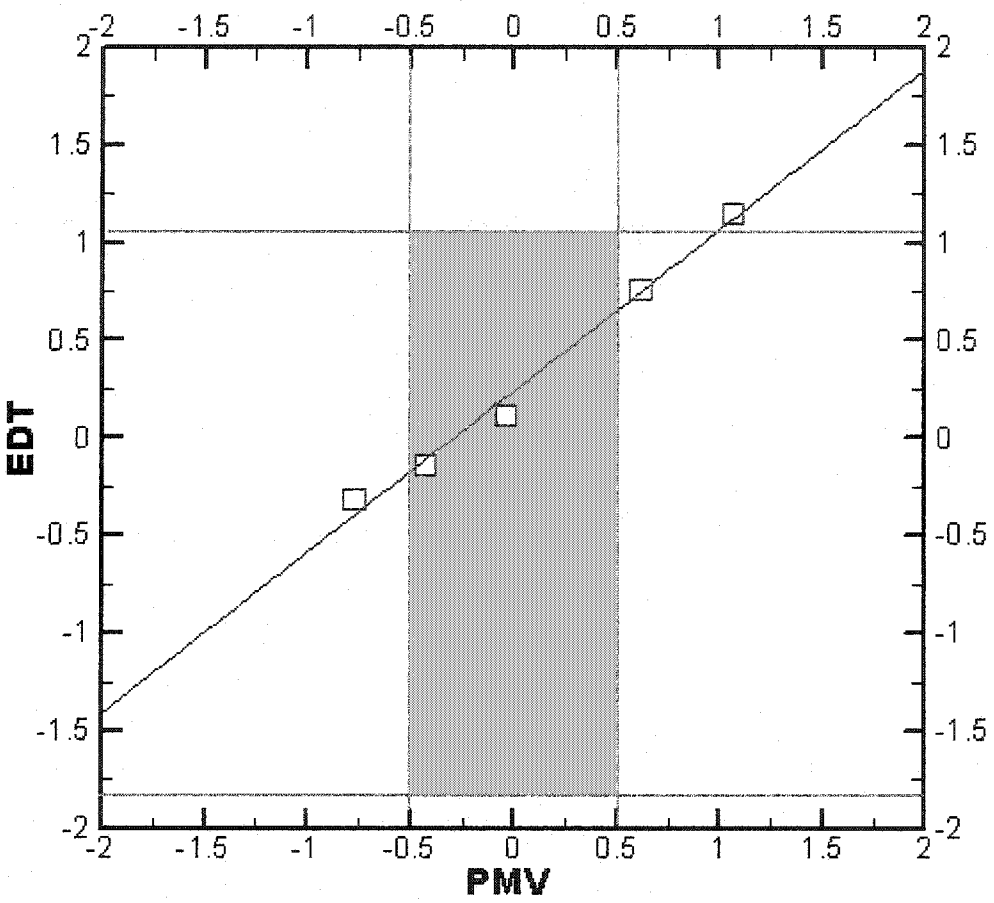

Figure 5.41 Thermal comfort zone for different inlet air temperature

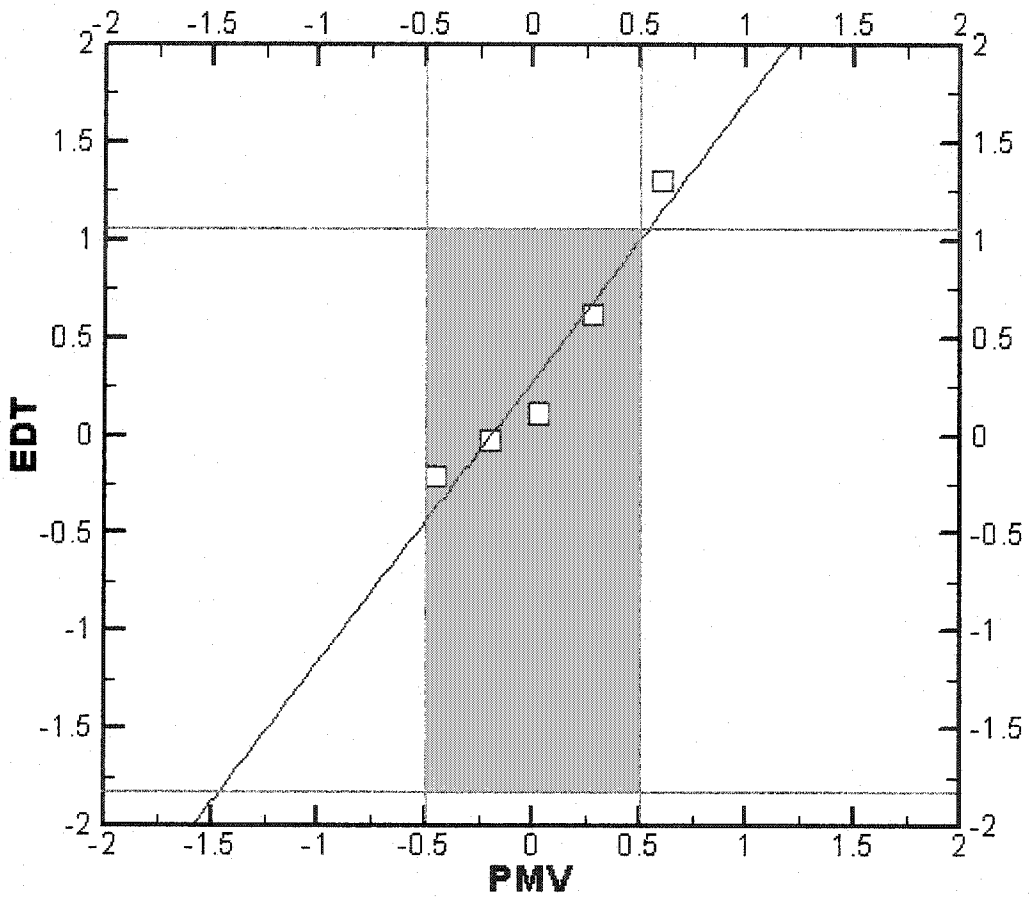

Figure 5.42 Thermal comfort zone for different inlet air velocity

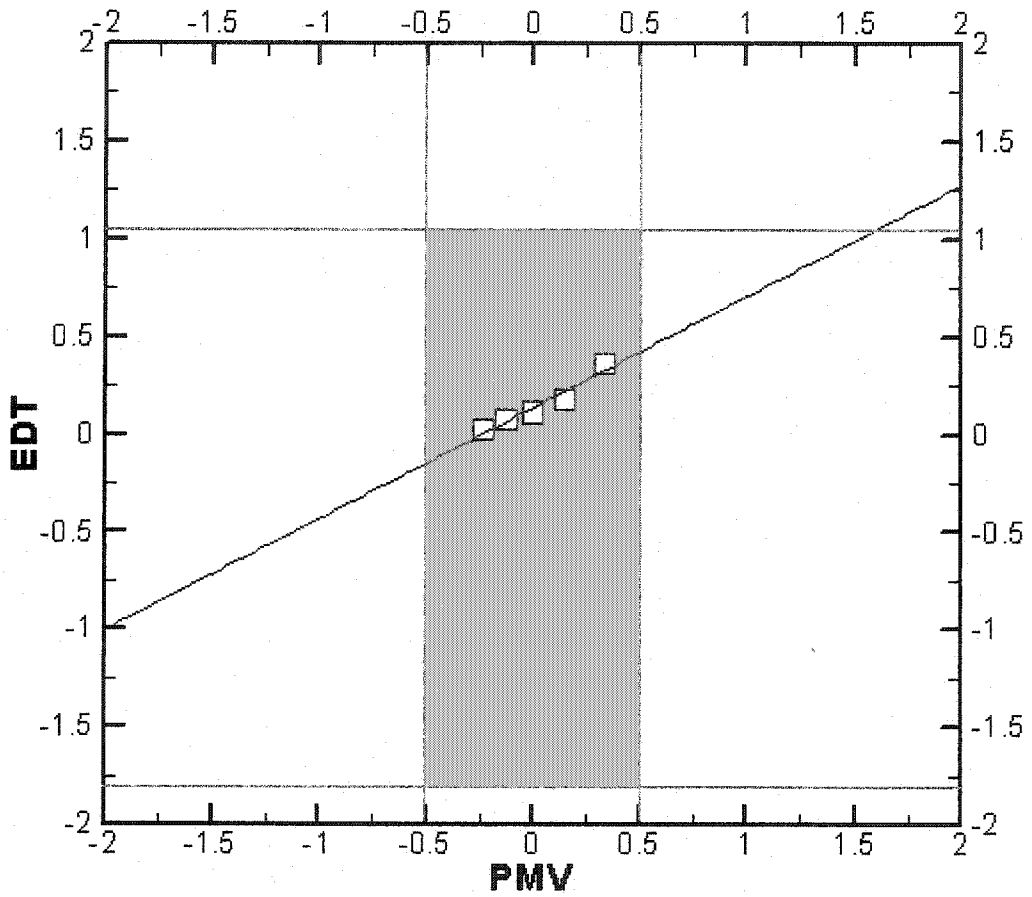

Figure 5.43 Thermal comfort zone for relative humidity

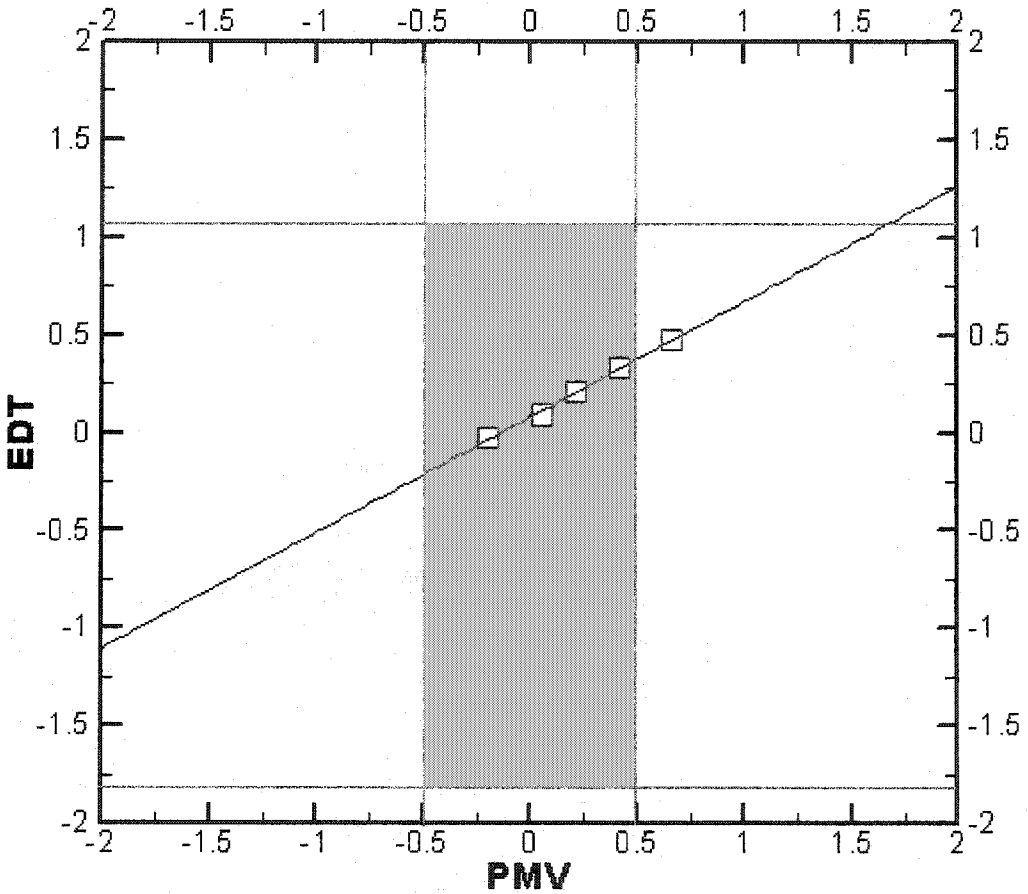

Figure 5.44 Thermal comfort zone for different metabolic rate

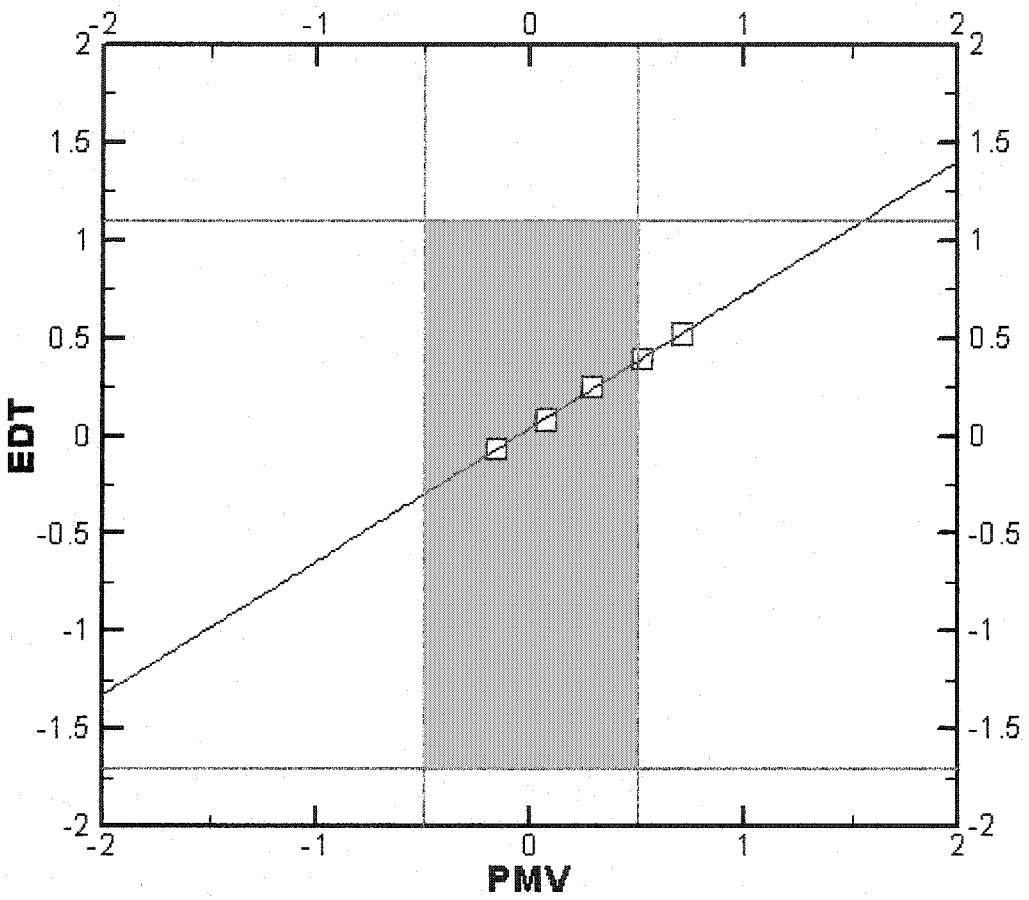

Figure 5.45 Thermal comfort zone for different metabolic rate (Segmented Body)

5.8 Correlation of Skin Temperature with PMV

The body skin temperature is a good indicator of thermal comfort or discomfort. High skin temperature may indicate warm discomfort while low skin temperature may be a result of cool discomfort condition. Since skin temperature can be easily measured, a relation between PMV and skin temperature will be valuable in assessing thermal comfort. With this objective in mind, predicted skin temperature values for all twenty cases are plotted as function of previously determined values of PMV index.

These results are shown in Fig. 5.46. One notes that all environmental variables (supply air velocity, humidity and temperature) nearly collapse on a single line. The metabolic rate for all these cases is kept at 100 W/m^2 (a sedentary person). The best fit line for these data points is given by the relationship $T_{sk} = A + B\ PMV$, where A and B are 33.70 and 0.96 respectively.

It is also noted that in Fig. 5.46 the points pertaining to metabolic rates other than 100 W/m^2 show a much steeper relationship. This indicates that slope B and intercept A are function of metabolic rate. Determination of A and B values as a function of metabolic rate is outside the scope of this study, since cases with environmental factors variation at metabolic rates higher or lower than 100 W/m^2 were not simulated. However, it will be of interest to determine these functional relationships if this linear relationship is to be extended to metabolic rates other than 100 W/m^2.

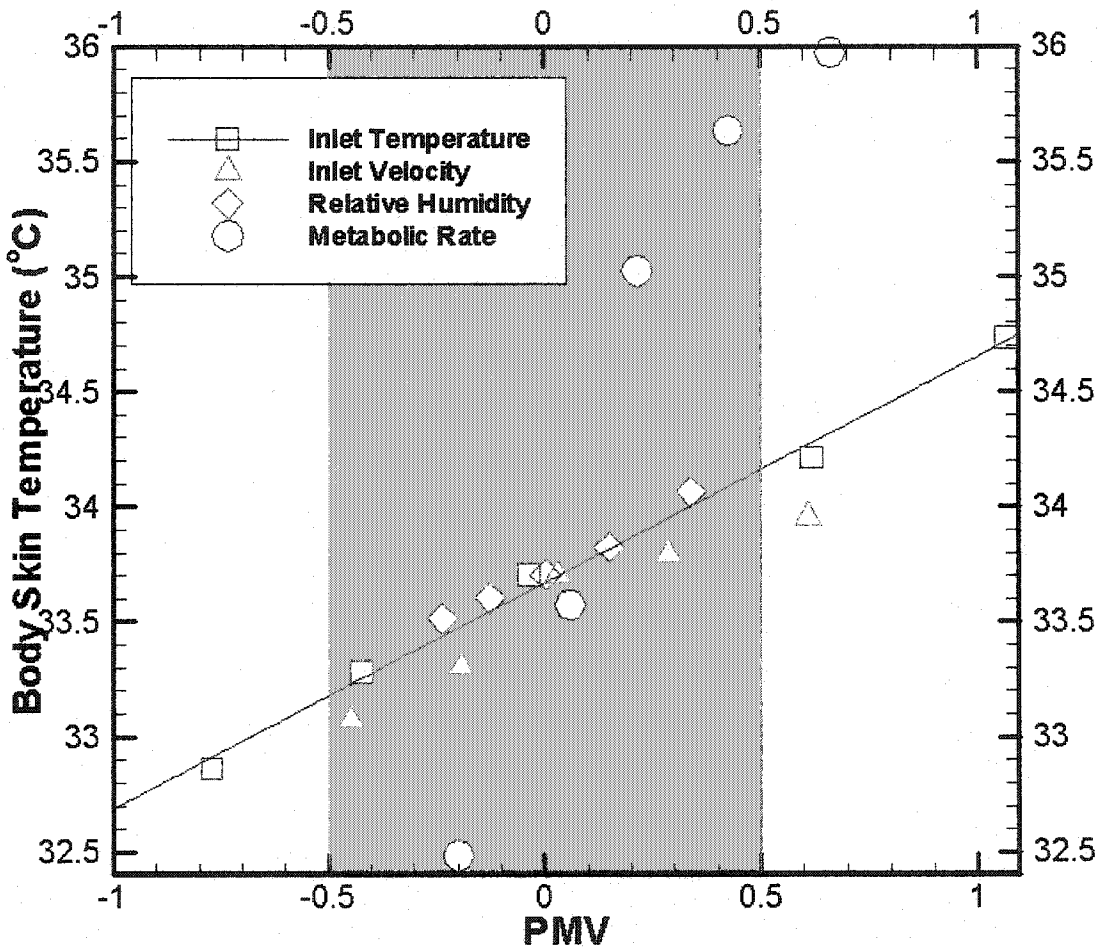

Figure 5.46 PMV index vs. body skin temperature for all different parameters

CHAPTER VI

CONCLUSIONS

Two numerical codes have been used to characterize the thermal environment around a human body. Both are coupled at the body surface through skin temperature. The two-node model was applied in this study to predict heat and mass transfer from a human body which in turn is used to set the boundary conditions at the human body surface for the CFD model for prediction of air flow and thermal characteristics of the occupied room. Effects of environmental factors such as supply air temperature, velocity, relative humidity, and turbulence intensity on human thermal comfort have been analyzed. Effects of human activity have been considered by varying the metabolic heat generation rate in the two-node human thermo-regulation model.

Results indicate that of the five parameters governing human thermal comfort, the supply air temperature has the most significant influence on human thermal comfort, followed by the metabolic heat generation rate and the supply air velocity. The effect of supply air relative humidity is relatively insignificant for chosen values of parameters in the analysis. The supply air turbulence intensity, according to calculated results, has a negligible effect on human thermal comfort for values of parameters considered in this study.

Both PMV and EDT comfort indices were successful in predicting regions of thermal comfort and discomfort. Furthermore, in majority of cases (75 %) prediction of

comfort or discomfort from these two indices were in broad agreement. The PMV index predicted 15 out of 20 specified parametric conditions to be in thermal comfort zone as compared to 18 (out of 20) for the EDT index case. Based on limited results obtained in this study, it is difficult to conclude if one index is better than the other for predicting thermal comfort conditions. However, limited results from this study do indicate that the PMV index produces conservative (least number of thermal comfort conditions) results.

The predicted value of room averaged PMV index and its relationship to the PPD index helped identify the optimal values of various supply parameters and metabolic heat generation rate. For instance, the optimal value of supply air velocity which minimized the PPD value (at 5 %) was determined to be 0.22 m/s after running five simulations in which the supply air velocity varied from 0.05 m/s to 0.35 m/s. This optimal value represents the case in which 95 percent of occupants are satisfied with maintained conditions as far as thermal comfort is concerned.

The segmented body model, developed in this study, gives a more realistic modeling of human thermo-regulatory processes. Results obtained from this model predict a wide variation of skin temperature, with the extremities such as feet and hand being at lower skin temperature as compared to head and neck regions. Consideration of human thermal comfort based on results from this model shows that it produces conservative results compared to the uniform skin temperature model. For instance, of the five metabolic heat generation rate cases only three are shown to lie in the thermal comfort zone as compared to four according to the uniform skin temperature model. Also, the optimal value of metabolic activity rate is 78 W/m^2 for the segmented body model as compared to 85 W/m^2 value for the uniform skin temperature body model.

The results also show that the PMV index can be correlated with the body skin temperature for all parameters except the metabolic activity rate. All computed values of skin temperature for 16 environmental parameter cases showed linear variation with PMV. Although all these results were for a metabolic rate of 100 W/m^2 , it can be speculated that the slope and intercept of the linear correlation between skin temperature and PMV should be functions of metabolic rate. Unfortunately, these functional relationships can not be determined in the present study because parametric variation of supply air conditions were not implemented at metabolic rates other than 100 W/m^2 . The linear relationship between PMV and skin temperature, once established on firm grounds, can be very useful since skin temperature can be sensed remotely and can be used to monitor thermal comfort sensation. This can permit manipulation of HVAC control system to maintain thermal comfort based on skin temperature sensing.

For future studies, further exploration of relationship between PMV and skin temperature and metabolic rate is recommended. Also, it is recommended that future studies include consideration of human thermo-regulation processes through the segmented body model to analyze thermal discomfort arising from excessive heat losses from body extremities such as hands and feet. Although the present study focused primarily on steady state cases, consideration of transient effects in a future study will be valuable for predicting thermal discomfort when environmental conditions or metabolic activity rate are changed with time.

REFERENCES

1. ASHRAE Standards, Standard 55, 1992.

2. Fanger, P., Thermal Comfort Analysis and Application in Environmental Engineering, McGraw-Hill, 1970.

3. Gagge, A.P., Forbelets, A.P. and Berglund, P.E., "Standard Predictive Index of Human Response to Thermal Environment,"ASHRAE Transactions, Part2, Vol. 92, 1986, pp. 709-731.

4. Brohus, H., Personal Exposure to Contaminant Sources in Ventilated Rooms, Ph.D. Thesis, Aalborg University, Denmark, 1997.

5. Loomans, M., The Measurement and Simulation of Indoor Air Flow, Ph.D. Thesis, Eindhoven University of Technology, Eindhoven, The Netherlands, 1998.

6. ASHRAE Fundamentals Handbook, [Chapter 8], 1997.

7. Nielsen, P.V., Flow in Air Conditioned Rooms, Ph.D. Thesis, Nordborg, Denmark, 1974.

8. Nielsen, P.V., Restivo, A. and Whitelaw, J. H., "The Velocity Characteristics of Ventilated Rooms," Journal of Fluids Engineering, Vol. 100, 1978, pp. 291-298.

9. Gosman, A.D. and Nielsen, P.V., "The Flow Properties of Rooms with Small Ventilation Openings," Transactions of the ASME, Vol. 102, 1980, pp.316-323.

10. Awbi, H.B., "Application of Computational Fluid Dynamics in Room Ventilation," Building and Environment, Vol. 24, 1989, pp. 73-84.

11. Awolesi, S.T., Awbi, H.B., Seymour, M.J., and Hiley, R.A., "The Use of CFD Techniques for the Assessment and Improvement of a Workshop Ventilation System" Computational Fluid Dynamics for the Environmental and Building Services Engineer, London: Mechanical Engineering Publications, 1991, pp. 39-46.

12. Awbi, H. B. and Gan, G., "Computational Fluid Dynamics in Ventilation," Computational Fluid Dynamics for the Environmental and Building Services, London: Mechanical Engineering Publications, 1991,pp. 67-79.

13. Chen, Q. and Kooi, J., "A Methodology for Indoor Airflow Computations and Energy Analysis for a Displacement Ventilation System," Energy and Buildings, Vol.14, 1990, pp. 259-271.

14. Chen, Q. and Jiang, Z., "Air Supply Method and Indoor Environment," Indoor Environment, Vol. 1, 1992, pp. 88-102.

15. Chen, Q. and Kooi, J., "Transient Heat Transfer through the Enclosures of a Room with Mixed Convection," Heat and Mass Transfer in Building Materials and Structures, 1991, pp. 697-706.

16. Chen, Q., Moser, A. and Suter, P., "A Numerical Study of Indoor Air Quality and Thermal Comfort under Six Kinds of Air Diffusion," ASHRAE Transactions, Vol. 98, Pt.1, 1992, pp. 203-217.

17. Murakami, S., Kato, S. and Suyama, Y., "Three-Dimensional Numerical Simulation of Turbulent Airflow in a Ventilated Room by Means of a Two-Equation Model," ASHRAE Transactions, Vol. 93, Pt. 2, 1987, pp. 621-641.

18. Murakami, S., Kato, S. and Suyama, Y., "Numerical Study on Diffusion Field as Affected by Arrangement of Supply and Exhaust Openings in Conventional Flow Type Clean Room," ASHRAE Transactions, Vol. 95, Pt. 2, 1989, pp. 113-127.

19. Murakami, S. and Kato, S., "Numerical and Experimental Study on Room Airflow-3-D Predictions using the k-ε Turbulence Model," Building and Environment, Vol. 24, No.1, 1989, pp. 85-97.

20. Fu, G., A Transient 3-D Mathematical Thermal Model for the Clothed Human, Ph.D. Thesis, Kansas State University, Manhattan, Kansas, 1995.

21. Givoni, B. and Goldman, R.F., "Predicting heart Rate Response to Work, Environment," Journal of Applied Physiology, Vol. 34, 1973, pp. 201-204.

22. Machle, W. and Hatch, F.F., "Heat: Man's Exchangees and Physiological Responses," Physiological Review, Vol. 27, 1947, pp. 200-227.

23. Gagge, A.P., Stolwijk, A.J. and Nishi, Y., "An Effective Temperature Scale Based on a Simple Model of Human Physiological Regulatory Response," ASHRAE Transactions, Vol. 77, pt. 1, 1971, pp. 247-262.

24. Gagge, A.P., Fobelets, A.P. and Berglund, L.G., "A Standard Predictive Index of Human Response, to the Thermal Enlivenment," ASHRAE Transactions, Vol. 92, pt.2, 1986.

25. Jones, B.W. and Ogawa, Y., "Transient Interaction between the Human and the Thermal Enlivenment," ASHRAE Transactions, Vol. 98, pt. 1, 1992.

26. Smith, C.E., A transient Three-Dimensional Model of the Human Thermal System, Ph.D., Thesis, Kansas State University, Manhattan, Kansas, 1991.

27. Murakami, S., Kato, S. and Zeng, J., "Flow and Temperature Fields around Human Body with various Room Air Distribution," ASHRAE Transactions, Vol. 103, pt. 1, 1996.

28. Alfahaid, A.F., Effect of Ventilation on human thermal Comfort in Rooms, Ph.D. Thesis, Old Dominion University, Norfolk, Virginia, 2000.

29. Arundel and Sterling, "Criteria for Human Exposure to Humidity in Occupied buildings." ASHRAE Transactions, Vol. 91, 1985, Part 1

30. Teodosiu, G. and Hohota, R., "Numerical Prediction of Indoor Air Humidity and its Effect on Indoor Environment," Building and Environment, Vol. 38, 2003, pp. 655-664.

31. Wright, D.N. and Bailey, G.D., "Survival of airborne Mycoplasma as affected by relative humidity," Journal of Bacteriology, Vol. 95, 1968, pp. 251-252.

32. Tennekes, H. and Lumley, J.L., A First Course in Turbulence, MIT Press, Cambridge, Massachusetts, USA, 1972.

33. Seppanen, O. and McNall, P.E., "Theramal Insulting Values for Typical Indoor Clothing Ensembles," ASHRAE Transactions, Vol. 78, 1972, pp. 120-130.

34. Rydberg J. and Norback, P., "Air Distribution and Draft,' ASHRAE transactions, Vol. 55, 1962, pp. 225.

35. Koestel A. and Tuve, G., "Performance and Evaluation of Room Air Distribution System," ASHRAE Transactions, Vol. 61, 1968, pp. 533.

36. Morton, B.R., Taylor, G.F. and Turner, J.S., "Turbulent Gravitational Convection from Maintained and Instantaneous Sources," Proceedings Roy. Soc. London, Vol. 234, 1954, pp. 1-23.

37. Zhao, B., Xianting, L. and Yan, Q., "A Simplified System for Indoor Airflow Simulation," Building and Environment, Vol. 38, 2003, pp. 543-552.

38. Chen, H.C. and Patel, V.C., "Near-Wall Turbulence Models for Complex Flows Including Separation;" AIAA Journal, Vol. 26, No. 6, 1988, pp. 641–8.

39. Launder, B.E and Spalding, D.B., "The Numerical Computation of Turbulent Flows," Computer Methods in Applied Mechanics and Engineering, Vol. 3, 1974, pp. 269–289.

40. Yakhot, V. and Orszag, S., "Renormalization Group Analysis of Turbulence," Journal of Scientific Computing, Vol. 1, No. 1, pp. 3-51.

41. Speziale, C. and Thangam, S., "Analysis of an RNG Based Turbulence Model for Separated Flows," Int. Journal of Engineering Science, Vol. 30, No. 10, 1992, pp. 1379-1388.

42. Fluent, Inc., Users Guide for Fluent, Release 6.02, Lebanon, NH, USA, 2002.

43. Dunnett, S.J., "A Numerical Study of the Factors Affecting Worker Exposure to Contaminated," Journal of Aerosol Science, Vol. 25, No. 1, 1994.

44. Niwa, K., Murakami, S. and Kato, S., "Numerical Analysis of Flow and Temperature Fields with Local Air-Conditioning by Supply Jets from the Seats in Hall," Proceeding Roomvent'96, Yokohama, Japan, Vol. 2, 1996, pp. 880-886.

45. Davidson, L. and Nielsen, P., "Large Eddy Simulations of the Flow in a Three-Dimensional Ventilated Room," Proceeding Roomvent'96, Yokohama, Japan, Vol. 2, 1996, pp. 161-168.

46. Heinsohn, R.J., Industrial Ventilation: Engineering Principle, John Wiley & Sons, New York 1991.

47. Iwamoto, S., "A Study on Numerical Prediction Methods of Thermal Environment around Occupants," Proceedings of Indoor Air '96, Nagoya, Japan Vol. 1, 1996, pp. 299-303.

48. Bluyssen, P.M. and Lemaire, T., "The Distrbution of Preceived Air Quality in an Office Space," Proceeding Roomvent'92, Aalborg, Denmark, Vol. 3, 1992, pp. 195-211.

49. Gan, G., Awbi, H.B. and Croome, D.J., " CFD Simulation of the Indoor Environment for Ventilation Design," ASME '93 Winter Meeting, New Orleans, USA, Paper No. 93.

50. Gan, G., "Numerical Method for a Full Assessment of Indoor Thermal Comfort," Proceedings of Indoor Air '94, Vol. 4, 1994, pp. 154-168.

51. Brohus, H. and Nielsen, P. V., "Air Flow in a Room Ventilated after the Mixing Principle with an Obstacle Placed in Occupied Zone," Proceedings of RoomVent '94, Budapest, Hungary, Vo. 2, pp. 559-564.

52. Awbi, H.B., "A CFD Study of the Air Quality at the Breathing Zone," Proceedings of Indoor Air '96, Nagoya, Japan Vol. 2, 1996, pp. 1009-1014.

53. Murakami, S., Kato, S. and Zeng, J., "Combined Simulation of Airflow, Radiation and Moisture Transport for Heat Release from a Human Body;" Building and Environment, Vol. 35, 2000, pp. 489-500.

54. Kato, S., Murakami, S. and Zeng, J., "Numerical Analysis of Contaminated Distribution around Body;" Proceeding Roomvent'96, Yokohama, Japan, Vol. 2, 1996, pp. 129-136.

55. Wurtz, E., "Two- and three-Dimensional Natural and Mixed Convection Simulation Using Modular Zonal Models in Buildings," International Journal of Heat and Mass Transfer, Vol. 42, Issue 5, 1999, pp. 923-940.

56. Ren, Z. and Stewart, J., "Simulating Air Flow and Temperature Distribution Inside Buildings Using a Modified Version of COMIS with Sub-Zonal Divisions;" Energy and Buildings, Vol. 35, 2003, pp. 257–271.

57. Chen, Q., "Computational Fluid Dynamics for HVAC: Successes and Failures," ASHRAE Transactions, Vol. 103, pt. 1, 1997, pp. 178–187.

58. Murakami, S. and Zeng, J., "CFD Analysis of Wind Environment Around a Human Body," Journal of Wind Engineering and Industrial Aerodynamics, Vo. 83, Issues 1-3, 1999, pp. 393-408.

CURRICULUM VITA
for
AHMED M. AL-MOGBEL

Education

Doctoral Philosophy, Old Dominion University, Norfolk, Virginia, December 2004
Master of Science, Old Dominion University, Norfolk, Virginia, August 2000
Bachelor of Mech. Engineering, King Saud University, Saudi Arabia, December 1991

Professional Membership

Student Member, American Society of Heating, Refrigerating and Air-Conditioning Engineers, 2000 – present
Student Member, American Institute of Aeronautics and Astronautics, 2001 – present
Member, Virginia Academy of Sciences, 2000 – present

Selected Publications

AL-Mogbel, A.M., Gorozabel, F.B. and Chaturvedi, S.K., " Thermodynamic Analysis of a Solar Assisted Heat Pump," Proceedings of the 79 Annual Meeting of Virginia Academy of Sciences, Harrisonburg, Virginia, May 2001.

AL-Mogbel, A.M. and Chaturvedi, S.K., "Numerical Analysis of Human Thermal Comfort in Occupied Rooms," Proceedings of the 81 Annual Meeting of Virginia Academy of Sciences, Charlesville, Virginia, May 2003.

AL-Mogbel, A.M. and Chaturvedi, S.K., "A Coupled Model for Predicting Heat and Mass Transfer from a Human Body to its Surroundings," AIAA Paper No. 2003-4211; 36th AIAA Thermo physics Conference, Orlando, Florida, June 2003.